DIPARTIMENTO SCIENZE DELLA VITA

DOTTORATO DI RICERCA IN SCIENZE DELLA VITA

CICLO XXXV

COORDINATORE Prof. Massimo Valoti

CHARACTERIZATION OF T CELL HOMEOSTASIS AND EFFECTOR FUNCTIONS

SETTORE SCIENTIFICO-DISCIPLINARE: BIO/11

TUTOR: Prof.ssa Cosima Baldari

DOTTORANDA: Dr.ssa Fabrizia Zevolini

CO-RELATORE: Prof.ssa Francesca Finetti

A.A. 2022/2023

TABLE OF CONTENTS

The intraflagellar transport protein IFT20 recruits ATG16L1 to early endosomes to promote autophagosome formation in T cells (Finetti *et al.*, 2021)

ABSTRACT

The orchestration of adaptive immune response crucially relies on homeostatic and effector functions of T lymphocytes. Among the array of pathways that concur to the regulation of T cell maintenance, activation and differentiation, an emerging leading factor is autophagy. Autophagy is a catabolic process that subserves the dual function of eliminating damaged substrates while providing endogenous energy sources and building blocks to maintain cellular functions. This mechanism depends on autophagy related (ATG) proteins and their interaction with the trafficking machinery that orchestrates the membrane rearrangements leading to autophagosome biogenesis. The intraflagellar transport (IFT) system, first identified for its role in the control of vesicular trafficking along the axonemal microtubules of the primary cilium, participates in the regulation of autophagy in both ciliated and non-ciliated cells. In the first part of this thesis, we investigated the mechanism by which IFT20, an integral component of the IFT system, regulates basal $CD4^+$ T cell autophagy. We show that IFT20 interacts with the core autophagy protein ATG16L1 and mediates its association with the golgin GMAP210 at the Golgi apparatus and the small GTPase Rab5 at early endosomes. GMAP210 downregulation, while leading to a dispersed Golgi-associated ATG16L1 pattern, did not affect basal autophagy. Nonetheless, we found that IFT20 is required for ATG16L1 recruitment to early endosomes tagged for autophagosome formation, thereby promoting autophagosome biogenesis in T cells.

Growing evidence indicates that IFT proteins participate in additional cilia-independent processes in the non-ciliated T cells. IFT20 plays a key role in T cell activation by regulating the assembly of the immune synapse (IS), the specialized membrane domain at the interface between the T lymphocyte and the antigen presenting cell (APC), controlling the intracellular traffic of T cell receptor (TCR) and Linker for Activation of T cells (LAT). More recently, the involvement of IFT20 in another vesicular trafficking-related process, the mannose 6-phosphate receptor (MPR)-dependent transport of acid hydrolases to lysosomes, on which lysosome biogenesis and function depend, opened the way to the second part of this work. $CD8^+$ cytotoxic T cells (CTLs) contain specialized secretory

lysosomes, named lytic granules, their main tool for target cell death delivery. We show that IFT20 controls MPR-mediated granzyme B targeting to lytic granules and CTL cytotoxicity. IFT20 depletion leads to a lytic granule phenotype associated to lysosomal biogenesis defect, a process orchestrated by the coordinated lysosomal expression and regulation (CLEAR) gene network and controlled by the master transcription factor EB (TFEB). Consistently, we found that IFT20 is involved in the TFEB-driven lytic granule biogenesis program, taking part to the main pathway of lethal hit delivery of CTLs.

Effective CTL killing relies on the proper biogenesis of lytic granules and on their polarized delivery to the IS. The dynamic reorganization of the microtubule cytoskeleton and centrosome reorientation at the IS is required for T cell effector functions, facilitating the polarized release of cytokines and cytolytic factors. In the third part of this thesis, the recent discovery that the kinase Aurora-A (AurA) promotes T cell activation, as well as the microtubule-driven delivery of CD3ζ-bearing vesicles to the IS, led us to investigate the potential involvement of AurA substrate Polo-like kinase 1 (PLK1), a mitotic regulator whose activation is pivotal for centrosome dynamics during cell cycle, in the assembly of the IS of CTLs. Our results show that PLK1 inhibition impairs TCR signalling and centrosome translocation towards the IS in CTLs, as well as lytic granule polarization towards the T-APC contact point, leading to defective CTL cytotoxic capability. The altered microtubule dynamics due to PLK1 inhibition may be the cause of defective IS assembly in CTLs, proposing PLK1 as a novel determinant of CTL-mediated killing.

All in all, this thesis deals with different aspects of T cell homeostasis and effector functions, shedding light on some missing points of the physiology of one of the main players of adaptive immunity.

INTRODUCTION

The immune system

The immune system was first identified as a protective factor against infectious diseases over a century ago (Kaufmann *et al.*, 2005). Throughout decades, countless studies have contributed to build the wide perspective that we currently have on this interactive network of lymphoid organs, cells, humoral factors, and cytokines. It is now clear that, beyond the host defence, the immune system is an integral part of other fundamental physiological processes that include development, homeostasis, and repair (Sattler *et al.*, 2017).

Immunity comprises two lines of defence, named innate and adaptive immunity, although they belong to a common network. The definition of innate immunity includes physical, chemical, and microbiological barriers, but the most effective players are the elements of the immune system, namely neutrophils, monocytes, macrophages, complement, cytokines, and acute phase proteins. This type of immunity provides immediate host defence, and the highly conserved nature of the response is direct evidence of its relevance in the survival of the organism (Smith *et al.*, 2019). The adaptive immunity consists of antigen-specific reactions driven by T and B lymphocytes. Whereas the innate response is rapid but can cause damage to normal tissues as it lacks specificity, the adaptive response is precise but takes several days or weeks to fully develop. Furthermore, the adaptive immune response has memory, so that subsequent exposure to the same trigger leads to a more rapid and vigorous response (Farber *et al.*, 2016).

Although the mechanisms that elicit innate and adaptive immune responses are distinct, they collude to improve the host defence against pathogens. Initiation of the innate immune response begins when germline-encoded intracellular or extracellular pattern recognition receptors (PRRs) of an immune cell recognize unique pathogen-associated molecular patterns (PAMPs) on a pathogen, such as bacteria-derived lipopolysaccharide, viral RNA, bacterial DNA, or a danger-associated molecular pattern (DAMP) found on proteins or other biomolecules that are released from stressed or injured cells. Activated PRRs trigger intracellular signalling cascades, which lead to transcriptional expression of pro-

inflammatory cytokines, type I interferons and other antiviral proteins aimed to eliminate pathogens and infected cells (Takeuchi *et al.*, 2010). The capability of non-self-recognition allows the innate immunity to recruit immune cells to the site of infection through cytokine production and to activate the adaptive immune system by antigen presentation (Janeway *et al.*, 2001).

The defining feature of the adaptive immunity is the presence of antigen-specific receptors on T and B cells that drive targeted effector responses. The adaptive immune response initiates when the antigen is presented to and recognized by the antigen specific T or B cell, leading to cell priming, activation, and differentiation. Antigen recognition triggers the effector response, which can be either due to the activated T cells leaving the lymphoid tissue and homing to the site of the disease, or to the release of antibodies into the blood and tissue fluids by activated B cells, and thence to the infective focus (Janeway *et al.*, 2001). B and T lymphocytes arise from progenitor cells within the bone marrow, but T cells migrate to the thymus at an early stage of their development. The production of antigen-specific receptors in both cell types is the result of an unusual process of random rearrangement and splicing of multiple DNA segments that code for the antigen-binding areas of the receptor. Gene rearrangement occurs early in the development of the cells and allows the production of a repertoire of over 10^8 T cell receptors (TCRs) and 10^{10} antibody specificities (Wartsila *et al.*, 2019), adequate to cover a wide range of pathogens before antigen exposure.

The B and T cells that emerge from the bone marrow and the thymus, respectively, have undergone gene rearrangement, but they are still naïve, as they have not yet encountered their specific antigen. These cells populate the secondary lymphoid tissues of the lymph nodes, spleen, tonsils, and mucosa-associated lymphoid tissue. The lymphoid tissues provide the microenvironment where naïve B and T cells can be more easily exposed to and recognize foreign particles, also through the activity of antigen-presenting cells (APCs) (Parkin *et al.*, 2001). Despite the similarities in the gene rearrangement processes, the T and B cell receptors recognize antigens differently. Specifically, T lymphocyte activation requires a processed small peptide antigen which is recognized by the T cell only if stably

bound to a polymorphic major histocompatibility complex (MHC)-encoded glycoprotein expressed on the surface of APCs, as the TCR does not recognize the antigenic epitope alone but recognizes the complex of the processed peptide in association with the MHC molecule (Jensen, 1999), while the B cell receptor directly recognizes conformational or linear epitopes of the antigen. T and B cells are able to respond to antigens and induce an immune response, however cell activation is tightly regulated to ensure that only pathogen- or cancer-cell derived antigens elicit a reaction.

T lymphocytes

The activation of T lymphocytes is a key element of the adaptive immunity and requires the coordinated activation of highly complex signalling networks (Fig.1). The T cell-mediated response relies on the ability of the TCR to recognize a peptide-MHC complex on the surface of an APC. TCRs on the surface of the T cell are associated with CD3 molecules (Wucherpfennig *et al.*, 2010). The TCR/CD3 complex is formed through noncovalent association of the TCRαβ subunit with a CD3 signalling apparatus, consisting of the dimeric subunits CD3γε, CD3δε and CD3ζζ. The eight subunits in the TCR/CD3 complex are type I transmembrane proteins. Both TCRα and TCRβ contain an extracellular portion with variable and constant domains, a transmembrane segment, and a short cytoplasmic tail (Dong *et al.,* 2019). Similarly, each CD3γ, CD3δ or CD3ε is composed of a single extracellular immunoglobulin domain, a transmembrane segment and a long cytoplasmic domain containing immunoreceptor-tyrosine-based activation motifs (ITAMs) (Wang *et al.*, 2012).

The TCR peptide-recognizing αβ heterodimer has no intrinsic catalytic activity. TCR engagement by peptide-MHC induces phosphorylation of the ITAMs in the CD3ζ subunits of TCR by the Lymphocyte specific kinase (LCK), anchored to the inner leaflet of the plasma membrane (Palacios and Weiss, 2004). Phosphorylated CD3ζ serves as recruitment and activation site to trigger the phosphorylation signalling events involving ζ-chain-associated protein kinase 70 (Zap70), containing tandem SH2 domains that bind phosphorylated ITAMs with high affinity (Chu *et al.*, 1998), and in turn the Linker for Activation of T cells

(LAT). LAT is an integral membrane protein with a cytoplasmic tail containing nine tyrosine residues. When phosphorylated, these residues act as docking sites for SH2-containing effector enzymes, resulting in the recruitment of the multiple downstream adaptors and signalling molecules composing the LAT signalosome (Rossy *et al.*, 2012). One of the enzymes recruited is the phospholipase Cγ (PLCγ), a critical molecule for lymphocyte activation (Cantrell, 2015). The subsequent tyrosine phosphorylation of PLCγ activates the enzyme, resulting in the hydrolysis of its substrate phosphatidylinositol 4,5-bisphosphate (PIP_2).

At the core of lymphocyte signal transduction is the control of intracellular calcium levels and the regulated metabolism of inositol phosphatases and lipids, including the polyunsaturated diacylglycerols (DAGs) (Oh-hora *et al.*, 2008; Matthwes *et al.*, 2009). Inositol 1,4,5-trisphosphate (IP_3) produced by PLCγ binds to IP_3 receptors on the endoplasmic reticulum (ER) membranes, initiating the release of calcium from stores into the cytosol (Bootman, 2012). The increase of cytosolic calcium concentration triggers further entry of calcium across the plasma membrane, whose high intracellular levels are required for T cell activation (Hogan *et al.*, 2010).

Ultimately, through the activation of several signalling pathways controlling phospholipids, calcium, and kinase signalling, the assembled LAT signalosome regulates the activity of transcription factors such as activator protein 1 (AP-1), the nuclear factor-κB (NF-κB) and nuclear factor of activated T cells (NFAT). Signalling events downstream of the transcription factors listed above result in cytoskeleton reorganization and induction of gene expression leading to T cell activation, proliferation, cytokine production and effector functions (Gaud *et al.*, 2018).

The TCR signalling response to antigen directs the differentiation of T lymphocytes into functionally diverse subsets. Moreover, the intensity and duration of TCR signalling have been related to effector versus memory T cell differentiation (Gaud *et al.*, 2018). Effector T cells comprise two groups, T helper (Th) and T cytotoxic (CTL), bearing either CD4 or CD8 molecules on their surface, respectively. $CD4^+$ Th cells are the orchestrating cells of the immune response, recognizing foreign antigens and activating other parts of the cell-

mediated immune response, including B cells, to eradicate the pathogen. $CD8^+$ CTLs are involved in antimicrobial and antitumor activity (Cassioli and Baldari, 2022). The activation of macrophages via $CD4^+$ cell cytokines to kill facultative intracellular pathogens and the role of $CD8^+$ T cells in killing virally infected cells, provide the control of intracellular infections that cannot be achieved by the innate immune system.

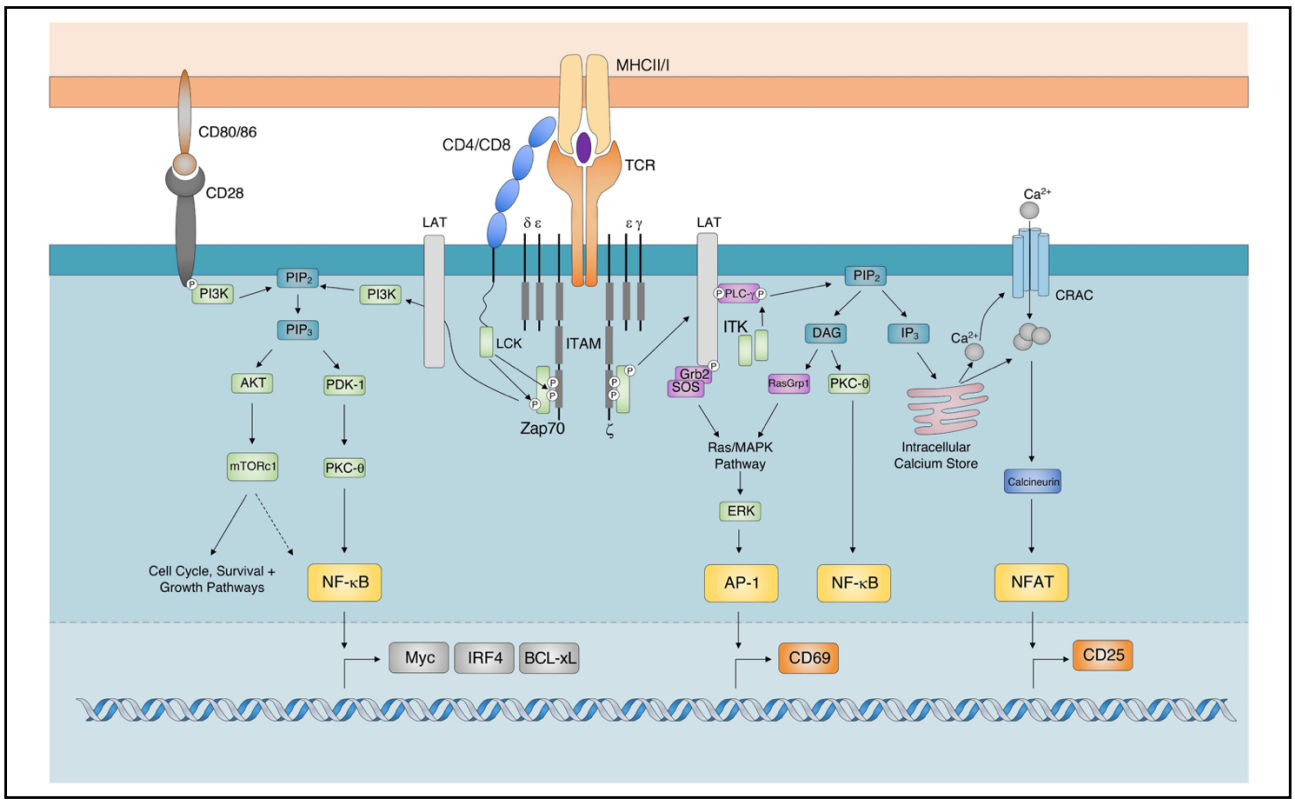

Figure 1| ***TCR signalling cascade leading to T cell activation.***

The recognition of the cognate peptide-MHC on the APC triggers TCR signal transduction, a complex pathway that involves several kinases and activates multiple transcription factors responsible for cell division (Myc) (Heinzel *et al.*, 2017), cell expansion (IRF4) (Krishnamoorthy *et al.*, 2017) and cell survival (BCL-xL) (Marinari *et al.*, 2004). The PLCγ-dependent cascade contributes to the establishment of the T cell activation program through the transcription factors AP-1, NF-κB and NFAT (Bhattacharyya *et al.*, 2020).

Foreign antigen can be loaded on the MHC following two pathways. The antigen can be produced endogenously within any cell of the organism and complexed with MHC class I through intracellular processing, as is the case for viral or tumour proteins. Endogenous antigens complexed with MHC I activate $CD8^+$ T cells. Because all nucleated cells express

MHC I, any cell that is infected with a virus or other intracellular pathogen, or is producing abnormal tumour antigens, can present these antigens with MHC class I and be removed by cytotoxic attack (Jongsma *et al.*, 2019). Alternatively, specialized professional APCs, namely dendritic cells, macrophages, and B cells, can endocytose exogenous antigen, process it and re-express it on the APC surface in association with MHC class II, whose expression is restricted only to these specialized cells (Pishesha *et al.*, 2022). $CD4^+$ lymphocytes recognize the antigen when presented with MHC class II. Whereas CD8-mediated responses are highly targeted to the cell that they recognize, CD4 activation leads to the production of cytokines, which in turn activate a wide range of cells around them. The fact that only a small number of APCs are able to drive $CD4^+$ lymphocyte activation ensures that the reaction is tightly controlled to avoid not only exacerbation of the response but also reactions against self-tissues (Reith *et al.*, 2005).

The first step in T cell activation is antigen recognition by the TCR. Antigen is presented by APCs after intracellular processing and expression in association with MHC, so that only the foreign molecules that have either invaded a host cell or induced an inflammatory response to activate endocytosis by APCs are recognized as dangerous and activate the immune response. Innocuous antigens are largely ignored (Kotsias *et al.*, 2019). The response of most naïve T cells to an MHC-bound peptide fails however to be triggered in the absence of an additional co-signal. This mechanism guarantees an additional safety net, as TCR binding to antigen-MHC complex alone is not sufficient to induce T cell activation. Notably, CD4 and CD8 molecules are not merely markers that define different T cell populations; they are co-receptors essential to facilitate TCR recognition of peptides presented on MHC molecules, and they take part in the transmission of the intracellular signals following TCR complex triggering (Gao *et al.*, 2002). In the absence of CD4/CD8 co-signals, the T cell will become anergic (Valdor *et al.*, 2010). Among the best established co-stimulatory pairs are CD28 on the T cell surface and its binding partners CD80/CD86, whose expression is restricted to specialized APCs, namely dendritic cells, macrophages, and B cells. CD28 co-engagement is required for a broad spectrum of functions that include

cell metabolism, cytokine production and the activation of transcription factors such as NF-κB, tightly related to cell survival (Schmitz *et al.*, 2006).

Fully activated T cells go through clonal expansion and differentiation. Most of the resulting progenies are armed effectors, which upregulate receptors and leave the lymphoid tissues to be guided to the site of inflammation, attracted by organ-specific adhesion molecules (Sallusto *et al.*, 1999). There, T cells will recognize target cells expressing the specific foreign antigen and initiate either a cytotoxic attack or stimulate an inflammatory response. Some of the activated T cells remain in the lymph nodes as central memory cells, which can react more quickly on subsequent exposure to their specific antigen (Gray *et al.*, 2018).

CD4$^+$ helper T lymphocytes

CD4$^+$ T cells play a central role in coordinating protective immune responses against bacterial, viral, parasitic, and fungal infections by regulation of antibody-producing B cells, CD8$^+$ T cells, and macrophages (Luckheeram *et al.*, 2012). To ensure that there are sufficient numbers of antigen-specific clones to combat pathogens at infection sites, activated CD4$^+$ lymphocytes undergo extensive cell division and differentiation, giving rise to a heterogeneous group of effector T cells. Effector CD4$^+$ T cells carry out multiple functions, ranging from supporting the activation of the cells of both the innate and adaptive immune systems, as well as nonimmune cells, to the suppression of the immune response (Swain *et al.*, 2012). The pattern of cytokines produced allows the functional identification of CD4$^+$ T helper cells (Luckheeram *et al.*, 2012). Two prevailing models explain how CD4$^+$ T cells integrate different signals to determine lineage commitment (Bhattacharyya *et al.*, 2020). The classic "qualitative" model suggests that Th cell responses are shaped dominantly by the cytokines produced by pathogen-exposed innate cells. The second "quantitative" model proposes that the strength of the signal delivered through the TCR regulates the differentiation program of CD4$^+$ T cells. Multiple T cell-associated factors influence the overall strength of TCR signals, including the quality of the interactions between MHC and TCR molecules, the amount of antigen, and the degree of co-stimulation (Corse *et al.*, 2011).

The best characterized subsets of CD4$^+$ T cells are Th1 and Th2. Th1 cells are involved with the elimination of intracellular pathogens (Sallusto *et al.*, 2016). They mainly secrete IFNγ, fundamental for the activation of mononuclear phagocytes (Brennan *et al.*, 2006), lymphotoxin α, whose depletion is associated with protection from autoimmune diseases (Chiang *et al.*, 2009), and interleukin 2 (IL2), that promotes proliferation of CD8$^+$ T cells with acquisition of a cytolytic phenotype (Pipkin *et al.*, 2010). Besides its role as T cell growth factor, IL2 was also found to promote the development of CD8$^+$ memory cells after antigen priming, thus ensuring a robust secondary immune response (Mitchell *et al.*, 2010). Th2 cells mount immune response to extracellular parasites and play major role in induction and persistence of allergic diseases (Henry *et al.*, 2017). Their key effector

cytokines include IL4, IL5, IL9 and IL13, all associated with immune reaction against parasites. Additionally, combinations of these cytokines drive B cell proliferation and immunoglobulin class-switching to immunoglobulin E, promoting the inappropriate immune responses that characterize allergic reactions (Fallon *et al.*, 2002). IL10, a cytokine with broad immunoregulatory function, was originally described as a unique product of Th2 cells but was later shown to be expressed in Th1 as well, with paracrine effect. Hence, IL10 affects T cell activity indirectly by inhibiting the function of antigen-presenting cells, with a major tissue-protective role for the cytokine in preventing Th1/Th17-mediated immunopathology and associated tissue damage (Jankovic *et al.*, 2010).

More recent findings have made clear that the specializations that can be acquired by $CD4^+$ T cells are not limited to Th1 and Th2. Thymocyte precursors can also differentiate into T cells specialized to assist B cell differentiation, known as follicular Th cells (Tfh), and into the pro-inflammatory Th17, along with regulatory T cells (Treg).

Tfh cells play a significant role in mediating humoral immunity through interaction with B lymphocytes. In the pre-germinal centre, they interact with antigen-primed B lymphocytes, with subsequent differentiation of the B cell into immunoglobulin-producing plasma cells, while in the germinal area they are involved in the development of long-lived B memory cells (Johnston *et al.*, 2009).

Th17 cells are responsible for mounting immune responses against extracellular bacteria and fungi, and they are involved in the pathogenesis of autoimmune diseases (Ouyang *et al.*, 2008). Among the cytokines produced are IL17, an inducer of the release of pro-inflammatory cytokines and also chemokines, that ensures the chemotaxis of inflammatory cells to the site on infection (Shahrara *et al.*, 2009; Halwani *et al.*, 2014), IL21, that triggers the production of anti-microbial and pro-inflammatory molecules, and IL22, known to exert a dual function contributing to the pathogenesis of autoimmune diseases and exhibiting tissue protective properties (Yeste *et al.*, 2014).

Tregs play important role in the maintenance of homeostasis and immunologic self-tolerance. After clearance of pathogens, they negatively regulate T cell proliferation and cytokine production, thereby preventing autoimmunity (Sugimoto *et al.*, 2006). Moreover,

self-reactive T cells that escape negative selection in the thymus have the potential to start dangerous reactions against the tissues. The establishment of peripheral tolerance is pursued also through the immune suppression activity of Tregs. Their main effector cytokines include IL10 and TGF-β, showing an important role in attenuating allergic inflammation (Jutel *et al.*, 2003). Furthermore, Tregs have gained a lot of attention for their role and function in cancer (Togashi *et al.*, 2019; Sakaguchi *et al.*, 2020; Dees *et al.*, 2021). Tregs participate to cancer progression by suppressing both $CD4^+$ and $CD8^+$ effector responses and exerting various other immunosuppressive effects on the tumor microenvironment (Li *et al.*, 2020).

Aside from the helper and suppressive roles of $CD4^+$ T cells in the induction and maintenance of $CD8^+$ responses, accumulating evidence points toa more direct role for $CD4^+$ T cells in antitumor immunity, sparking increased interest in the potential exploitation of $CD4^+$ T cells in cancer immunotherapy (Kravtsov *et al.*, 2022). Accordingly, $CD4^+$ T cells represent a unique branch of the adaptive immune system that is crucial in achieving a regulated effective immune response to pathogens and their proper functioning is vital for survival. Through their distinct phenotypes and respective cytokine profile, Th cells modulate the functions of the innate immune cells as well as the members of the adaptive immune system. To execute their wide spectrum of functions, they are required to integrate a large number of signals from the environment and transduce them based on their commitment (Bhattacharyya *et al.*, 2020). Beyond the classical TCR-induced pathways, we are now aware that the maintenance of T cell homeostasis and their effector functions involve also other signalling networks, one of which is autophagy, a conserved catabolic process that eliminates damaged macromolecules and organelles to provide endogenous energy sources to maintain cell homeostasis (Jacquin *et al.*, 2018).

CD8$^+$ cytotoxic T lymphocytes

CTLs are the main cellular effectors of the adaptive immune system, specialised in identifying and killing infected or malignant cells. They originate from naïve CD8$^+$ T cells (Gray *et al.*, 2014), although cytotoxic effectors can develop from CD4$^+$ cells as well (Takeuchi *et al.*, 2017). CTLs are endowed with an arsenal of cytotoxic mediators stored in organelles, called lytic granules, which are released upon target cell recognition, causing homeostatic perturbation and widespread intracellular proteolysis (Stinchcombe *et al.*, 2001). The release of the lytic granule contents must be tightly controlled to prevent non-specific killing of innocent bystander cells and occurs only at the site of contact with the target cell (Podack *et al.*, 1991).

Naïve CD8$^+$ T cells circulate between the lymphatic system and the blood. In peripheral lymphoid organs, TCR binding to specific antigen triggers naïve CD8$^+$ T cell activation, which is orchestrates at a highly specialized cell-to-cell contact, known as the immunological synapse (IS). Naïve CD8$^+$ T cells require 5-8 days after antigen recognition to differentiate into mature CTLs, proliferate and migrate to the affected tissue. During this time window, cytotoxic moieties are produced and stored within maturating cytotoxic granules. Furthermore, CTLs show an increased size and develop a more sophisticated cytoskeletal apparatus, required for the delivery of lytic granules to the IS. Once in the tissue, CTLs recognize and associate with the target cell bearing the specific cognate antigen and, within minutes, a sequence of coordinated events culminates in the killing of the target cell (de la Roche *et al.*, 2016).

The initial events of IS assembly involve the formation of TCR micro-clusters that move centripetally, coalescing at the centre of the IS, which will form the central supramolecular activation cluster (cSMAC) (Potter *et al.*, 2001). The microtubule cytoskeleton plays a prominent part in the delivery of the lethal hit. The assembly of the cSMAC relies on both actin and microtubule cytoskeleton dynamics, as the F-actin flow regulates TCR micro-cluster movement from the periphery toward the centre of the IS (Beemiller *et al.*, 2012), whereas the dynein-mediated transport of TCR complexes along microtubules occurs at the IS centre (Hashimoto-Tane *et al.*, 2011). The actin cytoskeleton contributes also to form

the peripheral SMAC (pSMAC), a ring of adhesion molecules surrounding the cSMAC and whose function is the stabilization of the cell-cell interaction (O'Keefe *et al.*, 2004) (Fig.2).

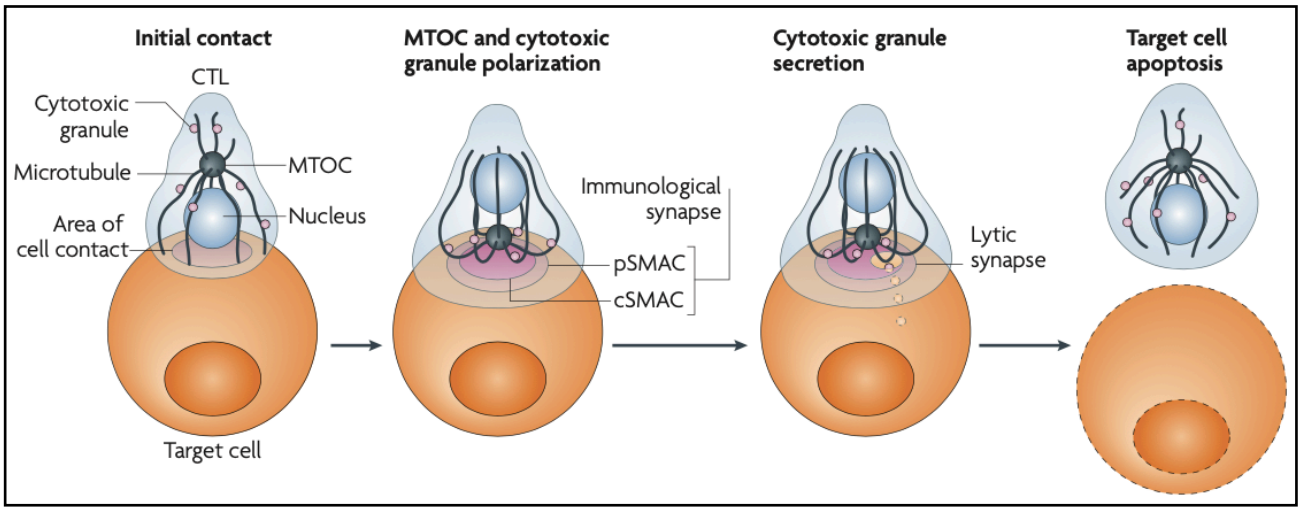

Figure 2| ***The sequential events of lytic synapse formation.***

Following peptide-MHC I recognition on APC, CTLs form a transient conjugate with the target cell. The CTL rapidly translocate its MTOC and the entire microtubule network towards the contact region, where the organization of the lytic synapse is proceeding. The IS is organized into a cSMAC, enriched with signalling molecules and TCRs, surrounded by a peripheral integrin-rich ring, the pSMAC, spatially delimiting the IS. Within minutes of stimulation, LGs move along MTs in a minus-end direction to cluster around the MTOC, to be delivered to the plasma membrane following MTOC translocation beneath the T-APC contact site. LGs release their content into the synaptic cleft, ensuring rapid target cell death by apoptosis. Only a part of the stored LGs is secreted, enabling CTLs to carry out repeated cycles of target cell recognition, killing machinery polarization and target cytolysis (de Saint Basile *et al.*, 2010).

The sustained signalling necessary for T cell activation is based not only on the stability of the T-APC interaction, but also on the vesicle-mediated delivery of TCRs and associated signalling molecules, including LCK and LAT, at the contact area (Soares *et al.*, 2013), highlighting the relevance of vesicular trafficking in CTL-mediated killing (Fig.3a).

Downstream TCR activation, the microtubule organizing centre (MTOC) polarizes towards the IS by means of the PLCγ signalosome-mediated mobilization of intracellular Ca^{2+} (Mullbacher *et al.*, 1999) and DAG accumulation at the IS (Quann *et al.*, 2009), allowing for

the recruitment of PKC isoforms. PKCθ facilitates centrosome translocation by mediating the sub-IS localization of dynein which pulls the centrosome forwards, and nonmuscle myosin II (NMII) to the opposite site of the cell where it pushes the centrosome towards the IS (Liu *et al*., 2013). Furthermore, PKCζ has also been implicated in the polarity of the killing machinery, taking part in centrosome positioning beneath the IS following TCR engagement (Bertrand *et al*., 2013).

Lytic granules are anchored to microtubules and, following their clustering around the centrosome, they migrate towards the IS together with the MTOC (Stinchcombe *et al*., 2006, Beal *et al*., 2009) (Fig.3b). Rapid lytic granule secretion on target cell binding can occur even in the absence of centrosome positioning beneath the IS, which is instead essential for the establishment of a stable conjugate (Bertrand *et al*., 2013), highlighting an alternative mechanism for the release of lytic granules into the synaptic cleft.

As soon as they have converged beneath the cSMAC region, lytic granules detach from the microtubules and use actin-based movement to fill the final short distance to the docking site (Langford, 1995), where cytotoxic granule fusion with the plasma membrane in an actin-depleted region allows for the secretion of the soluble components of the granules (Blott *et al*., 2002).

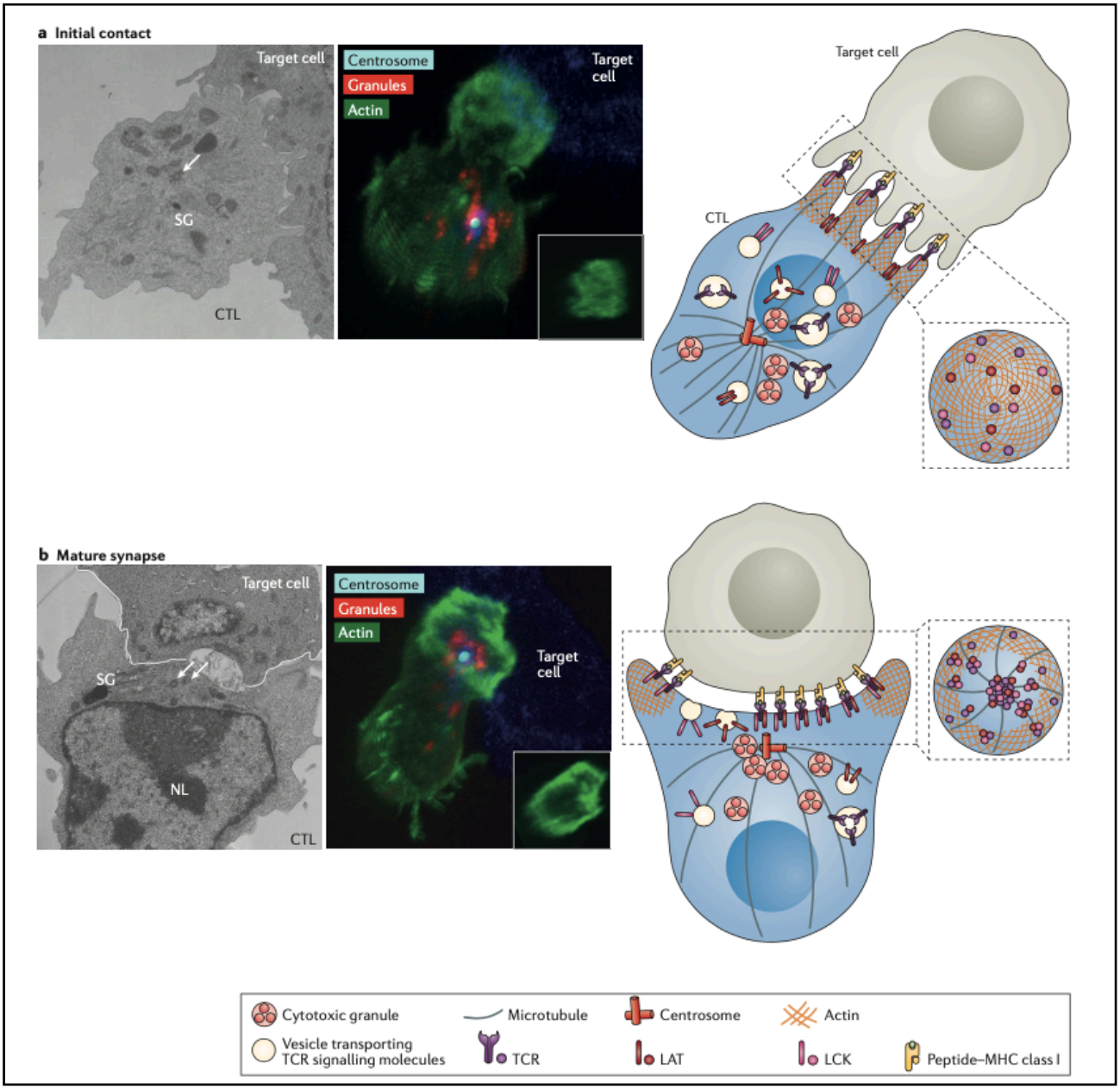

Figure 3| ***Schematic representation of the architecture of early and mature IS.***

(a) Early IS formation. The initial T-APC contact is mediated by actin-rich filopodia of the CTL, with the TCR-pMHC interaction taking place at the tips of these interdigitations. At this early stage, the MTOC is not polarized at the IS and secretory vesicles are dispersed throughout the cytosol. **(b)** Mature IS formation. At a more advanced stage of the IS maturation, the actin is depleted from the centre of the contact site, in correspondence of the cSMAC, and the actin-rich lamellipodia focus on the periphery of the IS. LGs migrate along the microtubules to the centrosome, that in turn translocates to the T-APC contact point beneath the IS membrane. Arrows point centrioles. NL, nucleus; SG, secretory/cytotoxic granules. In the figure are shown electron microscopy images (left), confocal microscopy images (centre) and a schematic representation (right) (de la Roche *et al.*, 2016).

A ciliary view of the immune synapse

The translocation of the centrosome towards the plasma membrane does not only occur during the assembly of the IS. Intriguingly, the IS shares some of its defining features with another signalling structure, the primary cilium (Finetti *et al.*, 2012). At a first glance, the IS and the primary cilium appear to have completely different architectures (Fig.4). Moreover, hematopoietic cells do not have a primary cilium, a fact that may rule out the presence of proteins that localize and function within this organelle. Surprisingly, closer analysis revealed that the IS and the primary cilium share several specialization traits and functions (Cassioli and Baldari, 2019).

The first considerations about the structural similarities between the IS and the primary cilium were done when centrosome docking at the IS was initially observed (Stinchcombe *et al.*, 2006). Additionally, both the Golgi apparatus and the endocytic recycling compartment were shown to polarize towards the plasma membrane, at the site of centrosome positioning, both at the IS and at the base of the cilium (Fig.4). These structural similarities are not limited to microtubule-mediated dynamics, but extend to the actin flow, as cortical actin is reduced in the region where the centrosome attaches to the plasma membrane during the maturation of both the IS and the primary cilium (Ritter *et al.*, 2015), and a peripheral actin ring is delineated thereafter.

The similarities between the IS and the primary cilium can be exploited to identify new components of the pathways orchestrating the assembly of the IS. In this regard, a pioneer work was done investigating the involvement of the intraflagellar transport (IFT) proteins in non-ciliated T cell signalling. The IFT system is essential for the assembly and maintenance of cilia, in which they dynamically control vesicular trafficking (Rosenbaum *et al.*, 2002), but IFT proteins were also found to be expressed in $CD4^+$ T cells (Finetti *et al.*, 2009; Finetti *et al.*, 2014), a cell type that is normally devoid of the primary cilium. In T cells, the ciliary protein IFT20 has been found not only to accumulate at the IS (Finetti *et al.*, 2009) but also to be involved in TCR signalling at multiple levels. Accordingly, cooperating with IFT88, IFT57 and IFT52, IFT20 promotes TCR recycling to the IS downstream of centrosome polarization (Finetti *et al.*, 2009). IFT20 is involved in early

vesicle trafficking by forming a complex with Rab5 and the TCR on early endosomes. In IFT20-depleted T cells, recycling TCRs remain sequestered in $Rab5^+$ endosomes, which fail to polarize at the IS despite a normal translocation of the centrosome, indicating that IFT20 regulates the trafficking of TCRs from early to recycling endosomes (Finetti *et al.*, 2014). Moreover, the loss of IFT20 has been linked to decreased TCR signalling and defective recruitment to the IS of the membrane-associated adaptor protein LAT (Vivar *et al.*, 2016), a crucial component of the scaffold that allows the assembly of the multimolecular complexes mediating the transduction of TCR-induced signals.

The shared features in the architectural framework of the primary cilium and the IS (de la Roche *et al.*, 2016), together with the variety of ciliary proteins taking part in IS assembly in T cells (Cassioli and Baldari, 2019), support the concept that the primary cilium and the IS are homologous structures. Notably, the majority of these ciliary proteins belong to the vesicular trafficking complex, suggesting the existence of a conserved traffic network involved in either cilium-dependent or cilium-independent functions in both ciliated and non-ciliated cells. Consistently, the IFT system was shown to be implicated in the autophagy of both ciliated cells (Pampliega *et al.*, 2013) and non-ciliated T cells (Finetti *et al.*, 2019; Finetti *et al.*, 2021), where this involvement is particularly interesting as it demonstrates that the IFT system controls T cell vesicular dynamics even beyond the IS assembly. IFT20 was recently found to be involved in the delivery of acid hydrolases to the lysosomes by controlling the retrograde transport of the MPR in both ciliated and non-ciliated cells (Finetti *et al.*, 2019), ultimately taking part in the final steps of autophagy. In this regard, the investigation of ciliogenesis-related proteins may lead to rapid progress in the understanding of immune disorders characterized by defective T cell-mediated responses. Hence, the homology between the primary cilium and the IS provides an extraordinary platform of investigation, with relevant implications in both physiological and pathological contexts.

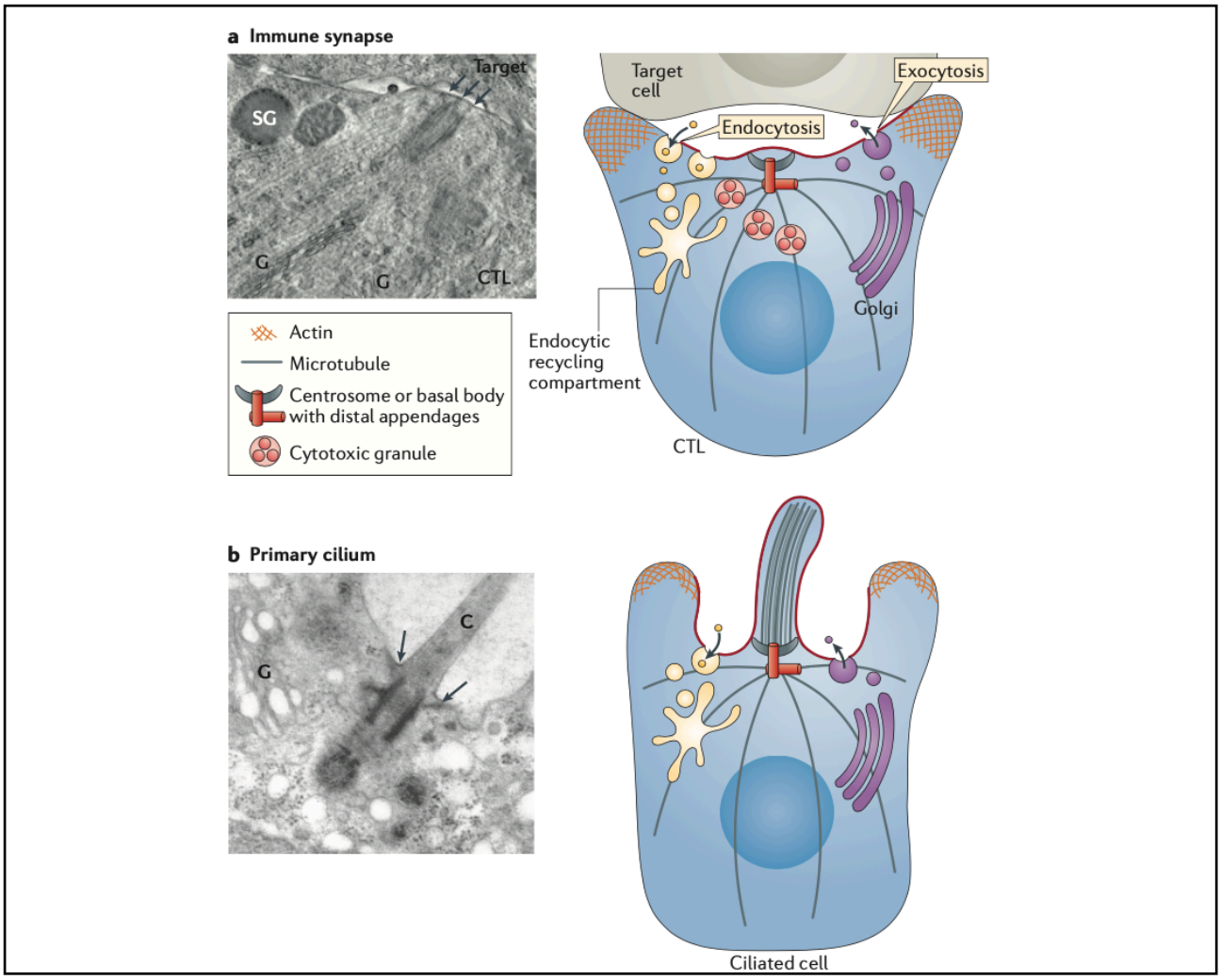

Figure 4| ***Structural similarities among the IS and the primary cilium.***

The IS **(a)** shows striking morphological similarities to the site of primary cilium (C) formation in ciliated cells **(b)**. In both structures, the centrosome is positioned beneath the plasma membrane, where it remains anchored by distal appendages proteins (black arrows) and where marked vesicle trafficking takes place. Other structure polarized beneath the plasma membrane, in both cases, are the Golgi apparatus (G), the endocytic recycling compartment and the secretory granules (SG). The plasma membrane at the IS and at the primary cilium has a characteristic composition compared to the rest of the cell, with a central actin-depleted region (red) and two peripheral actin-rich regions in both structures. Electron microscopy images are reported on the left, schematic representations on right (de la Roche *et al.*, 2016).

AIM OF THE THESIS

T lymphocytes play a central role in antigen-specific immune responses, serving as primary effectors for cell-mediated immunity. Emerging evidence highlighted that T cell maintenance, activation and differentiation depend on autophagy, an evolutionary conserved catabolic pathway that balances sources of energy through the elimination of damaged substrates (Dikic *et al.*, 2018). Autophagy regulation relies on the interplay between ATG proteins and the trafficking machinery that orchestrates the membrane rearrangements necessary for the biogenesis of the autophagosome. The IFT system, first identified for dynamically control vesicular trafficking along the primary cilium, participates in the regulation of autophagy in both ciliated and non-ciliated cells (Pampliega *et al.*, 2013). The first part of the work focuses on the mechanism by which IFT20, an integral component of the IFT system, regulates basal $CD4^+$ T cell autophagy, and in particular on the role of IFT20 in ATG16L1 localization to promote autophagosome biogenesis (Finetti *et al.*, 2021).

The extra-ciliary functions in which IFT proteins are involved in T cells are not limited to autophagy. IFT20 takes part to T cell activation by regulating the assembly of the IS, a specialized membrane structure at the T cell-APC interface (Finetti *et al.*, 2009; Finetti *et al.*, 2011), controlling the intracellular traffic of TCR and LAT (Finetti *et al.*, 2014; Vivar *et al.*, 2016). Furthermore, IFT20 is involved in lysosome biogenesis and function by controlling the MPR-dependent transport of acid hydrolases to lysosomes (Finetti *et al.*, 2019). $CD8^+$ T cells contain specialized secretory lysosomes, named lytic granules, whose release at the IS is pivotal to induce target cell death (Stinchcombe *et al.*, 2001). In the second part of the thesis, we investigated not only the potential outcomes of IFT20 deletion on the biogenesis and functions of CTL lytic granules but also the potential involvement of the CLEAR gene network, the main driver of lysosome biogenesis (Settembre *et al.*, 2013). CTL lethal hit delivery depends not only on the biogenesis of lytic granules but also on their polarized clustering to the IS. The dynamic microtubule cytoskeleton rearrangements allow for centrosome translocation to the IS, facilitating the localized release of lytic granule

contents (Stinchcombe *et al.,* 2006). The recent discovery that the kinase AurA helps T cell activation, as well as the microtubule-driven delivery of CD3ζ-bearing vesicles to the IS (Blas-Rus *et al.*, 2016), opened the way to the third part of the work. We investigated the potential involvement of AurA substrate PLK1, a mitotic regulator controlling centrosome dynamics during cell cycle progression (Joukov *et al.,* 2018), in the assembly of lytic synapse and the microtubule-dependent transport of the lytic granules to the IS.

MATERIALS AND METHODS

Cells, stimulations, and antibodies

$CD8^+$ T cells were isolated from the peripheral blood of anonymous healthy donors obtained from the Siena University Hospital blood bank. The study was approved by the local ethics committee (Siena University Hospital). Informed consent was obtained from blood donors by the physician in charge of the Siena University Hospital blood bank. Samples were anonymized before distribution. Primary $CD8^+$ T cells were isolated by negative selection through the RosetteSep™ Human $CD8^+$ T Cell Enrichment Cocktail (StemCell technologies) and centrifugation over a buoyant density medium (Lympholyte Cell Separation Medium, Euroclone).

Immediately after isolation, $CD8^+$ T cells were resuspended in the culture medium RPMI 1640 with 25 mM Hepes (Sigma-Aldrich), supplemented with 10% BCS (Bovine Calf Serum, Hyclone) inactivated at 56 °C for 30 minutes, 20 U/mL Penicillin (Sigma-Adrich) and 1X non-essential amino acids (MEM non-essential amino acids solution 100X, Gibco). Cell cultures were maintained at 37 °C and 5% CO_2.

Freshly isolated $CD8^+$ T cells were differentiated *in vitro* to CTLs by incubation of 48 h with anti-CD3/CD28 coated magnetic beads (Dynabeads Human T-activator CD3/CD28, Gibco) for cell expansion and activation and 50 U/mL of IL2 (human Interleukin-2, Miltenyi Biotech) for cell proliferation and differentiation. Mature CTLs were employed in the assays from days 5 to 8 of differentiation (Onnis *et al.*, 2022).

The treatment with the inhibitor BI2536 [100 nM in dimethyl sulfoxide (DMSO)] was carried out in serum-free medium for 3 h at 37°C and 5% CO_2 and maintained throughout the whole assays. Control samples were incubated with the same amount of DMSO.

Other cells used were Raji B cells and Jurkat T cells (ATCC, Manassas, VA), maintained in RPMI 1640 supplemented with 7.5% BCS and 20 U/ml Penicillin. TCR triggering in the absence of target cells was performed on 5 μg/ml anti-CD3 antibody (clone OKT3)-coated slides.

All primary commercial antibodies employed in the assays are listed in the Table T1, together with information about the dilutions used for immunoblotting and immunofluorescence. Polyclonal anti-IFT20 antibodies (Pazour *at al.*, 2002) were kindly provided by G. Pazour. Secondary horseradish peroxidase (HRP)-labelled antibodies were purchased from Jackson ImmunoResearch Laboratories and Alexa Fluor 488-, 555- and 647-labeled secondary antibodies from ThermoFisher Scientific.

Generation T cell transfectants and gene editing using CRISP-R/Cas9 technology

Control, IFT20KD and GMAPKD Jurkat T cell lines were generated as previously described (Finetti *et al.*, 2009; Galgano *et al.*, 2017). Jurkat T cells were stably transfected with the pEGFP-N1 plasmid construct encoding full-length IFT20, or a deletion mutant of IFT20 lacking amino acid residues 73-132, which include the coiled-coil domain (ΔCC IFT20), or the respective empty vector. Stably transfected cells were selected in G418-containing medium at the final concentration of 1 mg/ml (Gibco/Thermo Fisher Scientific, MA, United States). Transient transfections on Jurkat T cells mutant were carried out by electroporation using pCMV-EGFP-C3-Rab5a (kindly provided by M. Zerial), pEGFP 2xFYVE (kindly provided by A. De Matteis), pEGFP-N1 IFT20-GFP, or pEGFP-N1 ΔCC IFT20-GFP [1 μg/1 x 10^6 cells in 800 μl of OPTI-MEM (Gibco/Thermo Fisher Scientific, MA, United States)] and analysed 24 h post-transfection.

Specific single guide RNAs (gRNAs) directing the nuclease Cas9 to IFT20 gene (Table T2) were designed using the web-based tool CRISPOR (Haeussler *et al.*, 2016). A gRNA transcription template was prepared by PCR amplification using the PX458 construct as a template and the primers listed in the table T2, and then transcribed in vitro using the HiScribe T7 high yield RNA synthesis kit (NEB). gRNAs were purified by RNA clean & concentration (Zymo Research). Freshly isolated $CD8^+$ T cells were transfected using the Human T cell nucleofector kit and the program V-024 of the Nucleofector II system (Amaxa) for naïve cells, with ribonucleoprotein complexes formed mixing 10 μg of Alt-R Cas9 Nuclease V3 protein (IDT) and 6 μg of gRNA. Cells were then activated with anti-CD3/CD28 magnetic beads in AIM V culture medium (ThermoFisher Scientific)

supplemented with 10% BCS and 500 U/ml of human IL-2 for 48 h. Once removed the beads, cells were expanded in AIM V 10% BCS with 50 U/ml human IL-2. Transfected blasts were tested for gene editing by immunoblotting 5 days after isolation and employed for the assays from days 5 to 7.

CTLs were transiently transfected with the pEGFP-N1 plasmid encoding the TFEB-GFP fusion protein (kindly provided by D. Medina) or the empty vector. Briefly, CTLs at 5 days of differentiation were resuspended in 800 μL of cold transfection medium (Opti-MEM, Gibco) and 1 μg/1 x 10^6 cells of pEGFP-N1 or pEGFP-N1-TFEB plasmids. The cell suspension was incubated at 4 °C for 5 minutes and the transfection was carried out by electroporation. Transfected cells were gently resuspended in the culture medium with 500 U/ml IL2 and analysed 48 hours post transfection.

Cloning and purification of recombinant proteins

GFP- and GST-tagged mutants of IFT20 were generated by cloning the sequences that encode the IFT20 N-terminus lacking the coiled-coil domain (ΔCC-IFT20, aa 1-73), the IFT20 C-terminus including the coiled-coil domain (CC-IFT20, aa 74-132), and the full-length protein (IFT20, aa 1-132) in-frame with the tags into the pEGFP-N1 and pGEX-6P-2 vectors (Addgene). The sequences were amplified by PCR using the primers listed in Table T2. The 5'- ends of the primers were modified to add compatible restriction sites (*XhoI* and *KpnI* for pEGFP-N1, *EcoRI* and *XhoI* for pGEX-6P-2) and extra base pairs that ensure efficient DNA cleavage by restriction enzymes.

The recombinant GST fusion proteins were affinity purified on GSH-Sepharose (GE Healthcare, Italy) from bacterial cultures incubated with 0.25 mM isopropyl-β-D-thiogalactopyranoside (Sigma-Aldrich) overnight at room temperature and lysed in B-PER Complete Bacterial Protein Extraction Reagent (Thermo Fisher Scientific, MA, United States) according to the manufacturers' instructions.

Immunoprecipitation, *in vitro* binding, cell lysis and immunoblotting

Immunoprecipitation experiments were performed as previously described (Finetti *et al.*, 2020). Briefly, 5 × 10^7 cells/sample were lysed in 0.5% (v/v) Triton X-100 in 20 mM Tris–HCl (pH 8), 150 mM NaCl in the presence of Protease inhibitor Cocktail Set III (Calbiochem®, Merck) and the phosphatase inhibitor sodium orthovanadate (Sigma-Aldrich). Post-nuclear supernatants (2 mg/sample) were immunoprecipitated for 2 h at 4°C with gentle agitation using 2 µg of rabbit anti-IFT20 antibody (Proteintech, United Kingdom), anti-ATG16L1 antibody (Cell Signaling) or mouse anti-BECLIN1 mAb (Santa Cruz), and protein A-Sepharose (PAS, 3 mg/sample, GE Healthcare, Italy), after a preclearing step on PAS (1 h, 3 mg/sample). Subsequently, all samples were washed 4X with 1 ml 0.5% Triton X-100 lysis buffer, resuspended in 15 µl Laemmli buffer (Life Technologies/Thermo Fisher Scientific, MA, United States), boiled for 5 min and then subjected to SDS-PAGE.

In vitro-binding assays were carried out using recombinant GST, IFT20-GST, ΔCC IFT20-GST, or CC IFT20-GST on GSH- Sepharose precleared post-nuclear supernatants from 5 × 10^7 cells/sample lysed in 0.5% Triton X-100 in the presence of protease and phosphatase inhibitors as described. The binding reaction was performed for 2 h at 4°C with gentle agitation. Samples were washed 4X with 1 ml 0.5% Triton X-100 lysis buffer in the presence of protease and phosphatase inhibitors, resuspended in 15 µl Laemmli buffer, boiled for 5 min and subjected to SDS-PAGE.

Cells (2x10^6/sample) were lysed in 1%(v/v) Triton-X100 in the presence of protease and phosphatase inhibitors for 5 min on ice. Protein extracts from post-nuclear supernatants were quantified with a Quantum protein assay kit (Euroclone) and denaturated in 4x Bolt LDS sample buffer (Invitrogen) supplemented with 10x Bolt sample reducing buffer (Invitrogen) for 5 min at 100°C. Proteins (10 µg) were subjected to SDS-Page on Bolt Bis-Tris mini protein gels (Invitrogen) and transferred to nitrocellulose (GE HealthCare) under wet conditions. Blocking was performed in 5% non-fat dry milk in PBS containing 0.2% Tween 20 (Sigma-Adrich). Membranes were incubated in primary antibodies for 1-3 h at room temperature (20-25°C) or overnight at 4°C, followed by incubation in 20 ng/ml HRP-

conjugated secondary antibodies (Jackson ImmunoResearch Laboratories) for 45 min at room temperature. Secondary antibodies were detected using SuperSignal west pico plus chemiluminescent substrate (Life Technologies). For quantification, immunoblot membranes were scanned using a laser densitometer (DuoScan T2500, Agfa) or Alliance Q9-Atom chemiluminescence imaging system (Uvitec), and densitometric levels were measured using ImageJ software (National Institutes of Health, USA).

Immunofluorescence and image analysis

Samples were seeded on to poly-L-lysine (Merck)-coated slides (ThermoFisher Scientific) and fixed in either methanol at -20°C for 10 min or with 4% paraformaldehyde/PBS at room temperature for 15 min. Alternatively, for LC3B labelling, Jurkat cells were incubated 10 min in 50 mM NH_4Cl after fixation in 4% paraformaldehyde for 10 min at room temperature, and then permeabilized in methanol for 10 min at -20°C. After washing with PBS, samples were stained with primary antibodies at 4°C overnight and then incubated at room temperature for 45 min with Alexa fluor 488- and 555-labeled secondary antibodies and mounted with 90% glycerol/PBS.

Confocal microscopy was carried out on a Zeiss LSM700 microscope (Carl Zeiss, Jena, Germany) using a 63x/1.40 oil immersion objective or a spinning disk confocal and super-resolution microscope (CSU-W1-SoRA Nikon), with 60x/1.49 oil objective. Detectors were set to detect the optimal signal below the saturation limits.

Co-localization analyses were performed on a medial optical section of single cells using ImageJ and the JACoP plugin to calculate Mander's coefficient M1, which indicates the proportion of the green signal coincident with a signal in the red channel over its total intensity, and M2, which is defined conversely for red (Manders *et al.*, 1992). Mander's coefficients range from 0 to 1, corresponding to non-overlapping images and 100% co-localization between both images, respectively. The ATG16L1 dispersion was quantified by measuring fluorescence intensity in concentric regions using ImageJ. Circular regions were centred on the point of ATG16L1 maximal intensity and designed proportionally to the cell size (inner circle, middle ring, and outer ring diameters, corresponding to 1/9, 1/4.5, and

1/2.25 of cell diameter, respectively) (Progida *et al.*, 2010). Alternatively, ATG16L1 dispersion was measured using ImageJ by calculating the distance of ATG16L1$^+$ dots (identified using the same fluorescence threshold in control and IFT20KD cells in each experiment) from the centrosome (identified by pericentrin staining). The number and area of LC3$^+$, Lamp1$^+$, and granzyme B$^+$ dots were determined by immunofluorescence. The area of vesicles was measured by manual gating using the ImageJ software.

Autophagic flux

To analyse the autophagic flux, 1×10^6 cells/sample were incubated in RPMI 1640 added with 7.5% BCS for 30 min at 37°C in the presence or absence of 40 μM chloroquine. Subsequently, cells were harvested and lysed in 1% Triton X-100 in 20 mM Tris–HCl pH 8.0, 150 mM NaCl in the presence of protease and phosphatase inhibitors and processed for immunoblotting with anti-LC3B antibodies. Autophagy flux was calculated as the difference in LC3-II levels, normalized to actin, between chloroquine-treated and untreated cells. Alternatively, following the incubation with RPMI 1640 supplemented with 7.5% BCS for 30 min at 37°C in the presence or absence of 40 μM chloroquine, cells were allowed to adhere to poly-L-lysine-coated wells. Subsequently, the samples were fixed, permeabilized and stained as described above for immunofluorescence analysis of the number of LC3$^+$ dots.

Membrane Fractionation

Cytosolic and membrane fractions were purified as previously described (Finetti *et al.*, 2014). Jurkat cells (3×10^7/sample) were resuspended in 1 ml homogenization medium (0.25 M sucrose, 1 mM EDTA, 10 mM Tris-HCl pH 7.4) in the presence of protease and phosphatase inhibitors. The samples were homogenized by 10 pestle strokes through Dounce homogenization (tight Dounce homogenizer, Wheaton, United States) and 10 passages through a 26-gauge syringe needle. The homogenate was centrifuged at 3,000 × g for 5 min at 4°C to remove nuclei and the supernatant was centrifuged at 65,000 × g for 1 h at 4°C. The supernatant (cytosolic fraction) was collected, while the pellet (membrane

fraction) was lysed in homogenization buffer containing protease and phosphatase inhibitors with 0.5% Triton and centrifuged at 16,100 × g for 20 min at 4°C to eliminate insoluble material. The same quantities of membrane protein-enriched supernatant and cytosolic fraction were analysed by SDS-PAGE.

Real-time calcein release-based killing assay

Raji B cells were loaded with 500 nM calcein-AM (Life Technology) in AIM V medium (ThermoFisher Scientific) with 10 mM Hepes at room temperature for 15 min, washed and plated into 96-well black plates with clear bottoms (BD Falcon). IFT20KO or BI2536-treated CTLs and respective controls were added at different ratios to $0.5x10^4$ settled target cells per well to measure killing at 37°C 5% CO_2. Triton X-100 (1%) was added to target cells alone to calculate maximal target cell lysis as control. Target cell lysis was measured every 10 min for 4 h. The decreased calcein fluorescence in target cells due to cell lysis was measured at 485 nm excitation wavelength and 528 nm emission wavelength in the bottom reading mode by using a Synergy HTX multi-mode plate reader (BioTek). The fluorescence for the experimental condition was adjusted by the parameter γ according to the live target cell control fluorescence. The γ value was measured at time zero: $\gamma = F_{live}(0)/F_{exp}(0)$. The cytotoxicity was calculated according to the loss of calcein fluorescence in target cells by using the equation: % target cell lysis = $(F_{live} - \gamma \times F_{exp})/(F_{live}-F_{lyse}) \times 100$, where F_{live} is the fluorescence of target cells alone, F_{exp} are CTL-APC samples and F_{lyse} is the maximal target cell lysis. All the experiments were performed in duplicates and averaged to obtain one dataset. The maximal CTL-induced target cell killing was assigned to the higher CTL-APC ratio, on which was based the relative values for the other samples (Chang *et al.*, 2017).

Conjugate formation and image analysis

Conjugates between $CD8^+$ T cells and superantigen-pulsed Raji B cells were carried out as previously described (Cassioli *et al.*, 2021). Raji B cells (used as APCs) were loaded with 10 μg/ml of a mix of Staphylococcal Enterotoxins A (SEA), B (SEB) and E (SEE) (Toxin Technologies) for 2 h at 37°C and labelled with 10 μM Cell Tracker Blue for the last 20 min

of the incubation with superantigens (SAgs). Antigen-free conjugates of CTLs with unpulsed Raji B cells were used as negative controls.

SAg-loaded or unloaded Raji B cells were mixed with CTLs (1:1) to allow conjugate formation at 37°C for the indicated time points. Samples were then seeded on poly-L-lysine coated slides and processed as indicated in the immunofluorescence section.

Once acquired the images of CTLs with either SAg-loaded or unloaded Raji B cells, relative distances of the centrosome from the contact site CTL:APC was measured using ImageJ. Polarization of CD3ζ, granzyme B^+ lytic granules and PLK1, and the translocation of the centrosome to the IS were based on the presence of the staining solely on the CTL:APC contact site and was expressed as the percentage of conjugates with synaptic staining *versus* the total number of conjugates analysed. The recruitment index was calculated as the ratio of CD3ζ or pTyr fluorescence intensity at the synaptic area, which is manually defined at the CTL:APC contact site *versus* the entire cell, using ImageJ. Values above 1 indicate an accumulation of the marker at the IS area compared to the total cell, whereas values below 1 indicate a depletion of the marker at the IS area compared to the entire cell.

RNA purification and RT-qPCR

RNA samples were obtained from CTLs using the RNeasy plus mini kit (Qiagen), reverse transcribed to single-strand cDNA using the iScript cDNA synthesis kit (Bio-Rad) and analysed by Real-time quantitative PCR (RT-qPCR) on 96-well optical PCR plates (Sarstedt) using the SsoFast EvaGreen supermix (Bio-Rad) and specific primers for human transcripts listed in Table T2. The quantity of the transcripts of interest was determined using the ΔΔCt method and normalized to the house-keeping gene 18S.

Statistics and reproducibility

Each experiment is the result of at least 3 independent repetitions. The exact number of cells analysed is specified in figure legends. Statistical analyses were performed using Prism software (GraphPad Software). Pairwise or multiple comparisons of values with normal distribution were carried out using Student's t-test (unpaired), one-sample t-test

(theoretical mean=1) and one-way ANOVA, whereas values without Gaussian distribution were analysed with Mann-Whitney test or Kruskal-Wallis test. Statistical significance was defined as: ****P≤0.0001; ***P≤0.001; **P≤0.01; *P≤0.05; n.s., not significant.

Table T1. List of the primary antibodies used in this work

Antibody (anti-)	Host species	Company	Dilution WB	Dilution IF
Actin	mouse	Millipore	1:10,000	-
ATG5	mouse	Santa Cruz	1:500	-
ATG16L1	mouse	Santa Cruz	1:500	1:50
ATG16L1	rabbit	Cell signaling	1:500	-
BECLIN1	mouse	Santa Cruz	1:500	-
BECLIN1	rabbit	Cell signaling	1:500	1:50
CD3ζ	mouse	Santa Cruz	-	1:200
pErk1/2 (T202/Y204)	rabbit	Cell signaling	1:1,000	-
ERK2	Rabbit	Santa Cruz	1:500	-
Giantin	rabbit	abcam	-	1:200
GFP	rabbit	Life Technologies	1:1,000	1:200
GMAP210	mouse	BD Biosciences	1:250	-
GM130	rabbit	BD Biosciences	1:500	1:100
Granzyme B	rabbit	Cell signaling	1:2,000	-
Granzyme B-488	mouse	Bio Legend	-	1:20
IFT20	rabbit	G.J. Pazour*	1:500	-
Lamp1	mouse	Millipore	-	1:400
Lamp1-647	-	Bio Legend	-	1:150
pLat (Y191)	rabbit	Cell signaling	1:1,000	-
LC3B	rabbit	Cell signaling	1:500	1:200
M6PR	rabbit	abcam	-	1:400
PCM1	mouse	Santa Cruz	-	1:300

Pericentrin	rabbit	abcam	-	1:200
PLK1	rabbit	Biotechne	1:500	1:300
pPLK1 (T210)	rabbit	abcam	1:1,000	1:300
Rab5	mouse	BD	1:2,000	1:50
Rab5	rabbit	Cell signaling	-	1:200
Thrombospondin1	mouse	Invitrogen	1:500	-
tgn38	mouse	Santa Cruz	-	1:300
pTyrosine (Y1000)	rabbit	Cell signaling	-	1:100
β-tubulin	rabbit	Cell signaling	-	1:100
γ-tubulin	mouse	Sigma-Aldrich	-	1:200

*Program in Molecular Medicine, University of Massachusetts Medical School, Worchester, MA 01605, USA.

Table T2. List of the primers used in this work

Oligo name	Sequence	Description
Common reverse primer	AGCACCGACTCGGTGCCACT	gRNA production
GFP gRNA	ttaatacgactcactataggGGGCGAGGAGC TGTTCACCGttttagagctagaaatagc	gRNA production
IFT20 gRNA	ttaatacgactcactataggGAGTGTAGCC CTGCTTCACCCGttttagagctagaaatagc	gRNA production
IFT20 gRNA	GAGTGTAGCCCTGCTTCACCCG	gRNA sequence cloned into pSpCas9(BB) -2A-GFP plasmid
ΔCC mutant-GFP XhoI fw	CCGCTCGAGATGGCCAAGGACATCCTG	PCR primer for IFT20 mutants
ΔCC mutant-GFP KpnI rev	CGGGGTACCCCGATGGCCTTCATCTTT	PCR primer for IFT20 mutants
CC mutant-GFP XhoI fw	CCGCTCGAGATGGGTGCTCGGAACT	PCR primer for IFT20 mutants
CC mutant-GFP KpnI rev	CGGGGTACCCCTTTCTGAAAAATAAATTGGTC	PCR primer for IFT20 mutants
GST-ΔCC mutant EcoRI fw	CCGGAATTCCGATGGCCAAGGACAT	PCR primer for IFT20 mutants
GST-ΔCC mutant XhoI rev	CCGCTCGAGTCAGATGGCCTTCATCTTTTC	PCR primer for IFT20 mutants

GST-CC mutant EcoRI fw	CCGGAATTCCGATGGGTGCTCGGAA	PCR primer for IFT20 mutants
GST-CC mutant XhoI rev	CCGCTCGAGTCATTTCTGAAAAATAAATTGGTCAA	PCR primer for IFT20 mutants
GST-IFT20 EcoRI fw	CCGGAATTCCGATGGCCAAGGACAT	PCR primer for IFT20 mutants
Granzyme A fw	AACCAGGAACCATGTGCCAA	qPCR primer
Granzyme A rev	GGCTTCCAGAATCTCCATTGC	qPCR primer
Granzyme B fw	TCAAAGAACAGGAGCCGAC	qPCR primer
Granzyme B rev	TTGGCCTTTCTCTCCAGCTG	qPCR primer
Perforin-1 fw	CCTGCAGTCACAGCTACACA	qPCR primer
Perforin-1 rev	GGGGCTCCAGTTAAGGCAA	qPCR primer
Thrombospondin-1 fw	GCAAGTCACCCAGTCCTACT	qPCR primer
Thrombospondin-1 rev	AATGAACCCGTCTTTGGCC	qPCR primer
Serglycin fw	GACGAGAATCCAGGACTTGAA	qPCR primer
Serglycin rev	GGGCAGATTCCTGTCAAGAG	qPCR primer
Granulysin fw	GGATAAGCCCACCCAGAGAAG	qPCR primer
Granulysin rev	ACAGATCTGCTGGGCAGTTT	qPCR primer
TFEB fw	GGAGTACCTGTCCGAGACCT	qPCR primer
TFEB rev	GGGCTATTGGGAGCACTGTT	qPCR primer
Lamp-1 fw	CCGCGGTGTCTTCTTCGTG	qPCR primer
Lamp-1 rev	TAGAGACAGCGGGCGTTACC	qPCR primer
Cathepsin D fw	CCAGTGCTTCACAGTCGTCT	qPCR primer

Cathepsin D rev	CACGTAGGTGCTGGACTTGT	qPCR primer
18S fw	CGCCGCTAGAGGTGAAATT	qPCR primer
18S rev	CTTGGCAAATGCTTTCGC	qPCR primer

RESULTS

1. Basal T cell autophagy is regulated by the ciliary protein IFT20

1.1 Autophagy

Autophagy is a highly conserved catabolic process that contributes to the maintenance of the energetic balance of the cell through the turnover of proteins and organelles (Fig.5) (Dikic *et al.*, 2018). The autophagic flux refers to a complete catabolic process that ensures the degradation and recycling of intracellular components in the cytosol (Merkley *et al.*, 2018). The induction of autophagy promotes the recruitment of proteins and lipids from different intracellular membrane sources to initiate the formation of the autophagosomes (Hamasaki *et al.*, 2013), double-membrane vesicles that sequester cytoplasmic material and deliver it through vesicular fusion to lysosomes for degradation (Yang *et al.*, 2010).

Together with the ubiquitin-proteasome pathway, autophagy constitutes one of the main cellular processes for protein degradation. Three main forms of autophagy have been described in mammalian cells, representing the different mechanisms through which the substrate reaches the lysosome for degradation. Microautophagy is characterized by invaginations of lysosomal membranes that capture cargo to be degraded by lysosomal hydrolases (Kocaturk *et al.*, 2019). Chaperone-mediated autophagy is achieved by the heat shock-cognate protein of 70 kDa (Hsc70)-mediated recognition of KFERQ-motif-bearing soluble proteins, that allows the interaction of the target with the lysosome-associated protein type 2A (LAMP-2A) on the lysosomal membrane. Substrate binding to LAMP-2A induces the assembly of multimers of this protein, to form a complex that translocates the cargo across the lysosomal membrane to be degraded (Yang *et al.*, 2019). The presence of the consensus sequence is mandatory for cargo selection, making this process highly specific. Macroautophagy is the third form of autophagy, characterized by the sequestration of cytoplasmic material by a double-membrane structure, called phagophore, which expands around the cargo to form a sealed, double-membrane vesicle named autophagosome, that will eventually fuse with the lysosome for degradation. Among the

three types, macroautophagy is the most prevalent pathway used by cells to remove the damaged cellular organelles and other related debris, so that the term "autophagy" generally indicates macroautophagy (Dowling *et al.*, 2018).

The mechanism of autophagy can be conceptualized in a series of steps, each one being crucial for the autophagy process to take place successfully. Disruption of either early or later stages would equally affect the entire mechanism (Ravananan *et al.*, 2017).

Signals that activate the autophagic process typically originate from stress-inducing conditions, including starvation, hypoxia, oxidative stress, protein aggregation, ER stress and others. These signalling pathways can activate the Unc-51-like kinase 1 (ULK1) complex, consisting of ULK1, autophagy-related protein 13 (ATG13), RB1-inducible coiled-coil protein 1 (FIP200) and ATG101 (Parzych *et al.*, 2014). This complex triggers the nucleation of the phagophore by phosphorylating components of the class III PI3K (PI3KC3) complex I, composed of class III PI3K, vacuolar protein sorting 34 (VPS34), BECLIN1, ATG14, activating molecule in BECLIN 1-regulated autophagy protein 1 (AMBRA1) and general vesicular transport factor (p115), which in turn activates local phosphatidylinositol-3-phosphate (PI3P) production at the omegasome, a sub-domain of the ER (Yu *et al.*, 2018). PI3P recruits in turn a member of the PI3P effector proteins WD repeat domain phosphoinositide-interacting protein family (WIPI2) and the zinc-finger FYVE domain-containing protein 1 (DFCP1) to the omegasome via interaction with their PI3P-binding domains. WIPI2 was recently shown to recruit the ATG12-ATG5/ATG16L1 complex through direct interaction with ATG16L1. This complex enhances the ATG3-mediated conjugation of ATG8 family proteins (ATG8s), including microtubule-associated protein light chain 3 (LC3) proteins and γ-aminobutyric acid receptor-associated proteins (GABARAPs) to membrane-resident phosphatidylethanolamine (PE), thus forming the membrane-bound, lipidated forms; in this conjugation reaction, LC3-I is converted into LC3-II, the characteristic signature for autophagic membranes (Dikic *et al.*, 2018). ATG8 attracts the components of the autophagic machinery that contain an LC3-interacting region (LIR) and are also required for the elongation and closure steps of the phagophore membrane. Moreover, in selective autophagy, LC3 is critically involved in the sequestration

of specifically labelled cargo into autophagosomes via LIR-containing cargo receptors. Several cellular membranes, including the plasma membrane, mitochondria, recycling endosomes and Golgi complex, contribute to the elongation of the autophagosomal membrane by donating membrane material. Sealing of the autophagosomal membrane gives rise to a double-layered vesicle, the autophagosome, which matures and finally fuses with the lysosome. Acidic hydrolases in the lysosome degrade the autophagic cargo, with nutrients recycled back to the cytoplasm (Ravanan *et al.*, 2017).

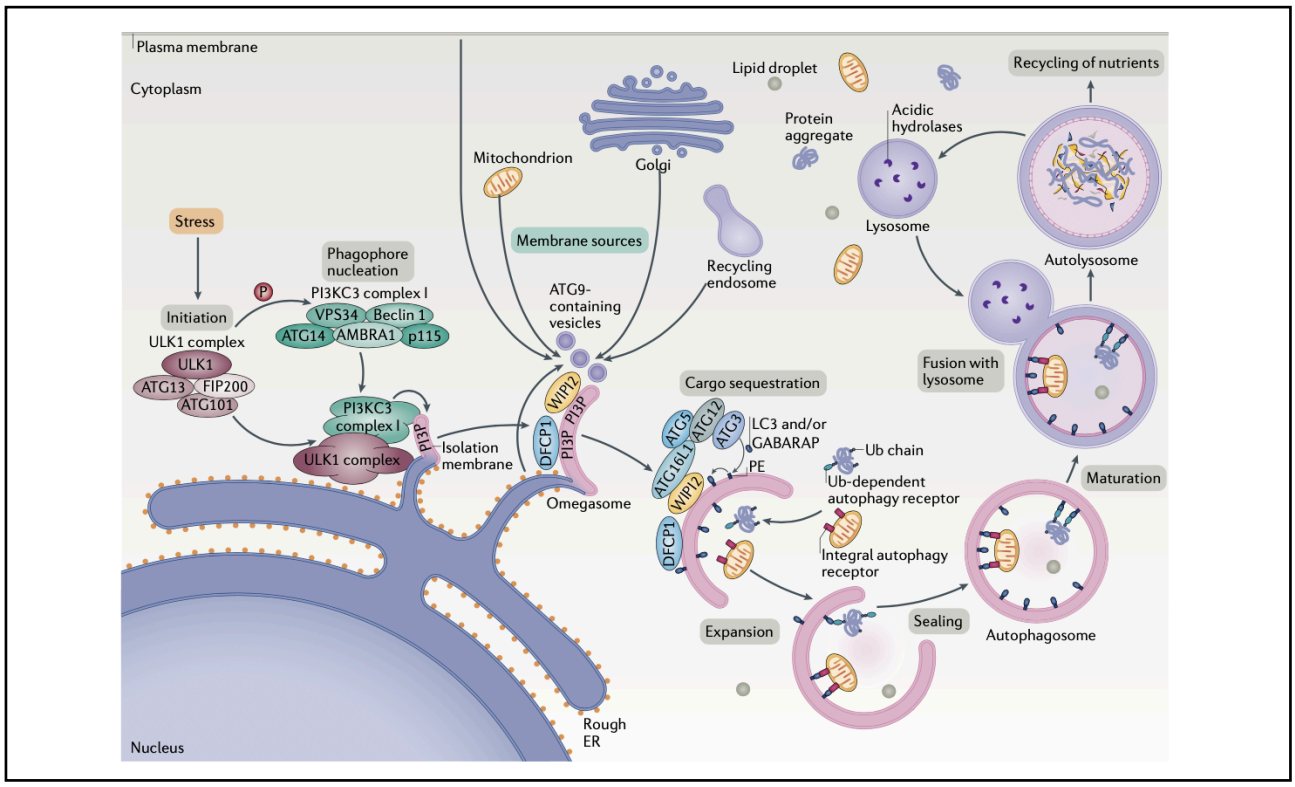

Figure 5| ***The autophagy process at a glance.***

Several condition of stress can trigger the initiation of autophagy. The activated ULK1 complex phosphorylates components of the PI3KC3 complex I and hence mediates the nucleation of the phagophore. The PI3KC3 complex activity allows for the generation of PI3P at a characteristic ER structure called omegasome, where other autophagy-related proteins are recruited, including the ATG5-ATG12/ATG16L1 complex. At this level, LC3-I is converted to LC3-II. Several cellular compartments, including the plasma membrane, mitochondria, recycling endosomes and Golgi apparatus, donate membrane material for the elongation of the auophagosome. Following the sealing of this structure, the mature autophagosome fuses with the lysosome, where acid hydrolases degrade the cargo and nutrients can be recycled (Dikic *et al.*, 2018).

The initiation of autophagy is primarily regulated through two energy sensors, the adenosine monophosphate–activated kinase (AMPK) and the mammalian target of rapamycin (mTOR) (Noda *et al*., 2015). Under steady state conditions, the major source of amino acids for cellular functions comes from the proteasome-mediated degradation of proteins. During starvation, however, autophagy plays a prominent role in amino acid generation (Wang *et al*., 2017). The increase in the autophagic activity occurs through the inhibition of the serine/threonine protein kinase mTOR, a part of the mTOR complex 1 (mTORC1), acting as negative regulator of autophagy. Under nutrient-rich conditions, mTORC1 is activated and suppresses the ULK1 complex, preventing autophagy activation (Kim *et al*., 2015). In contrast, the serine/threonine kinase AMPK is a positive regulator of autophagy. AMPK is rapidly activated by the high AMP/ATP ratio caused by nutrient deprivation and contributes to the energy balance of the cell by inhibiting activities that use energy and increasing those that produce energy, including autophagy (Li *et al*., 2019). In response to low energy levels, AMPK activates ULK1 by phosphorylation. Activated ULK1 itself phosphorylates BECLIN1, thereby activating the VPS34–BECLIN1 complex and promoting the induction of autophagy (Wang *et al*., 2017).

During the autophagy process, selected cytoplasmic materials are enclosed by an isolation membrane that elongates to form an autophagosome and eventually fuses with the lysosome to degrade the enclosed contents. This dynamic transport process is orchestrated by the Rab proteins, small GTPases belonging to the Ras-like GTPase superfamily (Ao *et al*., 2014). Rabs are considered markers of membrane identity and function as central organizers of vesicle-mediated transport between organelles.

Rab proteins switch among an active GTP-bound state (Rab-GTP) and an inactive GDP-bound form (Rab-GDP). This exchange can be performed in the presence of two regulatory proteins, the guanine nucleotide exchange factor (GEF), that catalyzes the dissociation of the GDP to allow the binding of GTP, and GTPase activating protein (GAP), that facilitates the hydrolysis of GTP to GDP (Langemeyer *et al*., 2018). Rab proteins use this guanine nucleotide-dependent switch mechanism to regulate each of the four major steps in membrane traffic: vesicle budding, delivery, tethering and fusion. These different processes

are carried out by several effector molecules that bind to specific Rabs in their GTP-bound state (Amaya *et al.*, 2015). Rab cascades seem to confer directionality to membrane traffic and couple each stage of transport with the next one along the pathway.

Early endosomes are characterized by the presence of the small GTPase Rab5 on the membrane, responsible for the recruitment of the PI3KC3-BECLIN1 complex (Skjeldal *et al.*, 2021). Another protein involved is Rab11, responsible for the membrane trafficking from the recycling endosome to the autophagosome (Lamb *et al.*, 2016). An additional pivotal protein in the initial phases of the autophagosome formation is Rab33, a Golgi-resident small GTPase first identified to be involved in retrograde traffic from Golgi to ER (Zheng *et al.*, 1998). The isoform Rab33B directly interacts with ATG16L1 in a GTP-dependent manner, modulating the recruitment of the ATG5-ATG12/ATG16L1 at Golgi (Itoh *et al.*, 2008). The progression from early to late endosomes is tightly regulated through the transition from $Rab5^+$ to $Rab7^+$ endosomes, that allows the traffic of the autophagosome towards the lysosomal compartment (Wen *et al.*, 2017), and therefore drives the final stages of the autophagy.

The role of autophagy in T lymphocytes

Autophagy is a quality control and pro-survival mechanism employed by T cells (Li *et al.*, 2012) and affecting multiple aspects of the immune response.

A comprehensive characterization of the mechanisms that drive autophagy, as well as the development of pioneer tools to study them, have led to the identification of new tissue-specific functions for the autophagic process. Several studies demonstrated the involvement of autophagy in many key functions of the immune system, including pathogen clearance (Kishi-Itakura *et al.*, 2020), antigen presentation (Oral *et al.*, 2017), regulation of cell activation and differentiation (Bronietzki *et al.*, 2015).

Mounting evidence has implicated autophagy and cellular metabolism in different stages of T lymphocyte differentiation, activation, and maturation. Autophagy participates in thymocyte development by sustaining the survival of double negative thymocytes and their transition to the double positive stage (Nedjic *et al.*, 2008) and regulates both positive and

negative selection via the MHC II loading pathway in thymic epithelial cells (Kasai *et al.*, 2009).

In the periphery, T cell activation and proliferation are fine-tuned by selective autophagy (Reggiori *et al.*, 2012; Zaffagnini *et al.*, 2016). Early after the first observation of autophagosomes in T lymphocytes (Pua *et al.*, 2007), autophagy has not only been shown to be activated upon TCR engagement, but also to modulate T cell proliferation in responses to this signal (Watanabe *et al.*, 2014). Selective autophagy has been recently shown to regulate specific signalling pathways activated by TCR engagement, supporting the idea that autophagy regulates peripheral T cell activation following TCR stimulation (Botbol *et al.*, 2016). Consistently, autophagy-deficient T cells fail to differentiate because of reduced numbers of active mitochondria upon T cell activation (Yang *et al.*, 2021). The regulation of autophagy also participates in helper T cell survival (Kovacs *et al.*, 2012; Kabat *et al.*, 2016; Wei *et al.*, 2016) and cytotoxic T cell effector functions (Puleston *et al.*, 2014). The autophagy pathway is dynamically regulated during the T cell response and seems to have a role in the metabolic homeostasis of effector T cells also during their transition to memory cells. Autophagy was found to decrease in activated proliferating effector T cells followed by upregulation when the cells stop dividing. Deletion of the gene encoding autophagy-related molecules has indeed little to no effect on the proliferation and function of effector cells, which instead showed survival defects that resulted in compromised formation of memory T cells (Xu *et al.*, 2014).

The intraflagellar transport (IFT) system in autophagy

The autophagy process is fine-tuned by a plethora of regulators and effectors. Among these is the intraflagellar transport (IFT) system (Prevo *et al.*, 2017), a multimolecular protein complex first described as promoter of primary cilium assembly and maintenance (Rosenbaum *et al.*, 2002). The primary cilium is a non-motile signalling organelle that grows in a specific region of the plasma membrane, where it detects changes in the surrounding environment and in response activates signalling pathways. It consists of an axoneme of nine doublets of microtubules that extend at the point of attachment to the cell

from the basal body, composed of microtubule triplets (Satir *et al.*, 2010). Cargo trafficking along the ciliary axoneme allows for the translation of environmental signals into a cellular response (Griffiths *et al.*, 2010) and is maintained by motor proteins and the two large multiprotein complexes IFT-A and -B (Tashner *et al.*, 2012). More in detail, while the anterograde IFT-B complex mediates the transport of molecules from the base to the tip of the cilium by interacting with kinesin, the retrograde IFT-A complex interacts with dynein to regulate the retrograde transport to the basal body (Tashner *et al.*, 2016). One of the subunits belonging to these complexes, namely IFT20, is associated also to other cellular compartments, such as the Golgi, from where it facilitates the mobilization of specific cargo to the basal body and cilium for ciliogenesis and ciliary signalling (Follit *et al.*, 2009).

The activity of the IFT system is not restricted to the primary cilium. An interesting link that has emerged in the last few years implicates autophagy in the growth of the primary cilium. In response to serum deprivation, many types of cultured cells undergo not only primary cilia growth (Takahashi *et al.*, 2018) but also autophagy (Onodera *et al.*, 2005) as adaptive mechanisms. Moreover, ATG proteins localize at the ciliary base and ATG16L1 is actively recruited to this location, suggesting that the sensing of nutrient deficiency and the activation of signalling from the primary cilium could initiate a cilia-mediated autophagic program. The temporal coincidence of the formation of both primary cilium and autophagosome at the early stages of nutrient deprivation may thus serve as a reciprocal regulatory brake for each of these processes (Pampliega *et al.*, 2013).

In this context, two integral components of the IFT system, IFT20 and IFT88, are actively involved in the transport of some components of the autophagic machinery towards the cilium during cell starvation, with IFT20 recruiting ATG16L1 at the Golgi apparatus and shuttling it to the ciliary base, wherefrom it enters the cilium assisted by IFT88 (Pampliega *et al.*, 2013). Therefore, both autophagy and ciliogenesis regulation involve IFT proteins, suggesting a reciprocal interplay between these two processes.

Despite their first characterization as promoters of assembly and function of the primary cilium, IFT proteins have been found to be not only expressed but also implicated in major processes in the non-ciliated lymphoid cells. Interestingly, IFT20 is involved in the

polarized recycling of the TCR and the adaptor protein LAT to the IS through the control of vesicular traffic in T lymphocytes (Finetti *et al.*, 2009; Vivar *et al.*, 2016).

Consistent with the autophagic function described for the IFT system in ciliated cells, T cells depleted of IFT20 show impaired autophagic activity either under starvation or under nutrient-rich conditions (Finetti *et al.*, 2019), indicating that IFT20 mediates autophagy-related functions also in non-ciliated T cells. Interestingly, the autophagy impairment observed in IFT20 depleted T cells was ascribed to a defect in the sorting of acid hydrolases to the lysosomal compartment (Finetti *et al.*, 2019), the latest destination of autophagosome cargo to be degraded.

1.2 IFT20 promotes autophagosome biogenesis in T cells

Given the role of autophagy in T cell homeostasis, our group also investigated the mechanism by which IFT20 regulates basal T cell autophagy (Finetti *et al.*, 2021 - further details in the attached paper). IFT20 interacts with the core-autophagy protein ATG16L1 localized in intracellular vesicles in ciliated cells (Pampliega *et al.*, 2013). Notably, ATG16L1 plays a leading role in the process of autophagosome formation through its capability to interact with proteins and lipids (Fig.6). Co-immunoprecipitation, immunofluorescence and *in vitro* GSH-Sepharose pulldown assays indicated that IFT20 interacts and colocalizes with ATG16L1 also in the non-ciliated T cells (Fig.7 A, B, D).

IFT20 is a small protein containing a single coiled-coil (CC) domain at its C-terminus, required for the heterodimerization with other CC domain-containing components of the IFT complex (Baker *et al.*, 2003; Omori *et al.*, 2008). We dissected the interaction of IFT20 with ATG16L1 by generating GST fusion proteins with only the IFT20 CC domain or the full-length IFT20 lacking the CC domain (Fig.7C). The GST-pull down assays showed that ATG16L1 binds to IFT20 regardless of the presence of the CC-domain (Fig.7D). These results indicate that IFT20 interacts with ATG16L1 mostly through a molecular determinant localized within its unstructured region, potentially using its CC domain to couple ATG16L1 to sites of autophagosome formation.

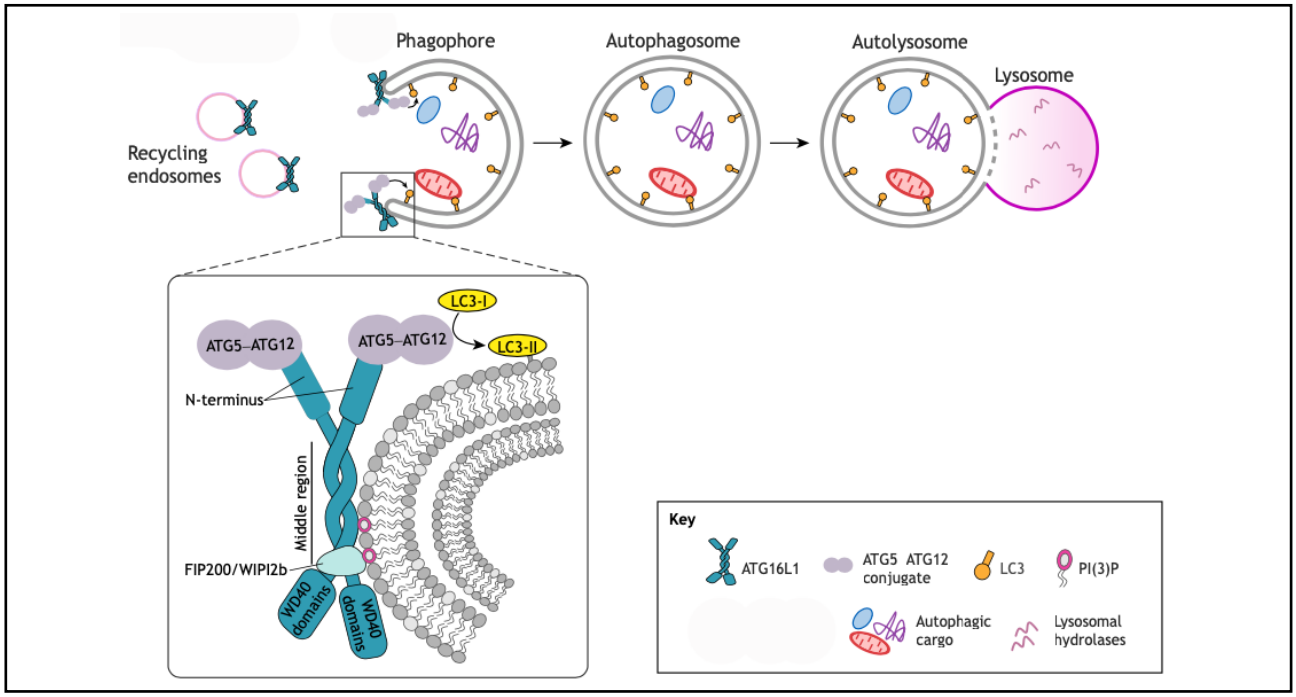

Figure 6| ***ATG16L1 is required for the biogenesis of the autophagosome.***

The interaction of ATG16L1 with the autophagy machinery components FIP200, WIPI2b and PI3P allows for its localization to the phagophore. Furthermore, ATG16L1 is thought to contribute to the elongation of the phagophore because of its localization to the endocytic compartment. Consistently, these events appear to be necessary for ATG8-mediated lipidation of LC3-I to LC3-II that in turn allows for the maturation of the autophagosome, which will fuse with the lysosome for cargo degradation (Gammoh *et al.*, 2020).

Next, we investigated the role of the IFT20 CC domain T cell autophagy in a Jurkat transfectant expressing either IFT20-GFP or a GFP-fused deletion mutant lacking the CC domain (ΔCC IFT20-GFP) (Fig.7E). In these transfectants, we exploited the standard immunoblot-based autophagy assay to measure the generation of LC3-II, the cleaved and lipidated form of LC3 localized at autophagosomal membranes (Klionsky *et al.*, 2016). Under basal conditions, the autophagic flux was decreased in cells expressing ΔCC IFT20-GFP compared to cells expressing full length IFT20-GFP (Fig.7F). Furthermore, immunofluorescence analysis of LC3 in IFT20 mutants showed an accumulation of $LC3^{+}$ dots in ΔCC IFT20-GFP Jurkat T cells compared to control (Fig.7G), confirming the impaired autophagic flux in this mutant and suggesting that the autophagy-promoting activity of IFT20 requires the CC domain.

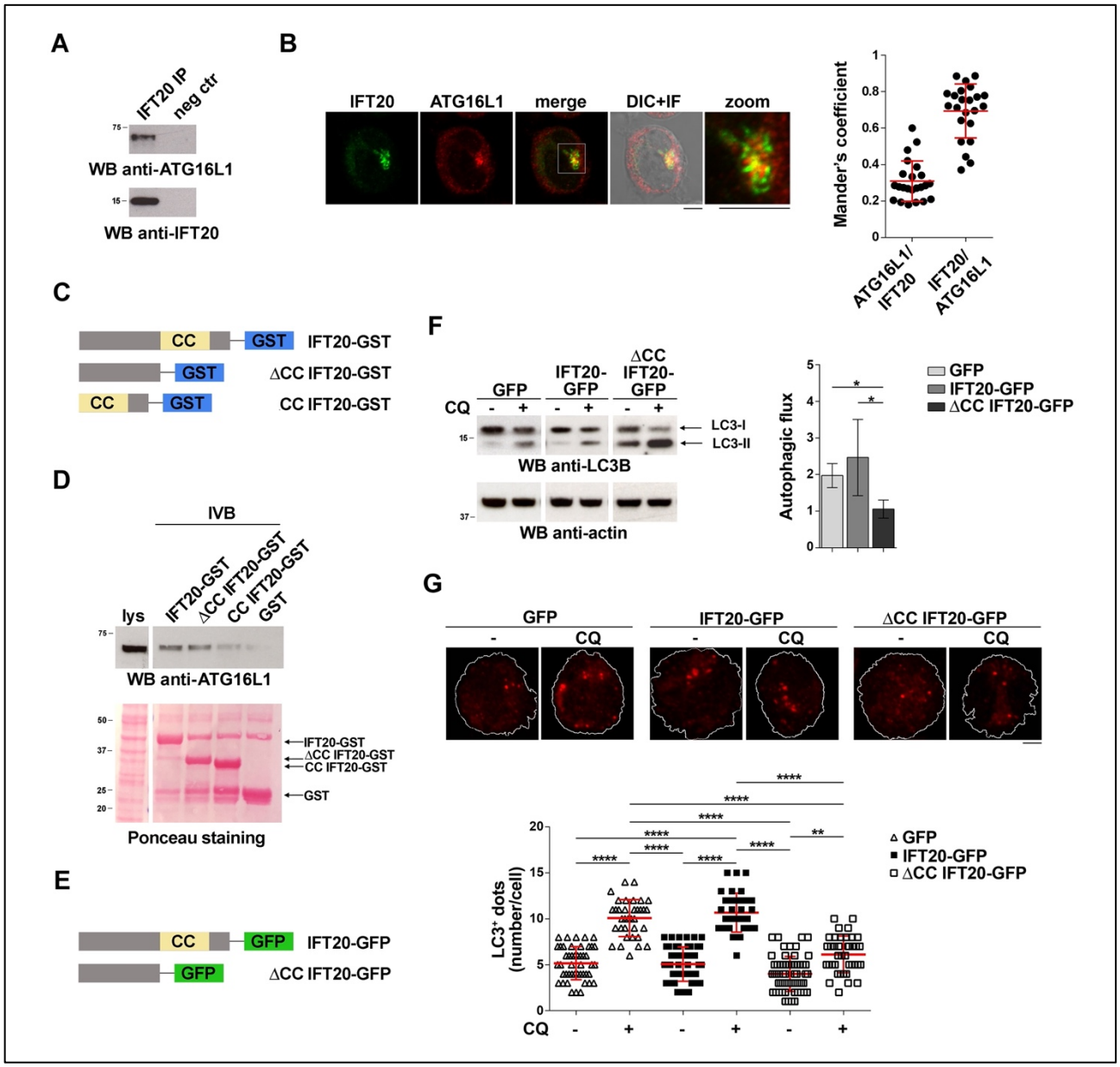

Figure 7| ***IFT20 interacts with ATG16L1 and promotes basal T cell autophagy through its CC domain.***

(A) Western blot (WB) analysis with anti-ATG16L1 antibodies of IFT20-specific immunoprecipitates (IP) from post-nuclear supernatants of Jurkat T cells. Each experiment included a pre-clearing negative control (neg ctr), in which proteins are bound to Protein-A–Sepharose before the addition of the primary antibody. The migration of molecular mass markers is indicated. Immunoblot images are representative of at least 3 independent experiments. **(B)** Confocal microscopy analysis of IFT20 and ATG16L1 in Jurkat T cells. Representative medial optical sections and overlay of immunofluorescence (IF) and differential interference contrast (DIC) images (IF + DIC) are shown. The graph shows the quantification of the weighted colocalization of IFT20 and ATG16L1 in Jurkat cells, calculated using Mander's coefficient (23 cells/sample, n =

3; mean ± SD). Scale bars: 5 µm. **(C)** Schematic representation of the GST fusion proteins with either the full-length IFT20 (IFT20-GST), or the full-length protein lacking the CC domain (ΔCC IFT20-GST) or only the CC domain (CC IFT20-GST). **(D)** Immunoblot analysis with anti-ATG16L1 antibodies of *in vitro*-binding assays carried out on Jurkat T cell lysates using IFT20-GST, ΔCC IFT20-GST and CC IFT20-GST fusion proteins or GST as negative control (n = 3). The Ponceau red staining of the same membrane is shown to compare the levels of fusion proteins and GST used in the assay. **(E)** Schematic representation of the GFP fusion protein with IFT20 (IFT20-GFP) or with the full-length protein lacking the CC domain (ΔCC IFT20-GFP). **(F)** Immunoblot analysis of LC3B in lysates of Jurkat cell mutants expressing either GFP, IFT20-GFP or ΔCC IFT20-GFP in the presence or absence of chloroquine (CQ, 40 µM), which blocks the degradation of LC3-II by impairing autophagosome fusion with lysosomes and resulting in the accumulation of degraded proteins (Mauthe *et al.*, 2018). The migration of molecular mass markers is indicated. The graph shows the autophagic flux in Jurkat transfectants, calculated as the difference in the levels of LC3II/actin between CQ-treated and CQ-untreated cells (n ≥ 3; mean fold ± SD, one-way ANOVA). **(G)** Immunofluorescence analysis of LC3B in Jurkat cells expressing GFP, IFT20-GFP or ΔCC IFT20-GFP either untreated or treated for 30 min with chloroquine (CQ, 40 µM). Representative images of the z-projection of maximum intensity and the quantification of the number of $LC3^+$ dots/cell are shown in the graph (35 cells/sample, n = 3; mean ± SD, Kruskal–Wallis test). *P < 0.05; **P < 0.01; ****P < 0.0001.

ATG16L1 is recruited from the cytoplasm to the cellular membranes that will contribute to the formation of the autophagosome (Xiong *et al.*, 2018). The interaction of IFT20 with the protein GMAP210 at the Golgi (Galgano *et al.*, 2017) and Rab5 at the early endosomes (Finetti *et al.*, 2014), both sources of autophagosome membrane (Itoh *et al.*, 2008), and with ATG16L1, led us to investigate the subcellular localization of ATG16L1 in IFT20-depleted T cells (IFT20KD). Immunofluorescence analysis of ATG16L1 and the centrosome revealed that, in control cell, ATG16L1-bearing vesicles cluster at the centrosome region, while in IFT20 deficient Jurkat T cells ATG16L1 shows a more dispersed pattern (Fig.8 A, B), supporting the idea that IFT20 tethers ATG16L1 to a vesicular compartment. Immunoblot analysis of cytosolic and membrane fractions confirmed the loss of ATG16L1

compartmentalization in favour of a cytosolic localization in IFT20KD cells (Fig.8C).

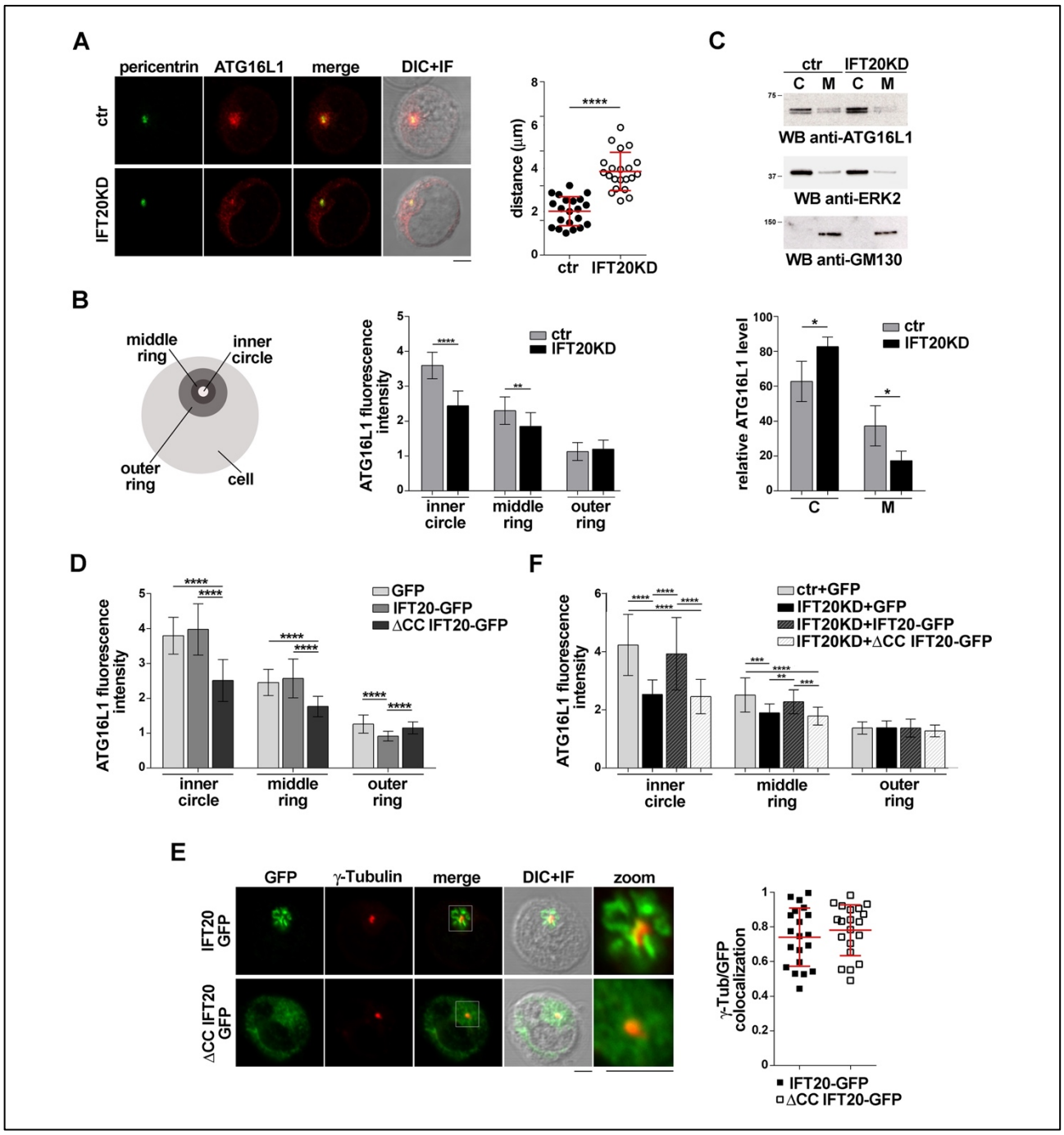

Figure 8| ***IFT20 mediates the vesicular localization of ATG16L1 in T cells.***

(A,B) Immunofluorescence analysis of ATG16L1 and the centrosomal protein pericentrin in control (ctr) and IFT20-deficient Jurkat cells. Representative medial optical sections are shown. Scale bars: 5 µm. (**A**) The graph shows the quantification of the distance of ATG16L1$^+$ vesicles from the centrosome (mean ± SD, Student's t-test; 21 cells/sample, n = 3). (**B**) The scheme shows the compartmentalization defined for each cell from the point of ATG16L1 maximal intensity. The

graph shows the quantification of the fluorescence intensity in the concentric regions (≥ 20 cells/sample, n = 3; mean ± SD, Mann–Whitney test). **(C)** Immunoblot analysis with anti-ATG16L1 antibodies in cytosolic (C) and membrane (M) fractions from either control or IFT20KD Jurkat cells. The cytosolic protein ERK2 and the cis-Golgi marker GM130 were used as controls for the purity of cytosolic and membrane fractions, respectively. The migration of molecular mass markers is indicated. The histogram shows the quantification of the percentage of ATG16L1 in the cellular fractions (n ≥ 4; mean ± SD, Student's t-test). **(D)** Confocal microscopy analysis of ATG16L1 in GFP, IFT20-GFP and ΔCC IFT20-GFP Jurkat T cell mutants. The graph shows the quantification of the fluorescence intensity in the concentric regions mentioned above (**B**) (≥ 25 cells/sample, n = 3; mean ± SD, Mann–Whitney test). **(E)** Quantification of the weighted colocalization of γ-tubulin with GFP of IFT20-GFP or ΔCC IFT20-GFP expressing cells, using Mander's coefficient (≥ 20 cells/line, n = 3; mean ± SD). Medial optical sections of representative images are shown. Scale bar: 5 μm. **(F)** Immunofluorescence analysis of ATG16L1 in control and IFT20KD Jurkat transiently transfected with the empty vector (GFP), or the IFT20-GFP or the ΔCC IFT20-GFP encoding constructs. The histogram shows the quantification of the ATG16L1 fluorescence intensity in the concentric regions described above (≥ 25 cells/sample, n = 3; mean ± SD, Mann–Whitney test). *P < 0.05; **P < 0.01; ***P < 0.001; ****P < 0.0001.

Although the IFT20 CC domain is dispensable for the interaction with ATG16L1 (Fig.7D), it is necessary for the pro-autophagic activity of IFT20 (Fig.7 F, G). Hence, we carried out an immunofluorescence analysis of the ΔCC IFT20-GFP mutant and found that the absence of the CC domain of IFT20 causes the loss of the typical ATG16L1 vesicular pattern (Fig.8D), similar to IFT20KD cells, while the centrosome localization of IFT20 lacking the CC domain was unaffected (Fig.8E). Importantly, the defect of ATG16L1 distribution observed in IFT20KD cells was rescued by restoring IFT20 expression, while ΔCC IFT20 was unable to rescue the defect (Fig.8F). Based on these findings, we hypothesize that IFT20 acts as an adaptor, coupling the core autophagy protein ATG16L1 to the sites of autophagosome formation through a molecular determinant that appears to involve its CC domain.

With the aim to identify the specific membrane localization of ATG16L1 in T cells, we

carried out a co-localization analysis of ATG16L1 with the Golgi apparatus, one of the most IFT20-enriched membrane compartments, where it binds the golgin GMAP210-CC domain (Follit *et al.*, 2006; Finetti *et al.*, 2009) (Fig.9A). A decreased ATG16L1 localization at the Golgi in IFT20KD cells suggested that IFT20 is necessary for the localization of ATG16L to this compartment. We found that the IFT20-mediated ATG16L1 localization to the Golgi is mediated by GMAP210, as immunofluorescence analysis of GMAP210-depleted Jurkat T cells (GMAP210KD) revealed a more dispersed ATG16L1 compartment (Fig.9B) and a decreased association of the protein with the Golgi (Fig.9C) compared to control. Consistently, IFT20 localization to Golgi was lost in GMAP210KD cells (Fig.9D), a result in agreement with the known interaction of IFT20 with GMAP210 in T cells (Galgano *et al.*, 2017; Zucchetti *et al.*, 2019). We took advantage of pull-down assays of IFT20 GST constructs to map GMAP210 binding site on IFT20. We confirmed GMAP210 interaction with the full-length IFT20 and, interestingly, we found that this interaction preferentially involves the CC domain of IFT20 (Fig.9E).

We further investigated the role of the IFT20 CC domain in GMAP210 localization to Golgi apparatus by immunofluorescence analysis of ΔCC IFT20-GFP mutants (Fig.9F). Autophagosome formation requires membrane source from several compartments, including the Golgi apparatus (Itoh *et al.*, 2008; Staiano *et al.*, 2019). We found that IFT20 recruits ATG16L1 to the Golgi in a GMAP210-dependent manner, suggesting a potential implication of this process in the pro-autophagic activity of IFT20. However, GMAP210 deficiency did not affect basal autophagy, as assessed by the measurement of the autophagic flux by both immunoblot and immunofluorescence analysis of LC3 (Fig.9 G, H). Hence, IFT20 couples ATG16L1 to the Golgi in T cells through its CC domain-dependent interaction with GMAP210, but this association does not lead to autophagosome formation.

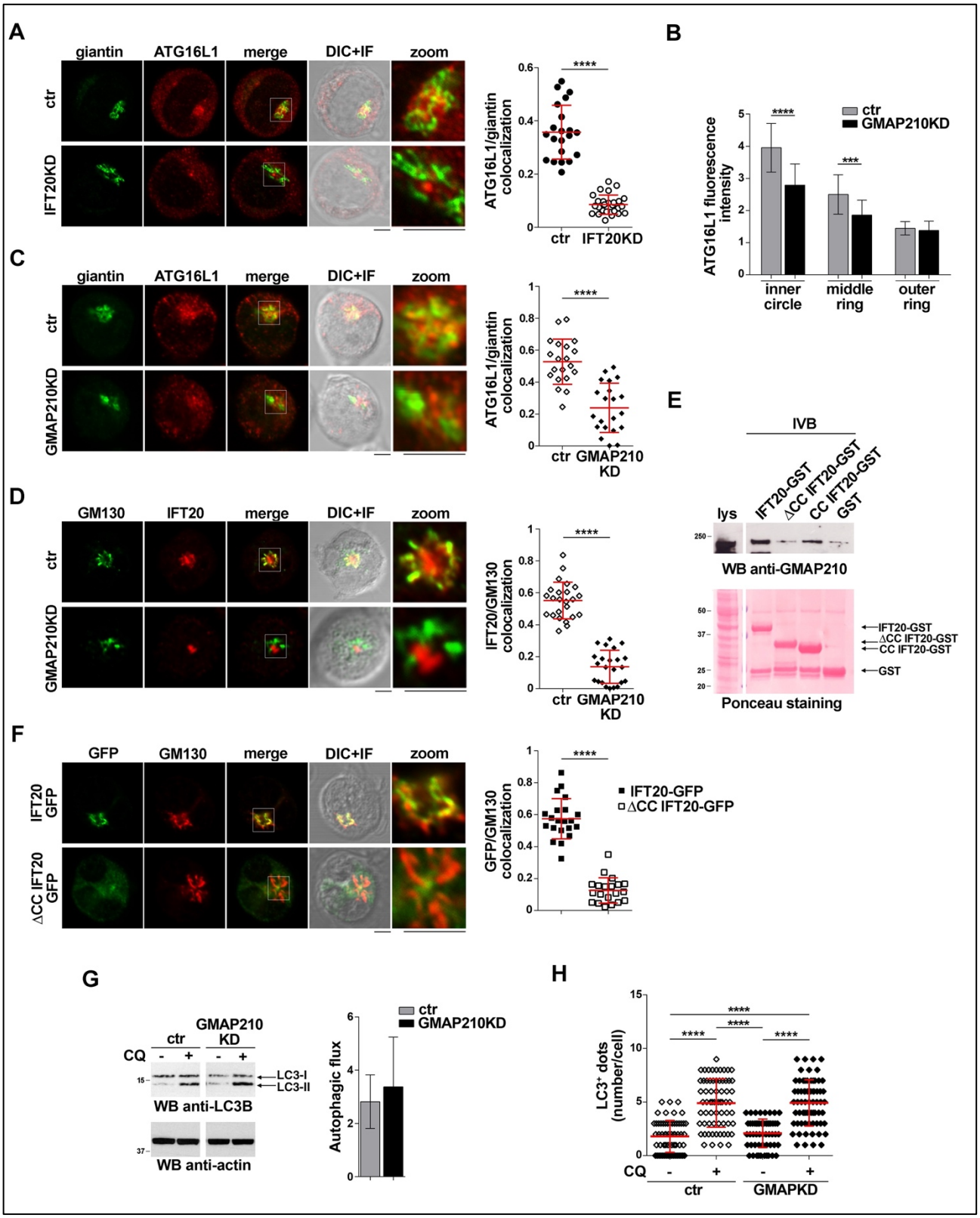

Figure 9| ***IFT20 recruits ATG16L1 to the Golgi through its CC domain-mediated interaction with GMAP210.***

(A) Quantification, using Mander's coefficient, of the weighted colocalization of ATG16L1 and the Golgi marker giantin in control and IFT20KD Jurkat cells (≥ 21 cells/sample, n = 3; mean ± SD, Student's t-test). Medial optical sections of representative images are shown. Scale bars: 5 µm. **(B)**

Quantification of ATG16L1 fluorescence intensity in the concentric regions previously described (Fig.8B) in control and GMAP210KD cells (≥ 25 cells/sample, n = 3; mean ± SD, Mann–Whitney test). **(C,D)** Immunofluorescence analysis of ATG16L1 and giantin (**C**) or IFT20 and the Golgi marker GM130 (**D**) in control and GMAP210KD cells. Representative medial optical section images are shown. The histogram shows the quantification of the weighted colocalization of ATG16L1 and giantin (**C**) or IFT20 and GM130 (**D**), calculated using Mander's coefficient (≥ 20 cells/sample, n = 3; mean ± SD, Mann–Whitney test). Scale bars: 5 µm. **(E)** Immunoblot analysis with anti-GMAP210 antibodies of *in vitro*-binding assays carried out on lysates of Jurkat cells using IFT20-GST, ΔCC IFT20-GST and CC IFT20-GST fusion proteins, or GST as negative control (n = 3). The Ponceau red staining of the same membrane is shown to compare the levels of fusion proteins and GST used in the assay. **(F)** Quantification, using Mander's coefficient, of the weighted colocalization of the cis-Golgi marker GM130 with GFP of IFT20-GFP or ΔCC IFT20-GFP expressing cells (≥ 20 cells/line, n = 3; mean ± SD, Mann–Whitney test). Medial optical sections of representative images are reported. Scale bars: 5 µm. **(G)** Immunoblot analysis of LC3B in lysates of either control or GMAP210KD cells in the presence or absence of chloroquine (CQ, 40 µM). The migration of molecular mass markers is indicated. The graph shows the autophagic flux calculated as the difference in the levels of LC3II/actin between CQ-treated and CQ-untreated samples (n ≥ 3; mean fold ± SD, Student's t-test). **(H)** Quantification of the number of $LC3^+$ dots/cell in control or GMAP210KD cells either untreated or treated with chloroquine (CQ, 40 µM) for 30 min (≥ 35 cells/line, n = 3; mean ± SD, Kruskal–Wallis test). **P < 0.01; ***P < 0.001; ****P < 0.0001.

In other cell types, ATG16L1 localizes not only to the Golgi but also to early and recycling endosomes (Ravikumar *et al.*, 2010; Puri *et al.*, 2013; Fraser *et al.*, 2019). IFT20 localizes to early endosomes by interacting with Rab5 (Finetti *et al.*, 2014). Interestingly, Rab5 is a component of the macromolecular complex containing the autophagosome formation regulators BECLIN1 and VPS34 (Revikumar *et al.*, 2008). Hence, we hypothesized that IFT20 could promote autophagy by exploiting its interaction with Rab5 to recruit ATG16L1 to early endosomes. Immunofluorescence analysis of ATG16L1 in either control or IFT20KD Jurkat T cells revealed that ATG16L1 localizes to the $Rab5^+$ compartment in control cells (Fig.10A), confirming this interaction in T cells. Moreover, this ATG16L1 sub-cellular localization was lost in the absence of IFT20 (Fig.10A). We confirmed both data by

co-immunoprecipitation experiments (Fig.10B).

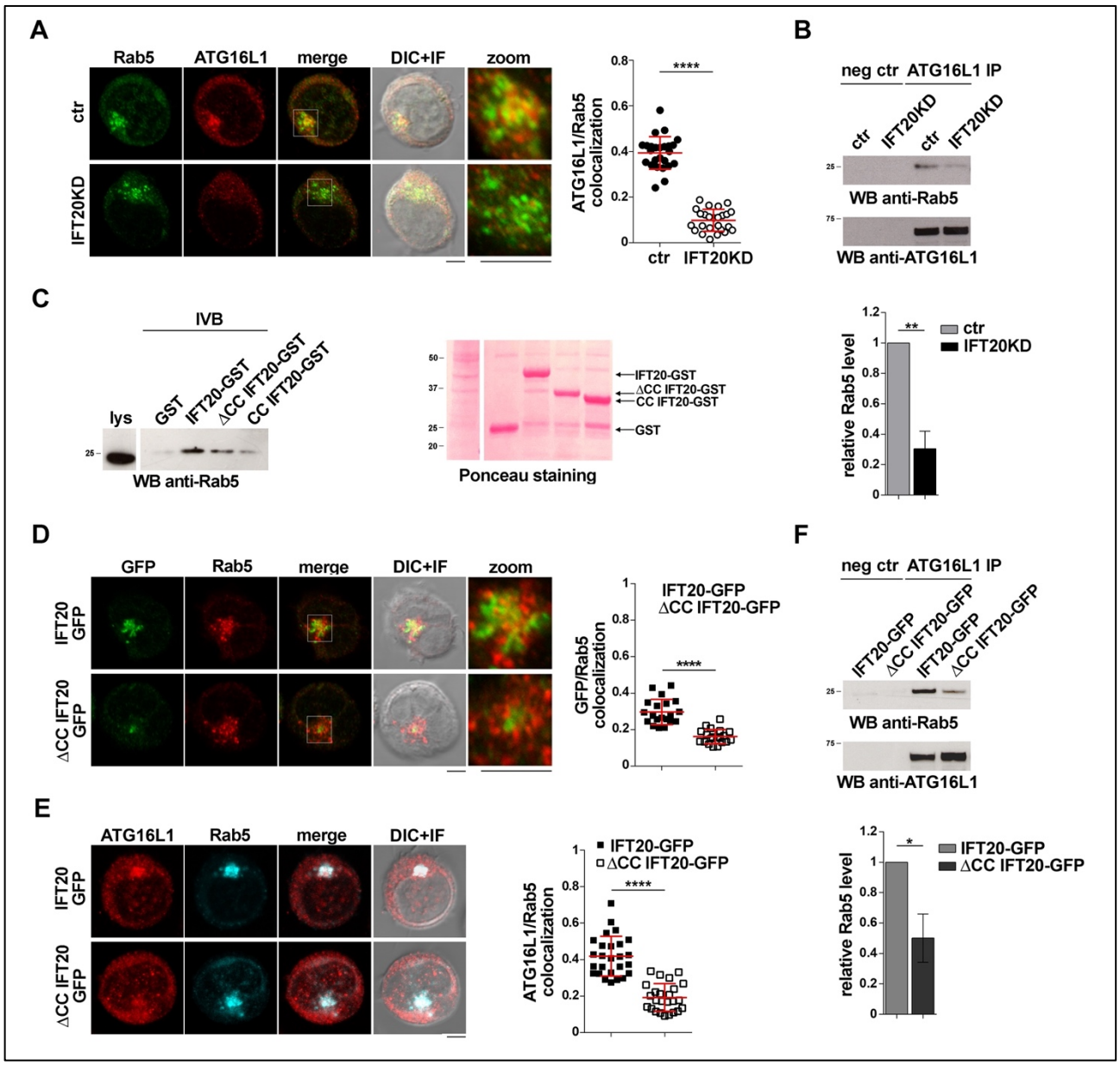

Figure 10| ***IFT20 is required for ATG16L1 localization to early endosomes through interaction with Rab5.***

(A) Immunofluorescence analysis of ATG16L1 in Rab5-GFP expressing control and IFT20KD Jurkat cells. Representative medial optical sections are shown. Scale bar: 5 μm. In the graph is reported the quantification of the weighted colocalization, using Mander's coefficient, of ATG16L1 and Rab5 in control and IFT20KD Jurkat cells (25 cells/sample, n = 3; mean ± SD, Student's t-test). **(B)** Immunoblot analysis with anti-Rab5 antibodies of ATG16L1-specific immunoprecipitates from post-nuclear supernatants of control and IFT20KD Jurkat cells. Pre-clearing controls (neg ctr) were run in parallel to each assay. The migration of molecular mass markers is indicated. The graph

shows the quantification of the relative protein expression normalized to ATG16L1 as mean fold ± SD, with the expression in control cells set as 1 (n = 3, Student's t-test). **(C)** Immunoblot analysis with anti-Rab5 antibodies of *in vitro*-binding assays carried out on lysates of Jurkat cells using IFT20-GST, ΔCC IFT20-GST and CC IFT20-GST fusion proteins, or GST as negative control (n = 3). The Ponceau red staining of the same membrane is shown to compare the levels of fusion proteins and GST present in the assay. **(D)** Immunofluorescence analysis of GFP and Rab5 in Jurkat cells expressing either IFT20-GFP or ΔCC IFT20-GFP constructs. The graph shows the quantification, using Mander's coefficient, of the weighted colocalization of GFP and Rab5 in Jurkat transfectants, reported as mean value/cell calculated on individual $Rab5^+$ dot (20 cells/sample, n = 3; mean ± SD, Student's t-test). Scale bars: 5 μm. **(E)** Immunofluorescence analysis of ATG16L1 and Rab5 in either IFT20-GFP and ΔCC IFT20-GFP expressing Jurkat cells. The graph shows the quantification of the weighted colocalization of ATG16L1 and Rab5 using Mander's coefficient (≥ 25 cells/sample, n = 3; mean ± SD, Student's t-test). Representative medial optical section images are shown. Scale bar: 5 μm. **(F)** Immunoblot analysis with anti-Rab5 antibodies of ATG16L1-specific immunoprecipitates from post-nuclear supernatants of Jurkat cells expressing either IFT20-GFP or ΔCC IFT20-GFP. Pre-clearing controls were included (neg ctr). The migration of molecular mass markers is indicated. The histogram shows the quantification of the relative Rab5 expression normalized to ATG16L1 as mean fold ± SD, with the expression in control cells set as 1 (n = 3; Student's t-test). **P < 0.01; ***P < 0.001; ****P < 0.0001.

By means of pull-down assays with IFT20-GST, CC IFT20-GST and ΔCC IFT20-GST, we were able to map the interaction of IFT20 with Rab5 (Fig.10C). We found that both IFT20 molecular determinants concur to the interaction with Rab5, but that the CC domain of IFT20 is required for its localization to early endosomes, as assessed by immunofluorescence staining of Rab5 in ΔCC IFT20-GFP mutants (Fig.10D). Additionally, ΔCC IFT20-GFP cells showed impaired ATG16L1 co-localization and interactions with Rab5 (Fig.10 E, F). These findings indicate that, through the interaction with Rab5 and ATG16L1, IFT20 recruits ATG16L1 to early endosomes using both its unstructured and CC domain.

The finding that IFT20 is required for ATG16L1 vesicular localization in T cells raised the

question whether IFT20 is directly involved in the ATG16L1-related autophagy process. Having ruled out the contribution of IFT20 to the Golgi localization of ATG16L1, early endosomes appeared as interesting candidates. Since the autophagy regulator BECLIN1 participates in ATG16L1 recruitment for autophagosome formation (Gammoh, 2020), we evaluated the participation of IFT20 in the interaction of ATG16L1 with BECLIN1 at early endosomes. We found that ATG16L1 co-immunoprecipitates (Fig.11A) and co-localizes (Fig.11B) with BECLIN1 in T cells. Interestingly, this interaction is impaired in IFT20-deficient T cells. Nevertheless, ATG16L1 still interacted with its downstream autophagy partner ATG5 in IFT20KD cells (Fig.11C). IFT20 deficiency did not affect either the interaction (Fig.11D) or the co-localization (Fig.11E) of BECLIN1 with Rab5 in T cells. Consistently, also the BECLIN1-dependent accumulation of PI3P at early endosomes was not impaired in IFT20-deficient T cells (Fig.11F), as assessed by the co-localization of Rab5 with GFP in T cells transiently transfected with a plasmid encoding for the fusion protein FYVE-GFP. FYVE is a tandem domain of hepatocyte growth factor-regulated tyrosine kinase substrate, specifically interacting with PI3P. Collectively, these findings indicate that IFT20 participates to the recruitment of ATG5-ATG12/ATG16L1 complex to early endosomes tagged for autophagosome formation by Rab5-associated BECLIN1.

ATG16L1 is involved in the determination of LC3 lipidation site and in the recruitment of ATG5-ATG12, allowing for the transfer of LC3 to the phagophore membrane (Fujita *et al*., 2008). By means of co-immunoprecipitation assays, we found that ATG16L1 interacts with LC3-I in T cells; this coupling was significantly impaired in IFT20KD cells (Fig.12A). This result suggests that the IFT20-dependent localization of ATG16L1 to early endosomes is necessary for the recruitment of LC3-I and to promote its local cleavage and lipidation to LC3-II. Accordingly, in IFT20KD cells not only the interaction of ATG16L1 with LC3-I, but also the localization of ATG16L1 to the $LC3^{+}$ compartment, were significantly impaired (Fig.12B). Moreover, a decrease in the co-localization of LC3 with the $Rab5^{+}$ compartment was observed in IFT20KD Jurkat cells (Fig.12C). An accumulation of LC3-II could be detected in IFT20-deficient T cells under basal conditions (Fig.12B), in agreement with the defect in the late steps of the autophagy pathway previously reported in these cells (Finetti

et al., 2020). Consistent with the previous work, we found that IFT20-mediated targeting of ATG16L1 and its partners ATG5-ATG12 to Rab5^{+}/BECLIN1^{+} vesicles allow for the recruitment of LC3, which in turn participates to the local generation of isolation membranes at early endosomes to promote the formation of the autophagosome.

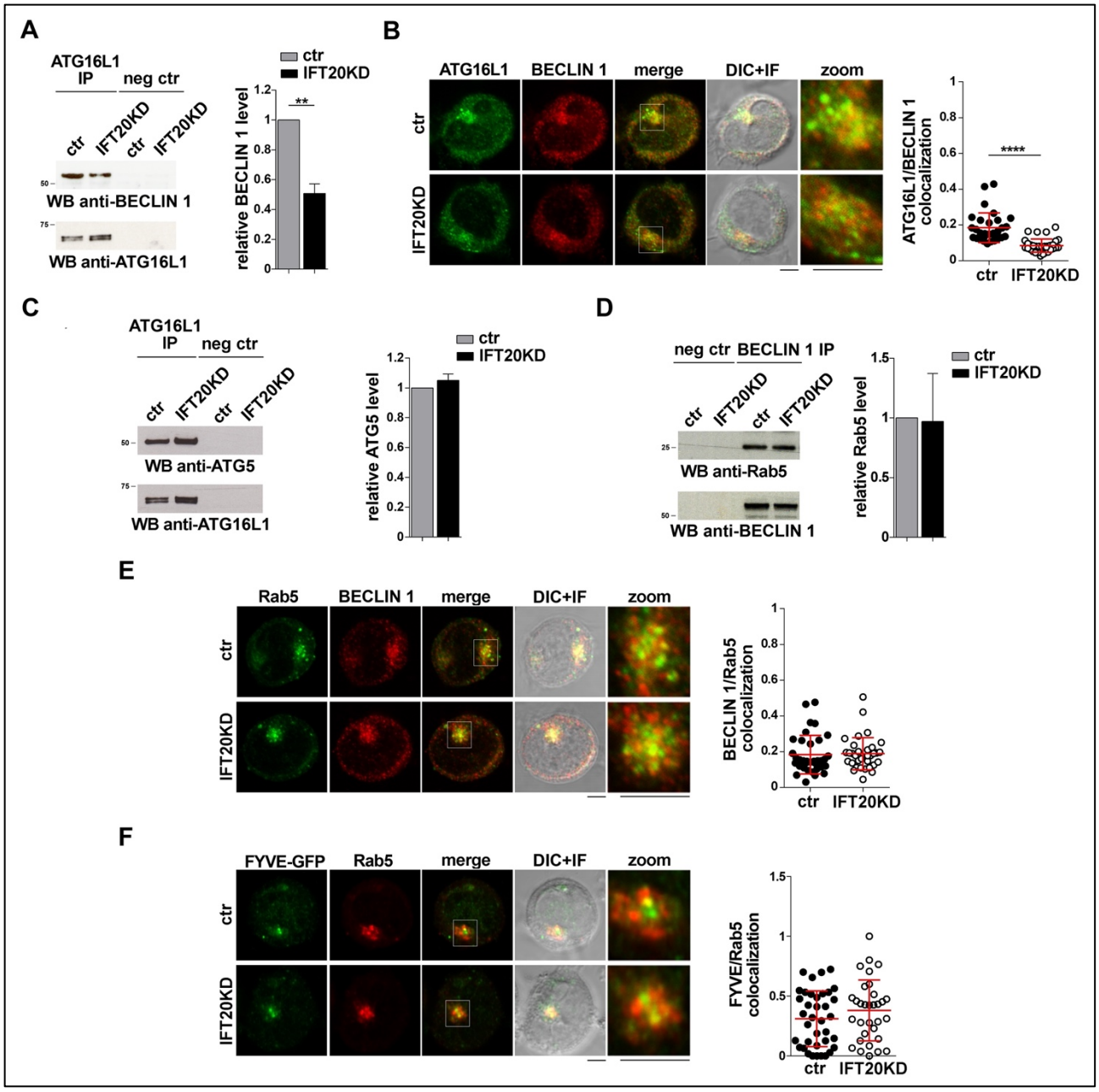

Figure 11 | ***IFT20 recruits ATG16L1 to early endosomes tagged for autophagosome formation.***

(A) Immunoblot analysis with anti-BECLIN 1 antibodies of ATG16L1-specific immunoprecipitates from post-nuclear supernatants of control and IFT20KD Jurkat cells. Preclearing controls are included in each blot (neg ctr). The migration of molecular mass markers is indicated. The

quantification of the relative BECLIN1 expression normalized to ATG16L1 is reported as mean fold ± SD, with the expression in control cells set as 1 (n = 3; Student's t-test). **(B)** Quantification of the weighted colocalization of ATG16L1 with BECLIN1, using Mander's coefficient, in medial confocal sections of control and IFT20KD Jurkat cells, reported in the histogram as mean ± SD (≥ 30 cells/line, n = 3; Mann–Whitney test). Representative images of medial section images are shown. Scale bars: 5 μm. **(C)** Immunoblot analysis with ATG5 antibodies of ATG16L1-specific immunoprecipitates from post-nuclear supernatants of control and IFT20KD cells. Pre-clearing controls are included (neg ctr). The migration of molecular mass markers is indicated. The quantification of the relative protein expression normalized to ATG16L1 is reported as mean fold ± SD, with the expression in control sample set as 1 (n = 3). **(D)** Immunoblot analysis with Rab5 antibodies of BECLIN1-specific immunoprecipitates from lysates of control and IFT20KD cells. Pre-clearing controls are included (neg ctr). The migration of molecular mass markers is indicated. In the histogram is indicated the quantification of the relative Rab5 expression normalized to BECLIN1 and reported as mean fold ± SD, with the expression in control cells set as 1 (n = 3). **(E,F)** Immunofluorescence analysis of BECLIN1 and Rab5 (**E**) or FYVE-GFP and Rab5 (**F**) in control and IFT20KD Jurkat cells. Representative medial optical section images are shown. Scale bars: 5 μm. The graphs show the quantification of the weighted colocalization of BECLIN1 (**E**) or FYVE-GFP (**F**) and Rab5 in control and IFT20KD cells, calculated using Mander's coefficient (≥ 32 cells/line, n = 3; mean ± SD, Mann–Whitney test). **P < 0.01; ****P < 0.0001.

To summarize, we found that IFT20 participates in basal autophagy by regulating the localization of ATG16L1 at early endosomes to promote autophagosome biogenesis. Hence, our data identify IFT20 as an integral part of the T cell autophagy apparatus, providing additional evidence of the participation of the ciliary machinery in the physiology and functions of the non-ciliated T cells. The identification of IFT20 as a new promoter of the basal autophagy in T cells (Finetti *et al.*, 2021), together with our previous implication of IFT20 in lysosome biogenesis (Finetti *et al.*, 2020), highlight a prominent function for IFT20 in the homeostasis of T cells.

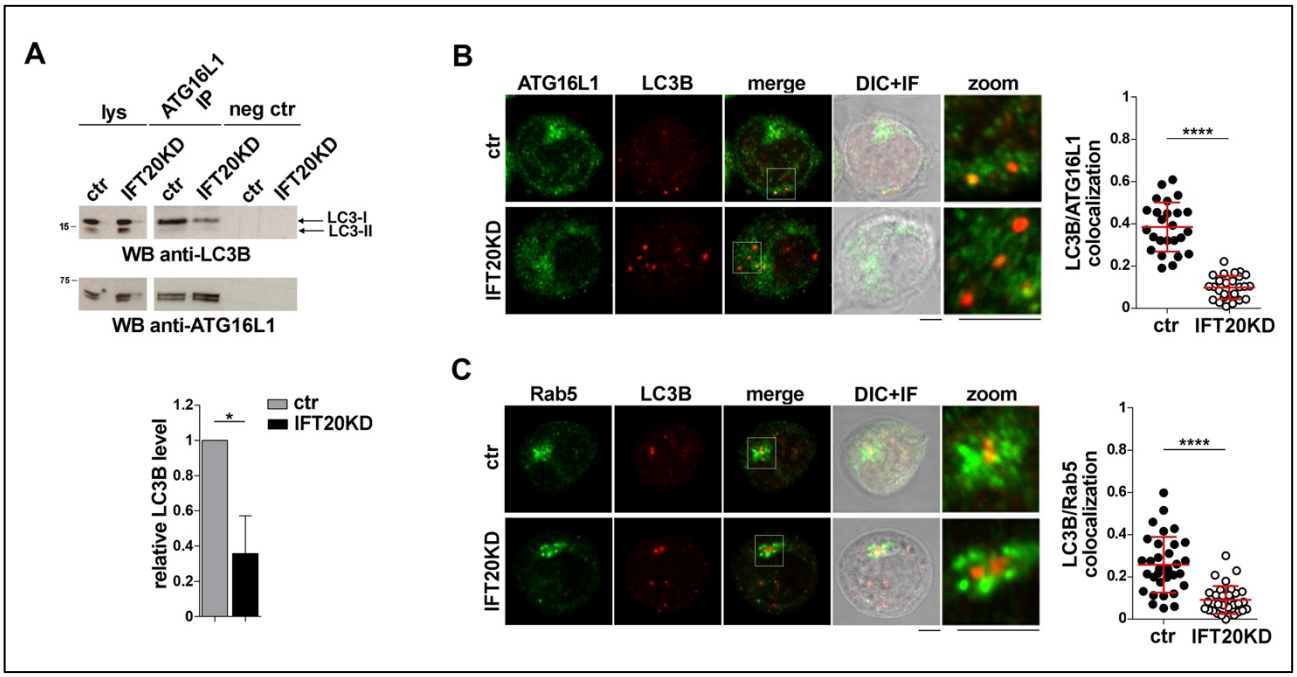

Figure 12| ***IFT20 mediates LC3 recruitment to ATG16L1 at early endosomes.***

(A) Immunoblot analysis using anti-LC3B antibodies on ATG16L1-specific immunoprecipitates from lysates of control and IFT20KD Jurkat cells. Pre-clearing controls and total cell lysates are included. The migration of molecular mass markers is indicated. The graph shows the quantification of the relative LC3B levels normalized to ATG16L1 and reported as mean fold ± SD, with the value of expression in control sample set as 1 (n = 3; Student's t-test). **(B,C)** Immunofluorescence analysis of ATG16L1 (**B**) or Rab5 (**C**) and LC3B in either control or IFT20KD cells. The histogram reports the quantification, using Mander's coefficient, of the weighted colocalization of LC3B and ATG16L1 (**B**) or Rab5 (**C**) in control and IFT20KD Jurkat cells, reported as mean value/cell calculated on single dot $LC3^+$ (≥ 25 cells/sample, n = 3; mean ± SD, Mann–Whitney test). Medial optical sections of representative images are shown. Scale bars: 5 μm. *P < 0.05; ****P < 0.0001.

2. The intraflagellar transport protein IFT20 participates in CTL-mediated killing

2.1 The biogenesis of lytic granules

CTLs are critical in orchestrating the protective immune responses against cancer and pathogen infected cells. Upon TCR triggering, CTLs can mediate target cell death and the integrity of the killing machinery is necessary for the fulfilment of CTL immune surveillance (McKenzie *et al.,* 2022). The main mechanism of target cell killing involves the secretion of lytic granules containing cytotoxic molecules (Podack *et al.,* 1991) and their exclusive release at the IS, the specialized membrane domain at the interface between the T lymphocyte and the APC (de la Roche *et al.,* 2016).

Lytic granules are characteristic of CTLs and are thought to derive from lysosomes (Stinchcombe *et al.,* 2004), the primary catabolic compartments of eukaryotic cells. The lysosomes degrade extracellular material that has been internalized by endocytosis and intracellular components that have been sequestered by autophagy (Ballabio *et al.,* 2020). In contrast to other cell types, which contain both secretory lysosomes and conventional lysosomes (Raposo *et al*., 2007), cytotoxic granules seem to be the only lysosome-type organelles present in mature CTLs. As secretory organelles, they contain a typical electron-dense core domain, where secretory proteins are localized (Peters *et al*., 1991) and, similar to endosomes, they incorporate extracellular proteins and surface receptors, such as the TCR, CD8 and MHC I (Peters *et al*., 1989). Lytic granules are generally thought to derive from lysosomes as not only do they bear a vesicular cortical domain surrounding the core (Burkhardt *et al*., 1990) and have a low intraluminal pH (Cuervo *et al*., 1996) required for the function of lysosomal enzymes, but they also contain lysosomal hydrolases, such as cathepsin D, and harbour lysosome-associated glycoproteins, namely Lamp1, on their outer membrane (Tian *et al*., 1991).

The main lytic granule content consists of granzymes, an array of serine proteases with different substrate specificity (Chowdhuri *et al*., 2008), and perforin, a protein with structural and functional similarities to bacterial pore-forming toxins (Spicer *et al*., 2017), packed together on a scaffold of the proteoglycan serglycin in the dense core (Kolset *et al*.,

2008). Cytotoxic granules also contain the processed isoform of granulysin, a bacteria membrane-disrupting protein (Sparrow *et al.*, 2020).

Naïve $CD8^+$ T cells do not contain lytic granules. Only after TCR triggering they express detectable levels of the secretory lysosome components (Sanchez-Ruiz *et al.*, 2015). The relative proportions of dense core and vesicular cortex vary among lytic granules (Burkhardt *et al.*, 1990), and this morphological heterogeneity may reflect sequential maturation stages of the cytotoxic granules. The appearance and maturation of lytic granules correlates with the killing ability of activated CTLs (Blott *et al.*, 2002).

The mechanisms involved in the biogenesis of lytic granules have been in part characterized. The multivesicular structure of the granules derives from sequential invaginations of the membrane of early endosomes (Gruenberg, 2001), where proteins endocytosed from the plasma membrane or deriving from the Golgi apparatus are sorted to the late endosomes and then to lysosomes for degradation, or alternatively recycled.

Granzymes, of which the best characterized is granzyme B, enter the ER as inactive precursors and reach the dense core of cytotoxic granules from the trans-Golgi network (TGN). The process of granzyme biosynthesis includes N-glycosylation and the addition of a mannose 6-phosphate (M6P) moiety. The multivesicular cortex of cytotoxic granules is enriched in the M6P receptor (MPR), known not only for its role in the targeting of acid hydrolases to the lysosomal compartment (Burkhardt *et al.*, 1990) but also for its participation in the sorting of granzymes, as well as other soluble lysosomal proteases, at the TGN (Fig.13). From the TGN, granzymes are directed to early endosomes within clathrin-coated vesicles (Stöckli *et al.,* 2004) and then sorted to late endosomes in multivesicular bodies, in a process involving the endosomal sorting complex required for transport (ESCRT) machinery (Hurley, 2008). In late endosomes, the low luminal pH is a crucial participant in the proteolytic maturation of the serine proteases, as it allows the dissociation of the bound ligand from the MPR, that is recycled back to the TGN (Braulke *et al.*, 2009). Of note, MPRs are detectable in the vesicular domain of cytotoxic granules, whereas they are completely absent in conventional lysosomes, suggesting that lytic granules are at a "pre-lysosomal" stage (Burkhardt *et al.*, 1990).

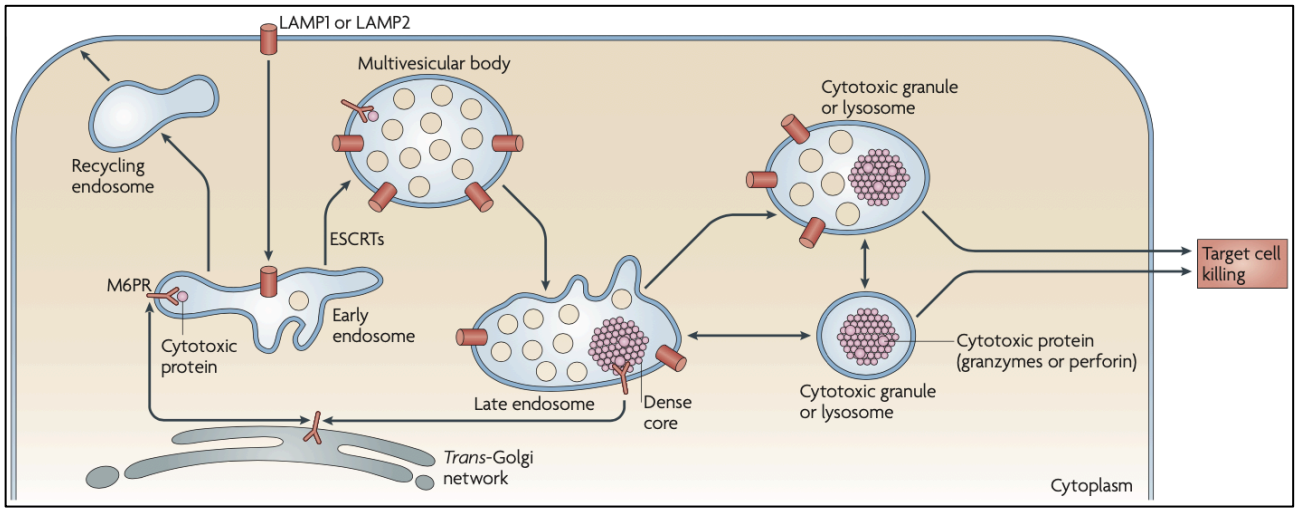

Figure 13| ***Schematic representation of biogenesis and exocytosis of cytotoxic granules.***
Granzymes and other soluble proteins, including lysosomal hydrolases, are sorted from the TGN by the MPR, to reach the endosomal compartment. In the late endosomes, the low pH allows for the dissociation of the ligand from MPR, that is recycled to the TGN. Lamp1 or Lamp2 travel directly to the plasma membrane wherefrom, following release of the lytic granule contents, they are internalized and sorted by the AP-1 complex to the endosomal pathway (not shown). The ESCRT machinery takes part in lytic granule protein trafficking to both early and late endosomes. Lytic granules are hybrid organelles containing both lysosomal and endosomal components. They contain various proportions of dense core domains, where cytotoxic proteins are stored, and multivesicular bodies (yellow circles), containing acid hydrolases (de Sainte Basile *et al.*, 2010).

Conversely, the pathway followed by perforin to enter the maturing lytic granules is largely uncharacterized. The export of the perforin from the ER and the localization to lytic granules require a molecular C-terminal domain and N-linked glycosylation (Brennan *et al.*, 2011), but also Lamp1 takes part to the sorting, interacting with the multimeric cytoplasmic adaptor proteins (AP-1) complexes (Krzewski *et al.*, 2013). The pore-forming activity of perforin on biological membranes requires its polymerization in the presence of Ca^{2+}. Inside cytotoxic granules, perforin is kept in a monomeric conformation by serglycin binding and by the low intraluminal pH that prevents Ca^{2+} binding (Lopez *et al.*, 2012). These protective mechanisms ensure that not only perforin but also the other cytotoxic proteins contained in lytic granules are kept inactive until release, to prevent damages to the cell itself.

Following their release into the synaptic cleft, perforin and granzymes cooperate to promote target cell death. The dissociation from serglycin and the higher pH of the synaptic cleft allows for the polymerization of perforin, whose monomers assemble to form pores in the plasma membrane of the target cell. Through these pores, granzymes reach the cytosol of the APC, where they trigger apoptosis by activating caspase-dependent and caspase-independent pathways (Chowdhury *et al.*, 2008). Lytic granules exert their cytotoxic activity also through the activity of granulysin that, by interacting with the target cell membrane by means of its positive charges, is able to induce the influx of Ca^{2+}, which leads to mitochondrial damage and activation of the caspase 3-mediated apoptotic program (Sparrow *et al.*, 2020).

Finally, integral lytic granule membrane proteins (Lamps) are sorted at the TGN through a tyrosine-based or a dileucine-based motif, that directly interact with the AP-1 sorting complex, mediating their delivery to the cortical domain of cytotoxic granules (Honing *et al.*, 1995).

Finetti and colleagues demonstrated that the ciliary protein IFT20 participates in biogenesis and function of lysosomes by regulating the MPR-mediated lysosomal targeting of acid hydrolases, as the retrograde transport of MPRs from endosomes back to the TGN in Jurkat T cells requires IFT20 (Finetti *et al.,* 2020). For the present work, we hypothesized that IFT20 could take part in the traffic of MPRs also in CTLs. Since the soluble lysosomal protease components of the cytotoxic granules, including the granzymes, are routed to lytic compartment through the MPR pathway (Griffiths *et al.,* 1993), IFT20 may be involved in lytic granule biogenesis.

2.2 CTLs depleted of IFT20 show lytic granule defects and impaired cytotoxic activity

The aim of this work is to provide insights into the participation of the ciliary protein IFT20 in the biogenesis of lytic granules of CTLs, a mechanism that is still poorly characterized and that initiates during the early phases of naïve $CD8^+$ cell development (Sanchez-Ruiz *et al.,* 2015). Therefore, the experimental procedures were performed on a CRISPR/Cas9-edited pool of human primary $CD8^+$ T cells knocked out for IFT20 expression (IFT20KO)

immediately after their isolation by negative selection from the peripheral blood of human healthy donors. The gene-edited cells were activated using beads coated with anti-CD3 and anti-CD28 mAbs in the presence of IL2, then $CD8^+$ T cells were allowed to differentiate *in vitro* to functional CTLs and used for the assays from day 5 to day 7 of maturation (Onnis *et al.,* 2022). Gene-edited cells were tested by immunoblot analysis at day 5 of maturation to assess the residual IFT20 expression and we selected for further analysis only the samples whose cells were at least 50% IFT20KO (Fig.14A).

With the aim to dissect the MPR retrograde traffic in IFT20-depleted CTLs, we set up a recycling assay that exploits the pool of MPRs that follows the constitutive secretion pathway and is associated with the plasma membrane. We incubated the cells with an anti-MPR antibody at 37°C for 4 hours to allow recycling of the antibody-tagged MPRs. These were then detected by confocal microscopy after staining with fluorochrome-labelled secondary antibodies. Cells were co-stained for tgn38, a marker of the TGN, where the MPR is recycled following bound-soluble hydrolase release into the late endosomes (de Saint Basile *et al.,* 2010). A decrease in the localization of MPR in the region of the TGN was observed in IFT20KO cells (Fig.14B), suggesting that IFT20 may be involved in the retrograde transport of MPR also in CTLs.

Granzyme B is one of the most relevant lytic proteins of the killing arsenal of CTLs, and it is sorted to the secretory granule compartment through a M6P tag (Griffiths *et al.,* 1993). A defective retrograde transport of MPR suggested a potential downstream defect in granzyme B transport to lytic granules. To test this hypothesis, we carried out a confocal microscopy analysis to verify the presence of granzyme B in the lytic granules in IFT20KO CTLs. The integral membrane protein Lamp1 is classically known as a lysosome marker (Cheng *et al.,* 2018), but it is also considered a gold standard marker for the most prevalent type of lysosomes present in CTLs, lytic granules (Blott *et al.,* 2002). The co-localization of granzyme B with Lamp1 was decreased in IFT20KO CTLs compared to control cells (Fig.14C), indicating that granzyme B is not correctly targeted lytic granules of IFT20-depleted CTLs. These results implicate IFT20 in the biogenesis of the main killing-mediating tool of CTLs.

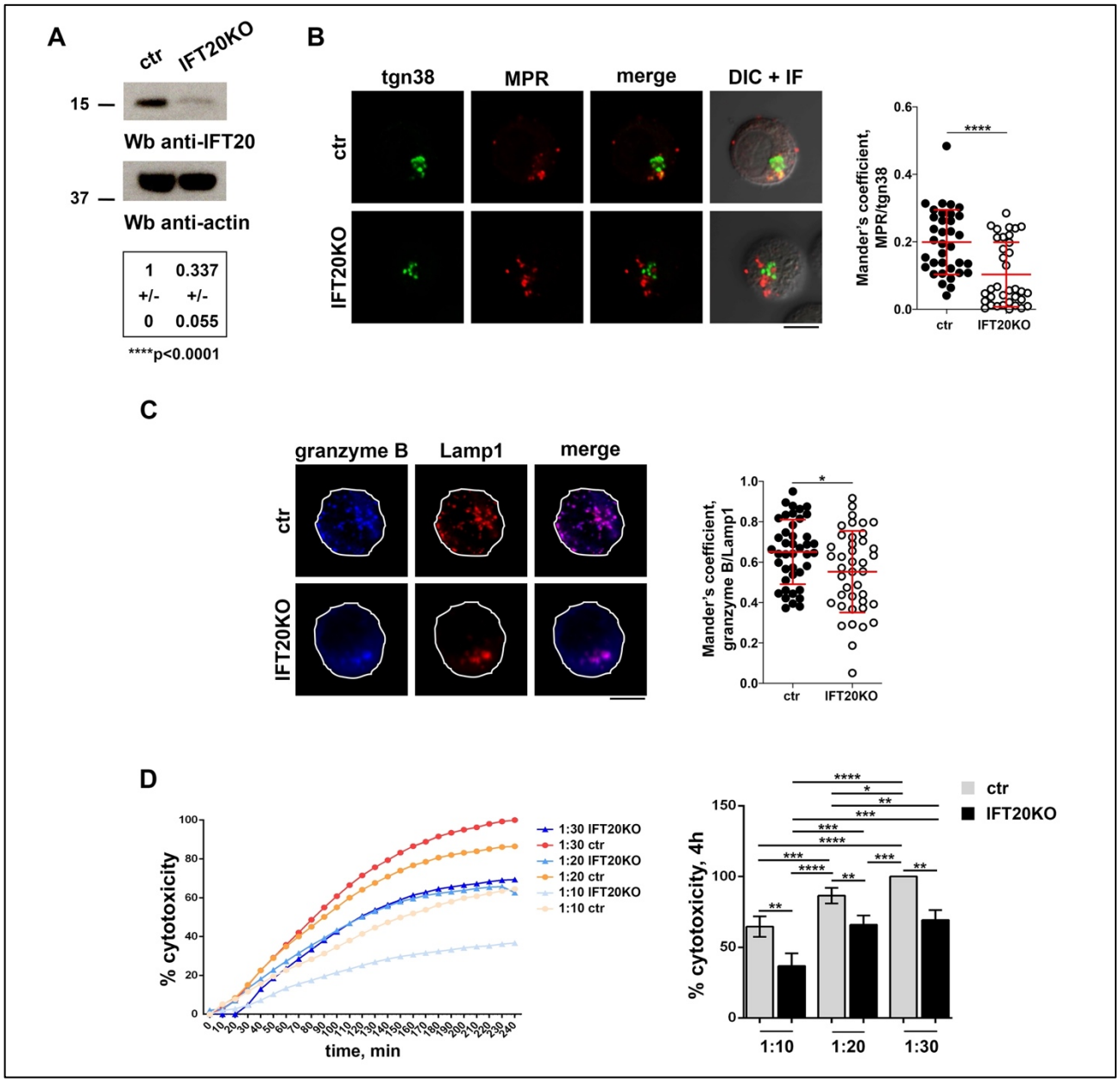

Figure 14| ***IFT20 controls MPR-mediated granzyme B targeting to lytic granules and CTL cytotoxicity.***

(A) Immunoblot analysis of anti-IFT20 antibody of either control or IFT20KO CTL lysates. A control anti-actin blot is shown below. The migration of the molecular mass marker is indicated. The quantification of the relative protein expression normalized to actin is reported below as mean fold ± SD, with control (ctr) value set as 1 (n ≥ 3; one sample t test). **(B,C)** Quantification using Mander's coefficient of the weighted colocalization of either MPR/tgn38 (**B**) or granzyme B/Lamp1 (**C**) in control and IFT20KO CTLs (unpaired t test; 15 cells/sample, n = 3). Representative medial optical sections and overlay of immunofluorescence (IF) and differential interference contrast (DIC) images (IF + DIC) are shown. Scale bars: 5 µm. **(D)** Real-time calcein release-based killing assay.

Control and IFT20KO CTLs were co-cultured with Raji B cells loaded with a mix of Staphylococcal Enterotoxins A, B and E (SAgs) at the indicated target:CTL ratios. Target cell lysis was measured every 10 minutes for 4 hours and reported as kinetic curves in the left graph. The graph on the right shows the percentage of target cell death at the endpoint (4 hours). The data from at least three independent experiments performed in duplicates are expressed as mean fold ± SD, with target cell lysis at the highest target:CTL ratio of the control sample set at 100% of cytotoxicity (ANOVA). *P < 0.05; **P < 0.01; ***P < 0.001; ****P < 0.0001.

Cytotoxic granule exocytosis is the main killing strategy of CTLs (Trapani *et al.,* 2002). Confocal microscopy analysis suggested that the cargo of these organelles was depleted of one of the most active lytic proteins in IFT20-depleted CTLs, therefore we decided to test the cytotoxic activity of IFT20KO cells. A time course analysis of fluorescent calcein release by target cells upon CTL-mediated killing (Chang *et al.,* 2017) revealed that, when IFT20 was depleted, the killing capability of CTLs was impaired at every effector:target cell ratio (E:T) tested (Fig.14D), indicating that IFT20 is required for the cytotoxic activity of CTLs. These data suggest that IFT20 is regulates the efficacy of CTL-mediated killing.

2.3 IFT20 couples the master transcription TFEB that regulates the lysosomal CLEAR network to the biogenesis of lytic granules

Previous work by our lab revealed that IFT20-deficient T cells show lysosomal compartment abnormalities, as not only the average size of their lysosomes is increased but these organelles are also present in reduced number when IFT20 is downregulated (Finetti *et al.,* 2020). This phenotype is consistent with a defect in the biogenesis of lysosomes (Settembre *et al.,* 2013). Consistently, also IFT20-depleted CTLs showed a similar phenotype of the lysosomal compartment, as the number of lysosomes, identified as Lamp1$^+$ vesicles, was decreased and their average size increased (Fig.15A), relating the downregulation of IFT20 to a defective lysosomal biogenesis also in CTLs. Staining CTL secretory lysosomes for granzyme B showed that IFT20-depleted CTLs contained a lower number of granzyme B$^+$ vesicles and their average size was increased compared to control

cells (Fig.15B). This result is a further validation of the lytic granule defect associated to IFT20 deficiency in CTLs, whose lysosome compartments are composed only of lytic granules (Blott *et al.*, 2002).

Lysosomal activity requires the concerted action of hydrolases, the acidification machinery and membrane proteins. The expression and activity of these components must be coordinated to allow optimal lysosomal function in different physiological and pathological conditions. The biogenesis of lysosomes is a process orchestrated by the coordinated lysosomal expression and regulation (CLEAR) gene network and regulated by the transcription factor EB (TFEB) (Settembre *et al.,* 2013). TFEB participates in a lysosome-to-nucleus signalling mechanism that conveys information on the lysosomal status to the nucleus to trigger a transcriptional response (Palmieri *et al.*, 2011). Consistent with its role as a modulator of the CLEAR network, TFEB positively regulates the expression of lysosomal genes, controls the number of lysosomes, and promotes the ability of cells to degrade lysosomal substrates (Ma *et al.*, 2012). In the case of lysosomal damage, the cell activates a compensatory enhancement of lysosomal component expression an attempt to bring lysosome dynamics back on track (Sardiello *et al.,* 2009). Accordingly, the mechanism activated by IFT20-deficient T cells to compensate for the defect in the lysosomal compartment is the upregulation of the TFEB-driven lysosome biogenesis program, that causes a lysosome enlargement (Finetti *et al.,* 2020). Consistently, we found that the transcription of Lamp1 and cathepsin D genes belonging to the CLEAR gene network, as well as TFEB, the master transcription factor responsible for its coordination (Settembre *et al.,* 2013), were upregulated in IFT20-depleted CTLs (Fig.15C). The activation of CLEAR gene network in IFT20-depleted CTLs not only further confirms a possible participation of IFT20 in the biogenesis of lytic granules but may also lead to the characterization of the mechanisms controlling the biogenesis of CTL cytotoxic granules.

Considering the lysosomal origin of lytic granules, we hypothesized that TFEB may take part in the biogenesis of lytic granules as well. The quantification of the expression of some lytic granule components revealed that IFT20KO CTLs upregulate the transcription of granzyme A, granzyme B, perforin, serglycin and granulysin (Fig.15D). Additionally, the

protein levels of granzyme B were upregulated in IFT20KO CTLs compared to control cells (Fig.15E).

The upregulation of secretory lysosome components at both transcriptional and protein levels in CTLs may suggest that TFEB coordinates not only lysosome but also lytic granule biogenesis. With the aim to deeper investigate the possible involvement of the CLEAR gene network in the biogenesis of cytotoxic granules, we decided to over-express TFEB in CTLs (Fig.15F, left). In agreement with the literature, we found that the transcription of Lamp1 and cathepsin D from the CLEAR gene network were upregulated as a consequence of TFEB overexpression (Fig.15F, centre) (Sardiello *et al.,* 2009). Strikingly, gene expression analysis revealed that also lytic granule component genes, namely granzyme A, granzyme B, perforin, serglycin and granulysin, were upregulated in CTLs over-expressing TFEB (Fig.15F, right). This evidence supports the presence of a tight relationship between the assembly of lytic granules and the TFEB-regulated transcription program.

2.4 IFT20 is implicated in SMAP biogenesis

Besides the release of classical lytic granules, the recent discovery of supramolecular attack particles (SMAPs) (Balint *et al.*, 2020) has unveiled an alternative mechanism of CTL-mediated cytotoxicity. While lacking membrane proteins, SMAPs possess a core of canonical lytic granule effectors, namely perforin, granzymes, and serglycin, and a glycoprotein shell, whose most prominent component is thrombospondin-1 (THSB1). Consistent with their lytic cargo, purified SMAPs have the ability to kill cells autonomously (Balint *et al.*, 2020). Classical lytic granule- and SMAP-mediated target cell killing show some differences. When released within the classical granules, perforin and granzymes are immediately available to interact with the target cell, with their release restricted to the IS (Murphy and Weaver, 2016). Conversely, once released by the CTL, SMAPs remain active for hours and thus may act in a different time frame and outside the IS (Ambrose *et al.*, 2020).

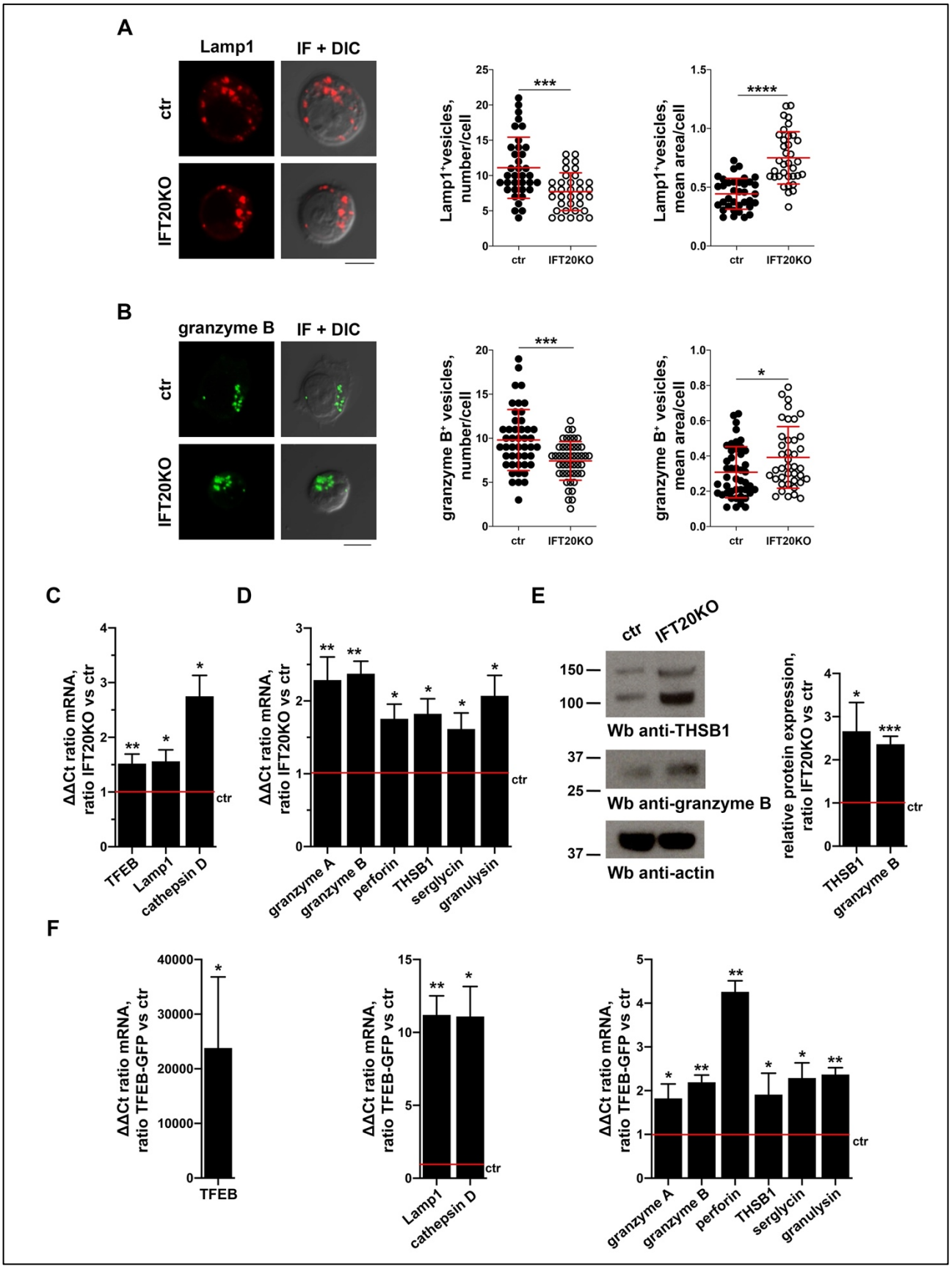

Figure 15| ***IFT20 is involved in the TFEB-driven lytic granule biogenesis program in CTLs.***

(A, B) Immunofluorescence analysis of Lamp1 (**A**) and granzyme B (**B**) in ctr and IFT20KO CTLs. Representative images (medial optical sections) are reported. Scale bars: 5 μm. The graphs show

the quantification of the number of Lamp1$^+$ or granzyme B$^+$ vesicles/cell (left) and their average size (μm^2) (right) (mean ± SD, ≥35 cells from three independent experiments, unpaired t test). **(C, D, F)** Quantitative RT-PCR analysis of TFEB and TFEB-regulated (**C**) and lytic granule component (**D**) genes in control and IFT20KO CTLs (**C, D**)or CTLs transiently transfected either with a construct encoding GFP-tagged TFEB or with the respective GFP empty vector (**F**) (n ≥ 3; one sample t test) (**F**). The relative abundance of gene transcripts was determined on duplicate samples using the ΔΔCt method and was normalized to human 18S. The data (mean ± SD) are expressed as normalized fold expression in IFT20KO or TFEB-GFP *versus* respective control samples, with the expression in control cells set for each gene as 1 (red line). **(E)** Immunoblot analysis with anti-THSB1 and anti-granzyme B antibodies of either control or IFT20KO CTL lysates. An anti-actin control blot is shown below. The migration of the molecular mass marker is indicated. The graph shows the quantification of THSB1 and granzyme B in IFT20KO CTLs as mean normalized fold ± SD, with the expression of each protein in control cells set as 1 (red line). *P < 0.05; **P < 0.01; ***P < 0.001.

Interestingly, CTLs were very recently shown to contain a homogeneous population of smaller granules with a single dense core (SCG), and a heterogenous population of larger granules with multiple dense cores (MCG). Proteomic analysis revealed a remarkably different composition of these two populations, as SCGs are enriched in lysosomal proteins, and hence are very likely to represent the classical lytic granules, while MCGs are enriched in endosomal trafficking regulators. THSB1 was found to selectively associate with MCGs and to be released in particles with a core-shell structure very similar to the SMAPs. SCGs and MCGs released were found to be involved in distinct fusion events, suggesting that the two classes of lytic granules mature and undergo exocytosis through independent pathways (Chang *et al.*, 2022).

As novel evidence revealed the existence of distinct population of lytic granules (Chang *et al.*, 2022), we analysed the gene expression of THSB1 in IFT20-depleted CTLs to assess the potential role of IFT20 in SMAP biogenesis. Interestingly, we detected an upregulation of THSB1 mRNA and protein in IFT20KO CTLs compared to control cells (Fig.15 D, E).

Collectively, these data highlight a defect in the lysosomal compartment in IFT20-depleted CTLs, as witnessed by the phenotype showed by IFT20KO CTLs. This phenotype can be explained by the accumulation of lytic granule components, which could be due either to increased production or reduced secretory granule exocytosis. According to our data, both these hypotheses could be valid. Indeed, we found that IFT20-depleted CTLs upregulate the biogenesis of lytic granule components, but these fail to reach the lytic granules because of impaired lysosomal targeting. Additionally, the cytotoxic capability of IFT20KO CTLs is reduced, which may be caused by the inability of CTLs to release the lytic granule contents onto the target cell. Besides the participation of IFT20, our work may shed a light on a possible role for the CLEAR gene network in the biogenesis of CTL lytic granules, a pathway that up to date has not been completely elucidated yet.

2.5 IFT20 participates in signalling at the IS of CTLs

T cell responsiveness is orchestrated by the dynamic modulation of the surface TCR. Resting T lymphocytes are characterized by constitutive cycles of TCR exposition, endocytosis and eventually either recycling or degradation (Geisler, 2004). This continuous mechanism subserves a dual function. First, it is a quality control check that ensures the identification and degradation of unsuitable TCR complexes. Additionally, it allows for the formation of an intracellular pool of functional TCRs that can be rapidly mobilized to the IS in response to the engagement of plasma membrane associated TCRs (Onnis *et al.,* 2016). The binding of a peptide-MHC complex triggers surface TCR activation and leads to receptor internalization. This event is followed by either polarized recycling to the plasma membrane or receptor degradation, and by the polarization to the IS of TCRs from the endosomal compartment (Alcover *et al.,* 2000). IFT20 is one of the proteins that promote TCR recycling to the IS downstream centrosome polarization in both Jurkat and primary T cells (Finetti *et al.,* 2009; Finetti *et al.,* 2014). IFT20 is involved in the intracellular trafficking pathway through its association with both Rab5 and TCR on early endosomes. In IFT20-deficient T cells, recycling TCRs accumulate in $Rab5^{+}$ endosomes, which fail to

cluster at the IS despite a normal polarization of the centrosome, indicating that IFT20 controls TCR traffic from early to recycling endosomes (Finetti *et al.,* 2014).

Based on this evidence, we investigated the possible implication of IFT20 in the signals activated after TCR engagement in CTLs. With this aim, we carried out the analysis of conjugates of IFT20-depleted CTLs and Raji B cells pulsed with a mix of superantigens (SAgs), including Staphylococcal enterotoxin A (SEA), Staphylococcal enterotoxin B (SEB) and Staphylococcal enterotoxin E (SEE) to cover a substantial proportion of the TCR Vβ repertoire and hence maximize the number of responding T cells (Fig.16A). Consistently with previous data on IFT20KD Jurkat T cells, we found that synaptic accumulation of TCR is impaired in CTLs, as well as the TCR-related phosphotyrosine (pTyr) enrichment at the IS region. The TCR-signalling defect was not associated to impaired centrosome translocation towards the T-APC interface, as we found centrosome repositioning beneath the IS membrane to occur normally in IFT20-depleted CTLs (Fig.16 B, C).

The IS acts as a platform where signals from the TCR and other co-stimulatory molecules are integrated to initiate and coordinate the T cell activation program (Gaud *et al.,* 2018). The proper assembly of the IS represents a crucial step in CTL lethal hit, as it drives the localized delivery of lytic granules and their release into the synaptic cleft (de Saint Basile *et al.*, 2010). Hence, a defect in the IS formation may concur to the impaired cytotoxic capability of IFT20-depleted CTLs.

Sustained signalling at the IS is fundamental to achieve a successful TCR signal transduction in response to peptide-MHC presentation (Soares *et al.,* 2013), and it crucially relies on the continuous cycles of TCR internalization and recycling that IFT20 contributes to regulate in freshly purified T cells (Finetti *et al.,* 2009; Finetti *et al.,* 2014). We asked whether this function of IFT20 extends to CTLs. Similar to $CD4^+$ T cells, we found that TCR clustering and TCR-dependent pTyr accumulation at the IS induced in response to the antigen binding in CTLs require the presence of IFT20. IFT20 is not required for the MTOC-mediated delivery of CD3-bearing vesicles to the synaptic membrane, as centrosome translocation beneath the IS region occurs normally in IFT20-depleted CTLs. The mechanism that is more likely responsible for the impaired TCR clustering to the IS in

IFT20-depleted CTLs may be a defect in TCR trafficking, that has already been demonstrated to be orchestrated by IFT20 in Jurkat and freshly purified T cells (Finetti *et al.*, 2014). We are planning to test this point experimentally.

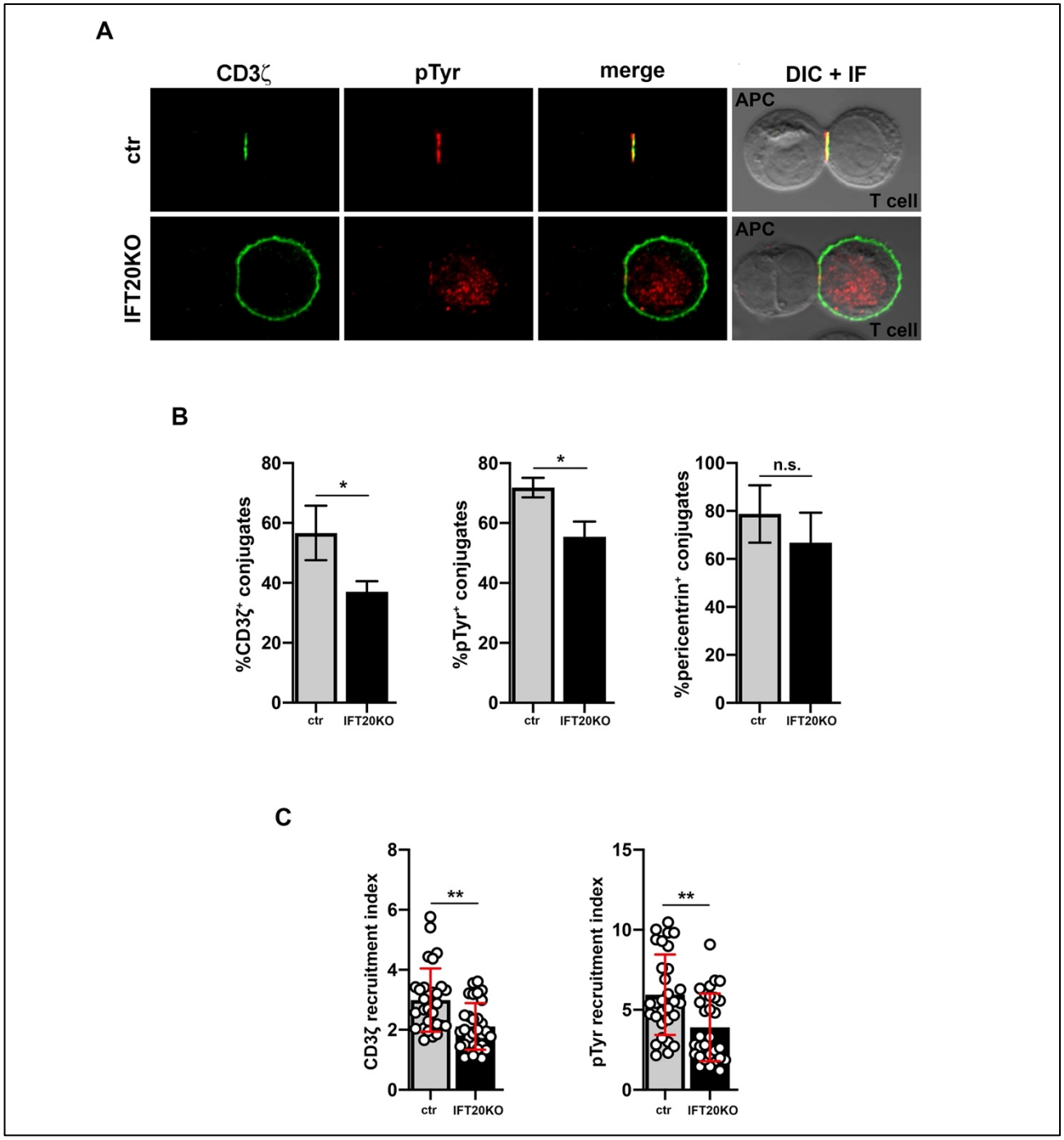

Figure 16| ***IFT20 is required for lytic synapse assembly in CTLs.***

(A) Immunofluorescence analysis of the TCR subunit CD3ζ and tyrosine phosphoproteins (pTyr) 15 min after conjugate formation of control and IFT20KO CTLs and SAg-loaded Raji cells. Medial optical sections of representative images from at least three independent experiments are reported.

Scale bar: 5 μm. **(B)** Quantification of the percentage of conjugates of ctr and IFT20KO CTLs harbouring CD3ζ, pTyr or centrosome marker pericentrin staining at the IS (≥ 30 cells/sample, n ≥ 3; mean ± SD, unpaired t test). **(C)** Relative CD3ζ or pTyr fluorescence intensity at the IS (recruitment index, ≥ 10 cells/sample, n ≥ 3; mean ± SD, unpaired t test). *P < 0.05; **P < 0.01; n.s. not significant.

Collectively, our results place IFT20 at two distinct steps of CTL-mediated cytotoxicity. Indeed, not only does IFT20 participate in the regulation of the biogenesis of lytic granules but it is also required for the vesicular traffic that sustains the signals at the IS, suggesting new implications for IFT20 in the cytotoxic capability of CTLs.

3. The mitotic regulator Polo-like kinase 1 (PLK1) is involved in the IS assembly of CTLs

3.1 Mitotic kinases as new players in IS assembly

The correct assembly of the IS is an essential event during the development of the adaptive immunity, as it is required for the proper activation, proliferation, and differentiation of T cells, hence allowing them to carry out multiple effector functions (Chakraborty *et al.,* 2014). The IS dynamics involve the microtubule-driven translocation of the centrosome beneath the IS membrane, together with the Golgi apparatus. In CTLs, centrosome polarization to the T-APC contact point is a critical step that sustains the secretion of lytic granules into the synaptic cleft (Martin-Cofreces *et al.,* 2014).

The profound changes that characterize the T cell response to an antigen require the transmission of activating signals from the IS to the cytoskeleton. In this regard, a crucial early event is Lck-dependent TCR/CD3 phosphorylation (Palacios and Weiss, 2004), which leads to receptor clustering at the cSMAC during IS maturation (Lee *et al.,* 2002). These early signals are amplified by the recruitment and phosphorylation beneath the IS membrane of a number of cytosolic enzymes and adaptors that propagate the activation signal. The network that is required for the transmission of the signals downstream TCR activation is hugely complex and, among the plethora of molecules involved in this process, the kinase Aurora-A (AurA) has recently emerged as a novel effector, promoting not only early T cell activation but also downstream effector functions (Blas-Rus *et al.,* 2016).

AurA is a serine/threonine kinase classically involved in cell cycle progression at the onset of mitosis, playing a critical role in centrosome and spindle dynamics. AurA expression and activity peak in late G2, when the protein is concentrated at the centrosomes (Carmena *et al.,* 2003). During centrosome maturation, AurA promotes microtubule assembly by recruiting nucleation and stabilization factors (Sardon *et al.,* 2008). Besides its role in cell cycle progression, the capability of AurA to orchestrate microtubule dynamics is extended also to the IS maturation in $CD4^+$ T lymphocytes. Interestingly, AurA is activated upon TCR stimulation and regulates the growth of the microtubules arising from the MTOC in

response to the signals downstream TCR triggering. The inhibition of AurA activity is associated with a decreased number of nucleated microtubules near the contact area which affects the polarized movement of CD3ζ-bearing vesicles to the IS and leads to impaired TCR clustering at the synaptic membrane. Furthermore, specific inhibition of AurA affects Lck activation and localization, thereby impairing the activation of TCR/CD3 complex-derived signals and preventing T cell activation (Blas-Rus *et al.,* 2016). Hence, AurA contributes to both early and late signalling events in T cells.

The mitotic regulator Polo-like kinase 1 (PLK1) is a substrate of AurA controlling the dynamics of the centrosome during cell cycle progression (Joukov *et al.,* 2018). The PLK family comprises five members, of which PLK1 is the most extensively characterized. A defining feature of PLKs is the presence of the C-terminal polo box domain (PBD), involved in the control of the kinase activity and target specificity. By means of its PBD, PLK1 docks into a myriad of proteins to perform critical mitotic functions (Reinardt *et al.,* 2013). The full activation of PLK1 requires not the only conformational changes caused by the PBD docking but also the phosphorylation of the kinase in a region known as the activation loop or T-loop (Xu *et al.,* 2013).

PLK1 is a key regulator of mitosis initiation. PLK1 expression is elevated in actively proliferating cells and is significantly different among the stages of the cell cycle. Several regulatory events coordinate the spatiotemporal dynamics of PLK1 activity (Joukov *et al.,* 2018). The expression of PLK1 is cell cycle dependent, as this kinase is barely detectable in G1 and S phases, gradually increases in G2 phase and peaks in M phase (Schmucker *et al.,* 2014), when its kinase activity is highest. After the completion of cell division, PLK1 expression declines and then moves into the next loop of cell cycles. Co-factors and kinases regulate the phosphorylation of the residues that are involved in PLK1 activation, thereby regulating its activity at multiple steps in the cell cycle. Among these kinases, AurA and its co-factor Bora activate PLK1 at its T-loop Thr210 residue to promote cell entry into mitosis (Bruinsma *et al.,* 2014).

During the cell cycle, the main PLK1 functions start in G2, during which it localizes to centrosomes. The centrosome is the major microtubule-organizing centre (MTOC) in

animal cells and is composed of two microtubule-based cylinders, the centrioles, which are surrounded by pericentriolar material (PCM). The centrioles maintain centrosome organization, while the PCM, which is highly enriched in γ-tubulin, is responsible for nucleating microtubule growth. Centrosomes duplicate at each cell cycle. Duplication starts at the G1/S transition and assembly occurs in the S phase. Subsequently, centrosomes undergo maturation at the end of G2, acquiring the ability to nucleate a higher number of microtubules characterized by increased dynamicity, and separate during mitotic phase. Within the centrosome, centriole assembly and maturation are pursued in a parallel manner. An important event that coordinates the centrosome cycle with the cell cycle is centriole disengagement within the centrosome, which occurs at the exit from mitosis and is required for centrioles to duplicate for the next cell cycle. PLK1 is a major mediator of centrosome maturation, separation, and centriole disengagement, orchestrating the coordination of these events within the cell cycle (Zitouni *et al.,* 2014).

Beyond cell cycle, a growing body of evidence describes additional roles of PLK1, more specifically in DNA damage response (Van Vugt *et al.*, 2004), chromosome instability (Liccardi *et al.*, 2019), autophagy (Ruf *et al.*, 2017), and apoptosis (Shao *et al.*, 2018). Furthermore, PLK1 has an indisputable role in cancer, as it controls several key transcription factors and promotes cell proliferation, transformation, and epithelial-to-mesenchymal transition (Iliaki *et al.,* 2021). Early observations on the overexpression of PLK1 in human tumours (Holtrich *et al.,* 1994) and the inhibition of cellular proliferation following neutralizing anti-PLK1 antibody treatment into HeLa cells (Lane *et al.,* 1996) initiated a series of studies evaluating a broad spectrum of inhibitors aiming to test the potentiality of PLK1 as a target for cancer therapy (Strebhardt, 2010). The identification of PLK1 as a functional node in the oncogenic network proved to be key in the advancement of effective therapies and led to intensive efforts to develop potent and specific small molecules that inhibit PLK1 activity (Liu *et al.,* 2017).

The ATP-binding pocket of kinases is a classical target for the design of inhibitors. The small molecule BI2536 is a highly selective ATP-competitive inhibitor of PLK1, that engages in a network of interactions involving residues from the N-terminal and C-terminal

lobes of the kinase domain (Kothe *et al.,* 2007). BI2536 treatment inhibits the proliferation of various tumour cell lines from different tissues by blocking cancer cells in the metaphase of mitosis and leading to apoptosis (Steegmaier *et al.,* 2007; Liu *et al.,* 2017). A number of studies have revealed that targeting PLK1 may be an effective strategy to control cancer cell proliferation (Liu *et al.,* 2017). However, PLK1 inhibitors, including BI2536, have not achieved a satisfactory therapeutic effect in clinical trials (Gutteridge *et al.,* 2016). One main reason is the dose-limiting toxicities of these molecules (Degenhardt *et al.,* 2010).

In addition to its several and well characterized roles in cell cycle progression, we hypothesize that PLK1-driven centrosome dynamics may be relevant also in T lymphocyte functions. The demonstration that its upstream regulator AurA is involved in the T cell activation through its capability of regulate TCR activation and microtubule dynamics (Blas-Rus *et al.,* 2016) opened the way for the investigation of the potential involvement of PLK1 in the assembly of the IS of CTLs.

3.2 PLK1 is recruited to the IS of CTLs

The localization of PLK1 at the centrosome is well described in several cell types (Colicino *et al.,* 2018), however its localization in T lymphocyte has not been investigated as yet. Hence, we first addressed this point in CTLs.

Before mitotic entry, pericentriolar material 1 (PCM1), a centriolar satellite protein, recruits PLK1 to the pericentriolar matrix, where PLK1 is activated by AurA (Wang *et al.,* 2013). We carried out a confocal microscopy analysis on CTLs at days 5 to 7 of differentiation and the co-localization analysis of PLK1 and PCM1 showed that the centrosome localization of PLK1 is conserved in T lymphocytes (Fig.17A, upper panel). We further confirmed this subcellular localization by co-staining with an additional centrosome marker, γ-tubulin (Fig.17A, lower panel).

To assess whether this mitotic regulator could be directly involved in centrosome dynamics at the IS, we first investigated the localization of PLK1 during the IS formation. Consistent with our hypothesis, PLK1 not only maintains a centrosomal localization in CTLs following antigen-specific engagement by APC, but it is also recruited to the CTL subsynaptic region

(Fig.17B). We carried out the analysis at either 5 or 15 minutes after conjugate formation, to visualize the events taking place at a stage when the IS has not yet achieved its final architecture *versus* a fully mature IS (de la Roche *et al.,* 2016). Interestingly, PLK1 is recruited beneath the synaptic membrane of CTLs at an early stage of IS maturation, suggesting that it might be involved in early events leading to CTL-mediated killing.

The kinase activity of PLK1 depends on its own phosphorylation. Immunoblot analysis of the phosphorylated form of PLK1 (pPLK1) in CTLs revealed that, while the active form of PLK1 is barely detectable in unstimulated cells, there is a sharp increase in the presence of the activated protein following TCR engagement by anti-CD3 mAb in CTLs, with the highest levels detected at the earliest time point (Fig.17C). Hence, TCR engagement promotes PLK1 phosphorylation and activation in CTLs.

To assess the specific localization of activated PLK1 following TCR engagement in CTLs, we performed a confocal microscopy analysis of pPLK1 in CTLs conjugated with either SAg-pulsed or unpulsed Raji B cells. While in unspecific conjugates pPLK1 remains localized at the centrosome, SAg-specific conjugates were characterized by the accumulation of pPLK1 at the IS membrane of CTLs (Fig.17D), clearly showing that TCR triggering promotes the recruitment of pPLK1 to the IS. Of note, we also detected an accumulation of pPLK1 in a perinuclear region (Fig.17D), a localization consistent with the reported activity of PLK1. Indeed, while PLK1 is phosphorylated on Thr210 in the cytoplasm by AurA and its co-factor Bora (Bruinsma *et al.,* 2014), PLK1 translocation to the nucleus seems to be required target phosphorylation, as downstream target phosphorylation by PLK1 first occurs in the nucleus (Bruinsma *et al.*, 2015).

Hence, our preliminary results on the PLK1-mediated orchestration of centrosome dynamics at the IS show not only that PLK1 is phosphorylated following TCR engagement in CTLs, but also that the phosphorylated form of PLK1 accumulates at the IS membrane, supporting the hypothesis that this mitotic regulator may have a function at the CTL IS.

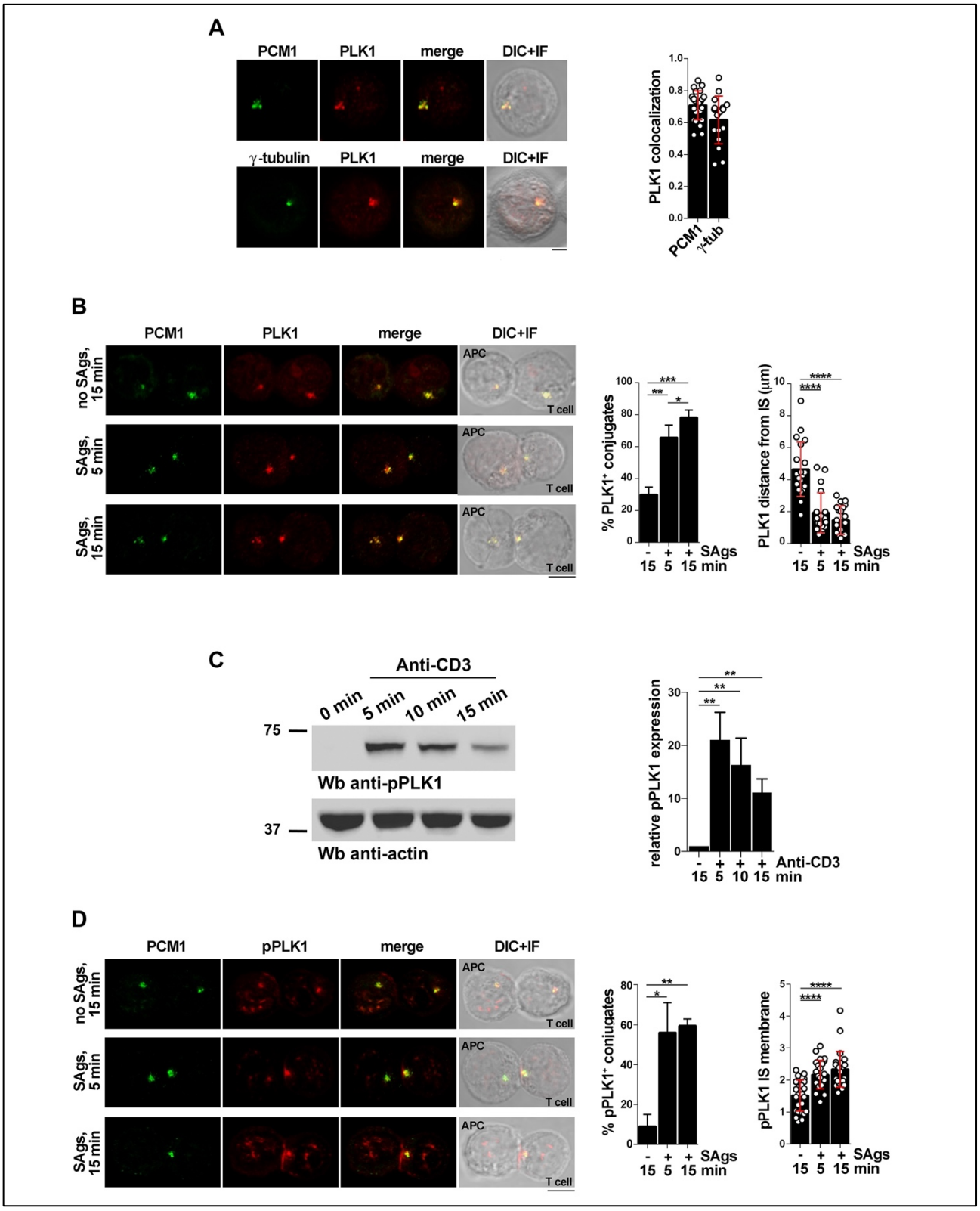

Figure 17| ***PLK1 is phosphorylated and recruited to the IS in CTLs.***

(A) Quantification using Mander's coefficient of the weighted colocalization of PLK1 and centrosome markers PCM1 or γ-tubulin, respectively, in CTLs (30 cells/sample, n = 3; mean fold ± SD). Medial optical sections of representative images are shown. Scale bar: 1 µm. **(B)** Immunofluorescence analysis of PLK1 and PCM1 in 5 or 15 minutes CTL:APC conjugates.

Conjugates formed in the absence of SAgs (no SAgs) were used as negative control. Scale bar: 5 μm. The graphs show the percentage of conjugates with PLK1 polarization to the IS (15 cells/sample, n = 3; ANOVA) and the quantification of the distance of PLK1 from the IS membrane (μm) (20 cells/sample, n=3; Kurskall Wallis test), respectively. **(C)** Immunoblot analysis with anti-pPLK1 antibody of CTL lysates either unstimulated or stimulated with anti-CD3 mAb for the indicated times. An anti-actin control blot is shown below. The migration of molecular mass marker is indicated. The quantification of PLK1 phosphorylation is reported in the graph (n=3; mean fold ± SD, one sample t test). **(D)** Immunofluorescence analysis of p-PLK1 and PCM1 in 5 or 15 minutes CTL:APC conjugates. Scale bar: 5 μm. The graphs show the percentage of conjugates harbouring accumulation of the phosphorylated form of PLK1 at the IS region (15 cells/sample, n = 3; mean ± SD, ANOVA) and the quantification of pPLK1 fluorescence intensity at the IS membrane (μm) (24 cells/sample, n=3; mean ± SD, Kurskall Wallis test), respectively. *P < 0.05; **P < 0.01; ***P < 0.001; ****P < 0.0001.

3.3 CTLs show an altered IS structure following PLK1 inhibition

To investigate the potential role of PLK1 at the IS of CTLs we took advantage of the highly selective ATP analogue BI2536, which inhibits PLK1 enzymatic activity at low nanomolar concentrations (Steegmaier *et al.,* 2007).

T cell activation requires the intracellular transduction of the signals emanated from the MHC-engaged TCR. The likelihood of a single receptor to initiate signalling upon ligand binding depends on the spatial reorganization of TCR complexes, with TCRs in dense clusters having the highest signalling efficiency (Pageon *et al.,* 2016). Furthermore, the polarized delivery of TCR/CD3-containing vesicles is necessary for the sustained signalling at the IS (Onnis and Baldari, 2019) and was recently proved to be impaired in the case of inhibition of the upstream PLK1 activator AurA (Blas-Rus *et al.,* 2016). Consistent with a possible involvement of PLK1 activity in the assembly of the IS in CTLs, confocal microscopy analysis of CTLs and SAg-loaded Raji B cells conjugates revealed that the synaptic accumulation of CD3ζ component of the TCR complex is decreased in BI2536-treated CTLs (Fig.18A). The entity of the defect was measured not only by the quantification of the T-APC conjugates positive for TCR accumulation at the IS (Fig.18B,

left) but also through the CD3ζ recruitment index, a value expressing the ratio of the fluorescence of CD3ζ at the IS compared to the fluorescence in the total cell membrane (Fig.18B, right). Taken together, these data show that the inhibition of PLK1 interferes with the recruitment of TCR complexes to the IS in CTLs.

The process of polarized TCR clustering is facilitated by the translocation of the centrosome towards the APC (Finetti *et al.*, 2015). The defective TCR clustering to the IS, as well as the central role of PLK1 activity for centrosome maturation during cell cycle, led us to investigate the potential outcomes of PLK1 pharmacological inhibition in centrosome translocation beneath the IS following TCR engagement. We performed confocal microscopy analysis of both the centrosome and lytic granules in conjugates of CTLs, either pre-treated with BI2536 or untreated, and conjugated with either SAg-loaded or unloaded Raji B cells (Fig.18A). Then we carried out different types of analysis to investigate the potential architectural aberrations of the IS when PLK1 was inhibited. The quantification of the percentage of conjugates positive for centrosome translocation towards the IS membrane revealed that this mechanism is impaired in BI2536-treated CTLs (Fig.18C, left). Furthermore, in physiological conditions, the distance of the centrosome from the IS membrane decreases in SAg-specific conjugates compared to non-pulsed samples, as the centrosome moves towards the maturating IS (Cassioli and Baldari, 2022). At variance, the distance of the centrosome from the IS membrane was increased in BI2536-treated cells compared to controls (Fig.18C, right), indicating that the treatment with the inhibitor impairs the polarization of the centrosome towards the IS.

We hypothesized that the impaired TCR/CD3 complex accumulation at the IS in CTLs following BI2536 treatment could be caused by defective TCR signalling, a speculation based also on the evidence that the PLK1 upstream activator AurA takes part in early TCR activation by helping Lck phosphorylation (Blas-Rus *et al.,* 2016). To assess the potential role of PLK1 in TCR signalling, we performed the immunoblot analysis of the active form of proteins that belong to the canonical signalling cascade downstream the TCR activation in response to anti-CD3 antibody binding (Bhattacharyya *et al.*, 2020). While TCR triggering induces the accumulation of the active form of LAT and Erk in untreated samples,

the analysis of BI2536-treated CTLs revealed a reduction in LAT and Erk phosphorylation when PLK1 activity was inhibited (Fig.18D). Taken together, this evidence suggests that the impaired TCR clustering at the IS following PLK1 inhibition prevents TCR activation.

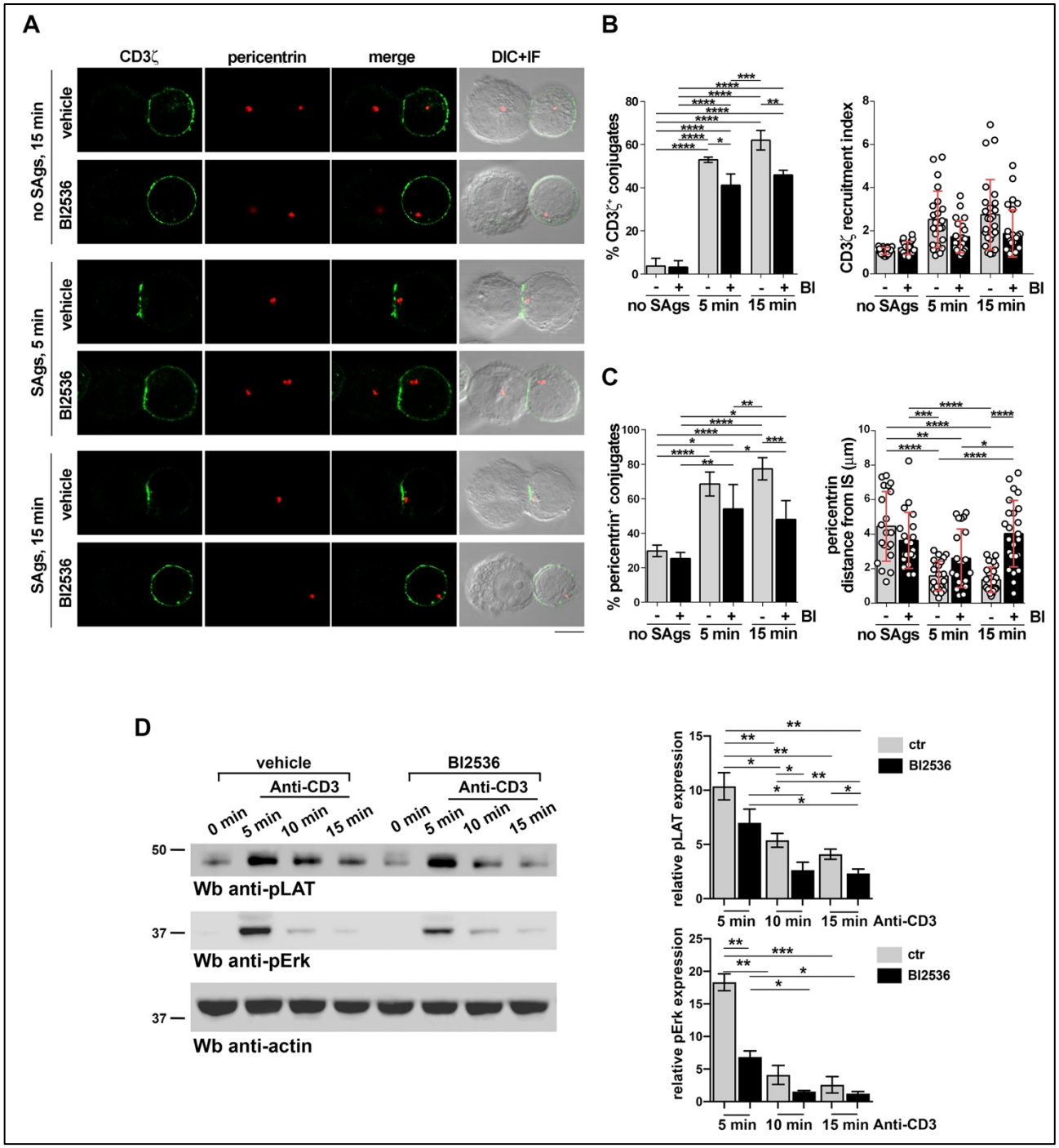

Figure 18| ***PLK1 inhibition impairs TCR signalling in CTLs.***

(A) Immunofluorescence analysis of CD3ζ and pericentrin in CTLs pre-treated with either vehicle or BI2536, mixed with Raji cells (APCs) either unpulsed or pulsed with SAgs, and incubated for 5 or 15 min at 37°C. Representative images of medial optical sections are shown. Scale bar: 5 μm. **(B)**

Quantification of percentages of conjugates positive for CD3ζ polarization to the IS (left) and of relative CD3ζ fluorescence intensity at the IS (recruitment index, right) (20 cells/sample, n ≥ 3; ANOVA) is reported in the graphs. **(C)** The graphs show the percentage of conjugates with pericentrin polarization to the IS (left) and the quantification of the distance of pericentrin-stained centrosome from the synaptic membrane (right) (μm) in conjugates of either control or BI2536-treated CTLs and Raji B cells either unpulsed or pulsed with SAgs (20 cells/sample, n ≥ 3; ANOVA). **(D)** Immunoblot analysis with anti-pLAT and anti-pErk antibodies of either control or BI2536-treated CTL lysates, unstimulated or stimulated with anti-CD3 mAb for the indicated times. An anti-actin control blot is shown below. The migration of molecular mass marker is indicated. The graph shows the quantification of pErk and pLAT, respectively (n ≥ 3; mean fold ± SD, one-way ANOVA). *P < 0.05; **P < 0.01; ***P < 0.001; ****P < 0.0001.

Full TCR activation and signal transduction are pivotal for the proper triggering of the killing machinery of CTLs. Despite the initial T cell activation occurs at the plasma membrane, its progression requires the contribution of intracellular components, including the MTOC and the microtubule-dependent vesicular traffic of endosomal TCRs and signalling mediators (Onnis *et al.,* 2016). Consistent with previous data available on its upstream regulator AurA in $CD4^+$ T cells (Blas-Rus *et al.,* 2016), our data suggest that also PLK1 may be required for the proper microtubule-mediated clustering of TCR complexes at the IS membrane of CTLs.

The dynamic reorganization of the microtubule cytoskeleton and centrosome reorientation at the IS is required for T cell effector functions, facilitating the polarized release of cytokines and cytolytic factors (Stinchcombe *et al.,* 2006). Polarized secretion into the synaptic cleft concentrates the lytic moieties delivered to the APC, while minimizing the damage to bystander cells in the surrounding tissue (Bettencourt-Dias *et al.,* 2007; Pihan, 2013). As PLK1 inhibition prevented centrosome translocation towards the IS, we hypothesized that also the related polarization of lytic granules could be impaired. Hence, we carried out a confocal microscopy analysis of granzyme B, used as a marker of cytotoxic granules, and the centrosome marker pericentrin (Fig.19A). The quantification of the percentage of conjugates positive for granzyme B-bearing vesicle polarization at the IS

revealed that this mechanism is impaired in BI2536-treated CTLs (Fig.19B, left). Furthermore, we measured the distance of granzyme B$^+$ granules from the IS and found that, in normal maturating IS, this distance decreases in SAg-loaded *versus* unloaded samples. Conversely, the distance of granzyme B$^+$ vesicles in BI2536-treated SAg-specific conjugates is comparable to the correspondent non-pulsed samples (Fig.19B, right), indicating that PLK1 inhibition affects the polarization of lytic granules towards the IS.

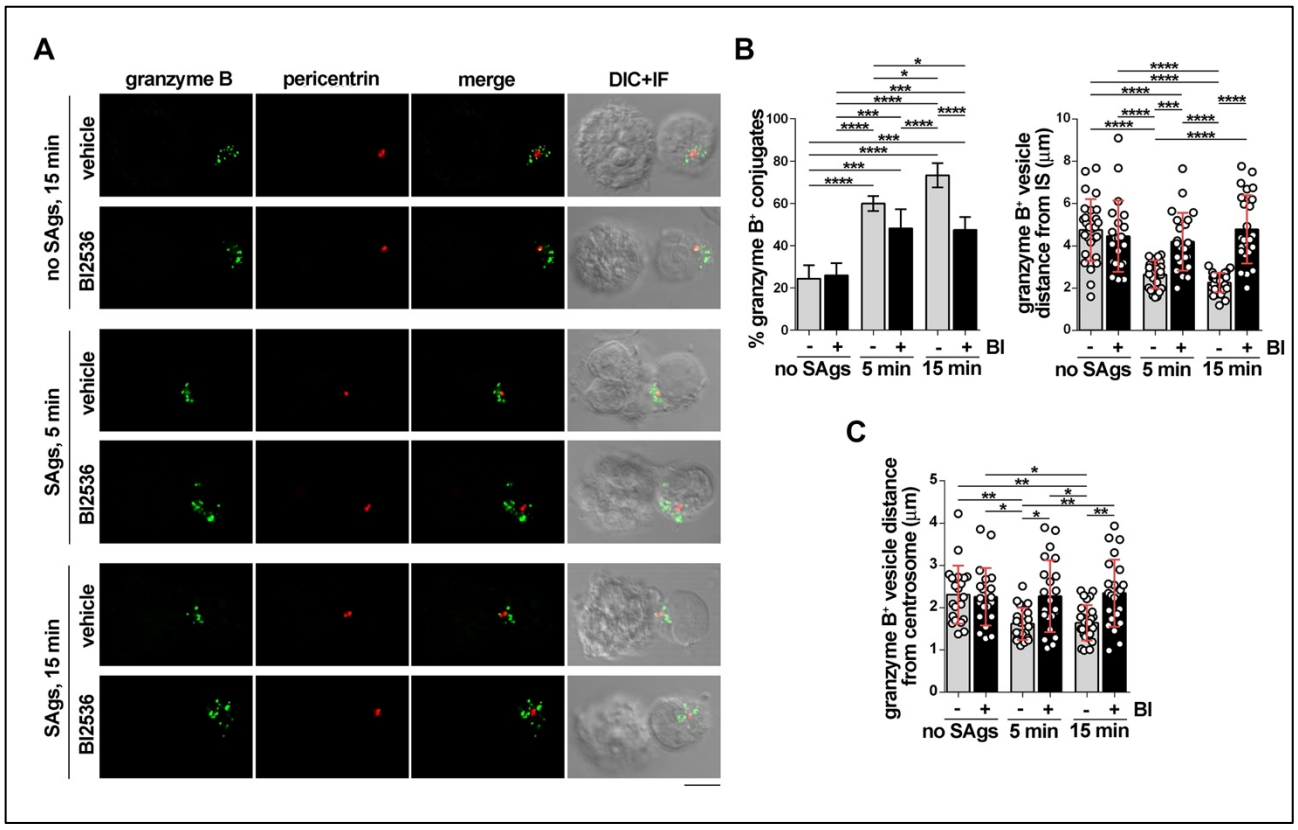

Figure 19| ***PLK1 inhibition impairs lytic granule polarization towards the IS in CTLs.***

(A) Immunofluorescence analysis of the lytic granule component granzyme B and the centrosomal protein pericentrin in 5 and 15 minutes conjugates of vehicle or BI2536-treated CTLs and SAg-pulsed Raji cells. Medial optical sections of representative images are reported in the panel. Scale bar: 5 µm. **(B)** The graphs show the percentage of conjugates with granzyme B polarization to the IS in either control and BI2536-treated CTLs (left) and the quantification of the distance of granzyme B-bearing vesicles from the IS membrane (µm) (right). **(C)** Quantification of the distance of granzyme B$^+$ vesicles from centrosome in 5 or 15 minutes CTL:APC conjugates (µm). **(B,C)** Data are reported as mean ± SD. Statistical analysis: 20 cells/sample, n ≥ 3; ANOVA. *P < 0.05; **P < 0.01; ***P < 0.001; ****P < 0.0001.

The centrosome-mediated delivery of lytic granules to the IS occurs in two distinct steps. TCR signalling triggers an initial convergence of granules towards the centrosome, causing a bolus of granules to be delivered simultaneously with centrosome polarization to the IS (Ritter *et al.,* 2015). To address this point in our model, we measured the distance of granzyme B^+ lytic vesicles from the centrosome in either control or BI2536-treated CTLs. The results showed that this distance was increased when PLK1 activity was inhibited (Fig.19C). Hence, pharmacological inhibition of PLK1 prevents the convergence of lytic granules towards the centrosome. These results highlight a role for PLK1 in orchestrating the correct architecture of the CTL IS, with a potential impact on the delivery of the lethal hit.

3.4 PLK1 is required for the cytotoxic activity of CTLs

Polarized clustering of the lytic granules at the IS secretory region is a central event for the delivery of the CTL lethal hit. The secretion of lytic granules occurs following distinct pathways. Rapid secretion of lytic granules upon target cell encounter can occur even in the absence of centrosome translocation towards the IS membrane (Bertrand *et al.,* 2013). However, even though lytic granule secretion is swiftly triggered in CTLs by TCR engagement as an immediate response to peptide-MHC, the polarization of the CTL lytic machinery ensures the prolonged and confined secretion of lytic molecules towards the target cell. Multiple studies have associated delayed or impaired centrosome reorientation with reduced cytotoxicity (Quann *et al.,* 2009; Tsun *et al.,* 2011; de la Roche *et al.,* 2013; Jenkins *et al.,* 2014). Of note, microtubule integrity is required for efficient cytotoxicity (Mastrogiovanni *et al.,* 2020). The evidence provided above suggests that the pharmacological inhibition of PLK1 leads to the formation of a structurally aberrant IS, which can be expected to result in defects in cytotoxicity. To test this hypothesis, we performed a time course analysis of fluorescent calcein release by target cells induced by either BI2536 treated or untreated CTLs (Chang *et al.,* 2017). Consistent with our observations, the killing capability of CTLs was impaired at every effector:target cell ratio

(E:T) tested (Fig.20) when PLK1 kinase activity was inhibited, providing a direct proof of a defect in CTL-mediated killing in the presence of the PLK1 inhibitor.

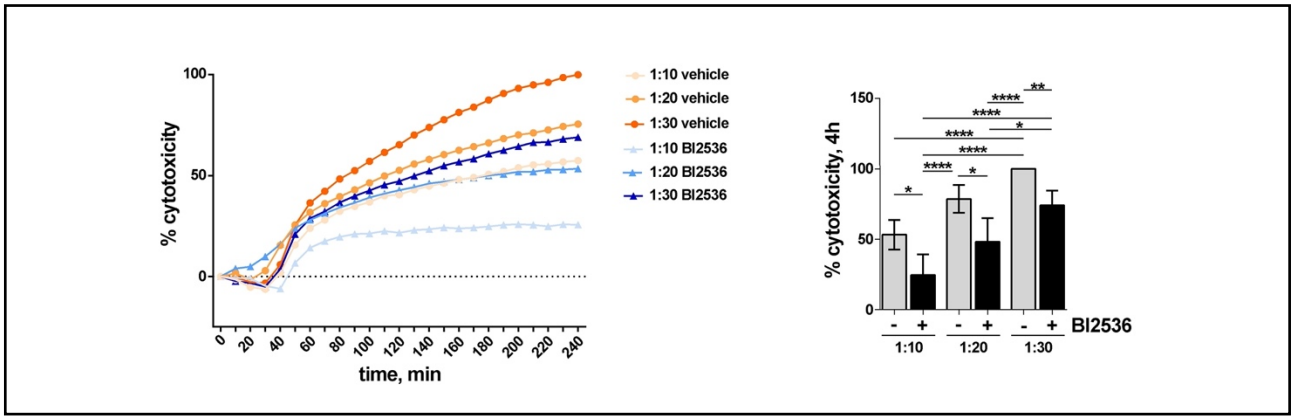

Figure 20| PLK1 inhibition impairs the cytotoxic capability of CTLs.

Real-time calcein release-based killing assay. CTLs either untreated or pre-treated with BI2536 were incubated with SAg-loaded Raji B cells at the target:CTL ratios indicated in the panel, and target cell killing was measured every 10 minutes for 4 hours as reported in the kinetic graph (left). The percentage of target cell death at the endpoint of the assay (4 hours) is shown on the right graph (≥3 independent experiments performed in duplicates, mean fold ± SD, target cell lysis at the highest target:CTL ratio of the control sample set at 100% of cytotoxicity, ANOVA). *P < 0.05; **P < 0.01; ***P < 0.001; ****P < 0.0001.

Collectively, these results reveal the presence of PLK1 in the killing arsenal of CTLs through the participation of this mitotic regulator in the process of lytic synapse assembly.

3.5 PLK1 inhibition affects microtubule architecture in CTLs

The polarized release of the lytic granule contents at the IS ensures effective CTL killing. Despite the precise role of the centrosome during the cytotoxic response remains elusive (Tamzalit *et al.,* 2020), our work provides further evidence supporting the importance of centrosome polarization in CTL-mediated killing.

Upon TCR stimulation, microtubule filaments are anchored to the pSMAC and mediate the recruitment of the centrosome to the contact zone. Some microtubules bend at the contact site, suggesting the presence of microtubule motor proteins anchored at the cell cortex,

which act on microtubules to pull the MTOC towards the IS (Kuhn and Poenie, 2002). Microtubules are large polymers composed of α/β-tubulin dimers that control intracellular organelle distribution and trafficking (Etienne-Manneville, 2010). These components of the cytoskeleton are endowed with an intrinsic polarity, with minus-ends anchored to the centrosome to avoid rapid depolymerization (Li *et al.,* 2008) and plus-ends characterized by dynamic instability. After centrosome polarization, microtubules actively polymerize at the IS. Interestingly, altering microtubule plus-end dynamics delays MTOC reorientation and movement of vesicles at the IS (Martin-Cofreces *et al.,* 2012), underling the importance of microtubule plasticity in the establishment of a functional IS.

During the IS maturation, the microtubule network organized around the centrosome subserves several functions, including TCR accumulation at the IS, vesicle movement for polarized secretion and maintenance of the contact area at the T-APC interface (Kopf and Kiermaier, 2021). Furthermore, microtubule dynamics are crucial for proper centrosome polarization towards the IS, a mechanism that we found impaired in PLK1-inhibited CTLs. In the light of the crucial role of PLK1 in orchestrating microtubule dynamics (Zitouni *et al.,* 2014), we hypothesized that the defective centrosome translocation that we detected following PLK1 inhibition in CTLs, and hence all the related IS dysfunctions, could be related to altered microtubule dynamics in our model. To address this point, we investigated the microtubule cytoskeleton architecture following TCR engagement in either BI2536-treated or untreated CTLs. To follow the microtubule organization at different time points following TCR engagement, CTLs were plated on slides coated with anti-CD3 mAb and fixed after 5, 15 or 30 minutes of stimulation at 37°C (Balagopalan *et al.*, 2018). Confocal microscopy analysis of the β-subunit of microtubule tubulin revealed that, upon TCR engagement, control CTLs reorientate the centrosome towards the anti-CD3 mAb-coated slides, and they show thin and copious microtubule filaments radiating from the MTOC at all the stimulation times tested (Fig.21A, upper panel). When PLK1 activity was inhibited, microtubules organized in thick and less numerous bundles compared to control cells (Fig.21A, lower panel). We compared the different rearrangement of microtubules in both conditions by measuring the ratio of the fluorescence of β-tubulin at the centrosome

versus the entire cell, obtaining a ratio of microtubule nucleation from the MTOC. The analysis revealed that this ratio was decreased in BI2536-treated CTLs compared to control cells (Fig.21B), indicating that, upon TCR engagement, the nucleation of microtubules from the centrosome is altered upon PLK1 inhibition.

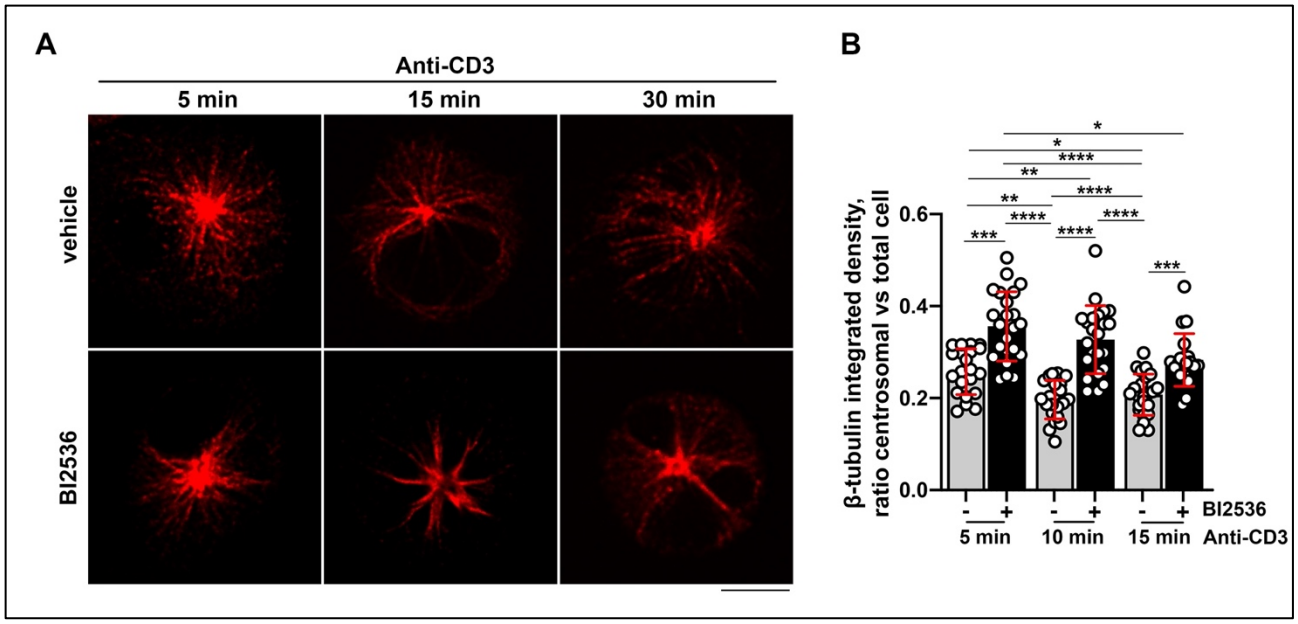

Figure 21| ***PLK1 inhibition impairs microtubule dynamics induced by TCR triggering in CTLs.***
(A) Immunofluorescence analysis of β-tubulin in control and BI2536-treated CTLs. Cells were plated on anti-CD3 mAb-coated slides for the indicated times. Representative images of Z-stack projections are shown. Scale bar: 5 μm. **(B)** Quantification of the relative density of fluorescence of β-tubulin at the centrosome, compared to the whole cell (15 cells/sample, n = 3; mean ± SD, ANOVA). *P < 0.05; **P < 0.01; ***P < 0.001; ****P < 0.0001.

The alteration in microtubule nucleation following PLK1 inhibition underlies the mechanism affecting IS assembly and cytotoxic capability of BI2536-treated CTLs. We hypothesized that PLK1 inhibition causes an impairment in centrosome dynamics due to defective microtubule nucleation upon TCR triggering in CTLs. Our data indicate that the impaired nucleation of microtubules from the centrosome may affect polarized secretion and vesicular trafficking at the IS. Accordingly, lytic granules are thought to traffic along microtubules to polarize towards the IS (Ritter *et al.,* 2015). Hence the thick bundles in

which BI2536-treated CTLs organize their microtubules may impair efficient cytotoxic granule trafficking.

The mechanisms behind the specification of the precise site of lytic granule exocytosis are still open to debate and there are multiple models that may be complementary. In this regard, pioneer studies demonstrated that the centrosome promotes cytotoxic specificity by guiding lytic granules to the IS for directional secretion (Stinchcombe *et al.,* 2006; Ritter *et al.,* 2015). More recent findings suggested that other mechanisms may join the CTL killing specificity, as it was demonstrated that altered microtubule architecture impairs the cytotoxic capability of CTLs but has no outcome on the polarization of lytic granules, the directionality of cytolytic secretion and the specificity of target cell killing (Tamzalit *et al.,* 2020). This study suggested that the microtubule cytoskeleton does not completely control the precise site of cytotoxic granule fusion and has a more determinant role in facilitating the efficient delivery of lytic granules to the cell surface. The model is consistent with a previous work indicating that target cell killing can occur prior to MTOC polarization (Bertrand *et al.,* 2013). If the microtubule cytoskeleton is not capable of determining the precise location of granule docking and fusion alone, other factors must be considered. Lytic granule exocytosis is known to occur at IS domains that have been depleted of F-actin, hence becoming accessible for vesicle fusion (Rak *et al.,* 2011; Brown *et al.,* 2011). However, granules do not fuse at actin-cleared regions outside the IS, implying that other factors must be involved. In this regard, signalling lipids, namely phosphatidylinositol and diacylglycerol, are interesting candidates. They not only orchestrate regulated secretion and polarity in other cell types (Balla, 2013) but they also play a central role in the patterning of architectural microdomains within the IS (Quann *et al.,* 2009; Gawden-Bone *et al.,* 2018). Moreover, local Ca^{2+} influx could also be involved, as it drives the regulated fusion at the neuronal synapse (Südhof, 2012).

Besides the debate on the specification of the precise site of secretion, the requirement for microtubule cytoskeleton integrity for the capacity of CTL killing is undeniable. Consistently, our latest findings suggest that microtubule alterations resulting from PLK1

pharmacological inhibition affect the cytotoxic capability of CTLs. Although the mechanism though which PLK1 activity is involved in microtubule orchestration upon TCR triggering in CTLs requires further investigation, we hypothesize that the altered microtubule organization that follows BI2536 treatment may account for the participation of PLK1 in IS formation and related cytotoxic capability of CTLs.

CONCLUSIONS AND PERSPECTIVES

The recent identification of IFT20 as a central regulator of lysosome function opened new perspectives on its ability to control the immune response at a more global level and paved the way to the present work. IFT20 not only indirectly promotes T cell autophagy by regulating the MPR-dependent transport of acid hydrolases to lysosomes (Finetti *et al.*, 2019) but it is also directly involved in autophagosome formation in ciliated cells (Pampliega *et al.*, 2013) and, as reported in this thesis, in the non-ciliated T cells. Our findings identify IFT20 as a new regulator of an early step of basal autophagy in T cells by regulating the localization of ATG16L1 at early endosomes to promote autophagosome biogenesis. Hence, IFT20 exerts a dual role in autophagy, directly promoting autophagosome formation by recruiting ATG16L1 at early endosomes and indirectly allowing for the degradation of the autolysosome contents by controlling lysosome biogenesis (Finetti *et al.*, 2019).

The potential outcomes related to the participation of IFT20 in lysosome biogenesis are not limited to T cell autophagy. Indeed, CTL lytic granules are specialized secretory lysosomes where their leading cytotoxic moieties, the granzymes, are routed through the MPR pathway (de Saint Basile *et al.*, 2010). We have provided evidence that IFT20 is involved in the biogenesis of lytic granules controlling the MPR pathway also in CTLs. Consistently, we found that, possibly as a consequence of defective MPR recycling, the contents of granzyme B in IFT20KO CTL lytic granules was reduced compared to control. The extent of this defect was limited, but this may be due to the presence of alternative sorting pathways. Although the M6P pathway is the primary sorting mechanism, it is becoming clear that alternative receptors are involved in the lysosomal sorting of some soluble proteins. The initial evidence of the existence of alternative receptors came from studies of immortalized cell lines of patients suffering from I-cell disease, a lysosome storage disorder in which the lysosomal hydrolases are not modified with M6P residues. Despite that, some soluble hydrolases normally sorted through the M6P tag can still be delivered to the lysosomes, implying that their transport is necessarily conducted in a M6P-independent

fashion (Rijnboutt *et al.*, 1991). Nonetheless, the M6P-dependent pathway is still the main cellular passageway for transporting soluble hydrolases to lysosomes and, despite the progresses that have been made over the last decades in its characterization (Coutinho *et al.*, 2012), important issues remain unresolved. In particular, the itinerary followed by lysosomal proteins after leaving the TGN, the participation of early *versus* late endosomes and the contribution of different molecular machineries to both forward and retrograde transport processes, still require to be studied. We have addressed in part this last point and found that IFT20 is required for acid hydrolase targeting to lysosomes by orchestrating the post-TGN sorting of the soluble cytotoxic moieties to the MPR pathway. Despite the defect in granzyme B cargo of IFT20KO lytic granules was only partial, the concrete relevance of this defect was demonstrated by the decreased cytotoxic capability of IFT20-depleted CTLs.

Alterations in lysosomal compartment functionality have been linked to a compensatory upregulation of the lysosome biogenesis program by the CLEAR gene network coordinated by the master transcription factor TFEB (Settembre *et al.*, 2013). Consistent with the increased lysosomal biogenesis previously reported in IFT20-depleted T cells, we found an accumulation of some lytic granule components in IFT20KO CTLs. The participation of TFEB in lytic granule biogenesis was further supported by the upregulation of TFEB and CLEAR gene network components in CTLs. We show that TFEB-overexpressing CTLs upregulate the transcription not only of the CLEAR gene network but also of lytic granule component genes, suggesting the interesting possibility that an expanded CLEAR gene network regulates the biogenesis of lytic granules.

The emerging scenario is that IFT20-mediated vesicular trafficking controls crucial processes, spanning from endosome recycling to lysosome biogenesis and T cell function. This evidence has important implications for the development of an effective immune response, as IFT20-deficient T cells are not only characterized by defective autophagy, but they also show impaired activation and differentiation both *in vitro* and *in vivo* in a T cell-specific conditional knockout mouse. The defects are partially due to the ability IFT20 to promote the polarized recycling to the IS of endosome associated TCRs and LAT described

in T cells (Finetti *et al.*, 2009; Vivar *et al.*, 2016). In this thesis we found that TCR clustering and related pTyr enrichment at the IS following cognate peptide-MHC engagement are impaired in IFT20-depleted CTLs, suggesting another level of implication for IFT20 in the cytotoxic capability of CTLs that, similarly to freshly purified T cells, could involve IFT20-related vesicular trafficking. Together, these findings identify IFT20 as a key player in T cell homeostasis, activation, and effector functions.

The proper assembly of the IS represents a crucial event during the development of the adaptive immunity. In the last part of the present work, we investigated the implication of the mitotic regulator PLK1 in IS assembly. We found that PLK1 localizes at the IS and is activated following TCR engagement in CTLs. Interestingly, our data show that the inhibition of PLK1 activity by means of its highly selective inhibitor BI2536 (Steegmaier *et al.,* 2007) leads to the formation of a structurally defective IS. Indeed, TCR clustering at the IS, as well as the translocation of the centrosome towards the T-APC contact point, were impaired in PLK1-inhibited CTLs, and the failure of the TCR to accumulate at the cSMAC may explain the lack of propagation of its signalling cascade. Furthermore, CTL BI2536 treatment prevented not only lytic granule polarization at the IS but also the convergence of cytotoxic granules around the centrosome. Importantly, defects in the architecture of the IS are associated to the impaired cytotoxic capability of BI2536-treated CTLs. Defective CTL cytotoxic capability related to PLK1 enzymatic inhibition represents a crucial finding for BI2536-based therapies. Indeed, the participation of PLK1 in CTL-mediated killing may be a concurring factor in BI2536-related toxicity (Liu *et al.*, 2017).

Finally, as the dramatic structural reorganization that characterize TCR-engaged CTLs requires proper cytoskeleton dynamics (Mastrogiovanni *et al.,* 2020), we hypothesized that the defects that we observed in the assembly of the IS may be linked to the alteration in microtubule architecture following CTL treatment with BI2536. Although this mechanism needs to be better characterized, this work proposes PLK1 as a novel and crucial player in the assembly of the IS and a determinant for effective killing by CTLs.

In conclusion, our work focused on different aspects of T cell homeostasis and effector functions, shedding light on some missing points of the physiology of one of the main players of adaptive immunity.

BIBLIOGRAPHY

Alcover A., Alarcón B. Internalization and intracellular fate of TCR-CD3 complexes. Crit Rev Immunol (2000), 20:325-46.

Amaya C., Fader C., Colombo M. Autophagy and proteins involved in vescicular trafficking. FEBS Letters (2015), 589(22):3343-3353.

Ambrose A.R., Hazime K.S., Worboys J.D., Niembro-Vivanco O. and Davis D.M. Synaptic secretion from human natural killer cells is diverse and includes supramolecular attack particles. Proc. Natl Acad. Sci. USA (2020), 117:23717–23720.

Ao X., Zou L., Wu Y. Regulation of autophagy by the Rab GTPase network. Cell Death and Differentiation (2014), 21:348-358.

Arstila T.P., Casrouge A., Baron V., Even J., Kanellopoulos J., Kourilsky P. A direct estimate of the human B and T cell repertoire diversity. Science (1999); 286:297-329.

Baker S. A., Freeman K., Luby-Phelps K., Pazour G. J., Besharse J. C. IFT20 links kinesin ii with a mammalian intraflagellar transport complex that is conserved in motile flagella and sensory cilia. Journal of Biological Chemistry (2003), 278:34211–34218.

Balagopalan L., Yi J., Nguyen T., McIntire K.M., Harned A.S., Narayan K., Samelson L.E. Plasma membrane LAT activation precedes vesicular recruitment defining two phases of early T-cell activation. Nat Commun. (2018), 9(1):2013.

Balla T. Phosphoinositides: Tiny lipids with giant impact on cell regulation. Physiol. Rev. (2013), 93:1019–1137.

Ballabio A., Bonifacino J. Lysosomes as dynamic regulators of cell and organism homeostasis. Nat. Rev. Mol. Cell. Biol. (2020), 21(2):101-118.

Balint S., Muller S., Fischer R., Kessler B.M., Harkiolaki M., Valitutti S., Dustin M.L. Supramolecular Attack Particles Are Autonomous Killing Entities Released From Cytotoxic T Cells. Science (2020), 368:897-901.

Beal A.M., Anikeeva N., Varma R., Cameron T., Vasiliver-Shamis G., Norris P., Dustin M.L., Sykulev Y. Kinetics of early TCR signalling regulate the pathway of lytic granule delivery to the secretory domain. Immunity (2009), 31(4):632-642.

Beemiller P., Jacobelli J., Krummel M.F. Integration of the movement of signaling microclusters with cellular motility in immunological synapses. Nature Immunology (2012), 13:787-795.

Bertrand F., Müller S., Roh K.H., Laurent C., Dupré L., Valitutti S. An initial and rapid step of lytic granule secretion precedes microtubule organizing center polarization at the cytotoxic T lymphocyte/target cell synapse. PNAS (2013), 110(15):6073-6078.

Bettencourt-Dias M., Glover D. Centrosome biogenesis and function: Centrosomics brings new understanding. Nat. Rev. Mol. Cell Biol. (2007), 8:451–463.

Bhattacharyya N., Feng C. Regulation of T helper cell fate by TCR signal strength. Frontiers in Immunology (2020), 11:624.

Blas-Rus N., Bustos-Moran E., Pérez de Castro I., de Carcer G., Borroto A., Camafeita E., Jorge I., Vasquez J., Alarcon B., Malumbres M., Martin-Cofreces N. and Sanchez-Madrid F. Auora A drives early signalling and vesicle dynamics during T-cell activation. Nature Communications (2016) 7:11389.

Blott E.J., Griffiths G.M. Secretory lysosomes. Nature Reviews Molecular Cell Biology (2002), 3:122-131.

Bootman M.D. Calcium signaling. Cold Spring Harbor Perspectives in Biology (2012), 4:a011171.

Botbol Y., Guerrero-Ros I., Macian F. Key roles of autophagy in the regulation of T-cell function. European Journal of Immunology (2016), 46(6):1326-1334.

Braulke T., Bonifacino J. Sorting of lysosomal proteins. Biochim Biophys Acta (2009), 1793(4):605-614.

Brennan F.M., Foey A.D., Feldmann M. The importance of T cell interactions with macrophages in rheumatoid cytokine production. Current Topics in Microbiology and Immunology (2006), 305:177-194.

Brennan A.J., Chia J., Browne K.A., Ciccone A., Ellis S., Lopez J.A., et al. Protection From Endogenous Perforin: Glycans and the C Terminus Regulate Exocytic Trafficking in Cytotoxic Lymphocytes. Immunity (2011), 34:879-92.

Bronietzki A.W., Schuster M., Schmitz I. Autophagy in T-cell development, activation and differentiation. Immunology and Cell Biology (2015), 93(1):25-34.

Brown A.C., Oddos S., Dobbie I., Alakoskela J., Parton R., Eissman P., Neil M., Dunsby C., French P., Davis I., Davis D. Remodelling of cortical actin where lytic granules dock at natural killer cell immune synapses revealed by super-resolution microscopy. PLoS Biol. (2011), 9:e1001152.

Bruinsma W., Macurek L., Freire R., Lindqvist A., Medema R.H. Bora and Aurora-A continue to activate Plk1 in mitosis. J. Cell Sci. (2014), 127:801-811.

Bruinsma W., Aprelia M., Kool J., Macurek L., Lindqvist A. and Medema R.H. Spatial separation of Plk1 phosphorylation and activity. Front. Oncol. (2015), 5:132.

Burkhardt J.K., Hester S., Lapham C.K., Argon, Y. The lytic granules of natural killer cells are dual-function organelles combining secretory and pre-lysosomal compartments. The Journal of Cell Biology (1990), 111:2327-2340.

Cantrell D. Signaling in lymphocyte activation. Cold Spring Harbor Perspectives in Biology (2015), 7:a018788.

Carmena M., Earnshaw W.C. The cellular geography of aurora kinases. Nat. Rev. Mol. Cell Biol. (2003), 4:842–854.

Cassioli C., Baldari C.T. A ciliary view of the immunological synapse. Cells (2019), 8:279.

CassioliC., Onnis A., Finetti F., Capitani N., Brunetti J., Compeer E.B., Niederlova V., Stepanek O., Dustin M.L. and Baldari C.T. The Bardet–Biedl syndrome complex component

BBS1 controls T cell polarity during immune synapse assembly. J. Cell. Sci. (2021), 134:jcs258462.

Cassioli C., Baldari C. The expanding arsenal of cytotoxic T cells. Frontiers in Immunology (2022), 13:883010.

Chang H.F., Mannebach S., Beck A., Ravichandran K., Krause E., Frohnweiler K., Feche-Trost C., et al. Cytotoxic granule endocytosis depends on the Flower protein. J Cell Biol (2017), 217(2):667-683.

Chang H.F., Schirra C., Ninov M.., Hahn U, Ravichandran K., Krause E., et al. Identification of a Novel Class of Cytotoxic Granules as the Origin of Supramolecular Attack Particles in T Lymphocytes. Nat Commun (2022), 13:1029.

Chakraborty A.K., Weiss A. Insights into the initiation of TCR signaling. Nat Immunol (2014), 15: 798-807.

Cheng X., Xie Y., Zhou B., Huang N., Farfel-Becker T., Sheng Z. Revisiting LAMP1 as a marker for degradative autophagy-lysosomal organelles in the nervous system. Autophagy (2018), 14(8):1472-1474.

Chiang E.Y., Kolumam G.A., Yu X., Francesco M., Ivelja S., Peng I., Gribling P., Shu J., Lee W., Refino C., Balazs M., Paler-Martinez A., Nguyen A., Young J., Barck K., Carano R., Ferrando R., Diehl L., Chatterjea D., Grogan J. Targeted depletion of lymphotoxin-alpha-expressing TH1 and TH17 cells inhibits autoimmune disease. Nature Medicine (2009), 15(7):766-773.

Choi A., Ryter S., Levine B. Autophagy in human health and disease. The New England Journal of Medicine (2013), 368(7):651-662.

Choi S.H., Cho K. LAMP2A-mediated autophagy involved in Huntington's disease progression. Biochemical and Biophysical Research Communications (2021), 534:561-567.

Chowdhury D., Lieberman J. Death by a Thousand Cuts: Granzyme Pathways of Programmed Cell Death. Annual Reviews in Immunology (2008), 26:389-420.

Colicino E., Hehnly H., Regulating a key mitotic regulator, polo-like kinase 1 (PLK1). Cytoskeleton (2018), 75:481-494.

Corse E., Gottschalk R.A., Allison J.P. Strength of TCR-peptide/MHC interactions and in vivo T cell responses. J Immunol. (2011), 186:5039-5045.

Coutinho M.F., Prata M.J., Alves S. Mannose-6-phosphate pathway: a review on its role in lysosomal function and dysfunction. Mol Genet Metab. (2012), 105(4):542-50.

Cuervo A.M., Dice, J.F. A receptor for the selective uptake and degradation of proteins by lysosomes. Science (1996), 273:501-503.

Dees S., Ganesan R., Singh S., Grewal I.S. Regulatory T cell targeting in cancer: Emerging strategies in immunotherapy. Eur J Immunol (2021), 51(2):280-291.

Degenhardt Y. and Lampkin T. Targeting polo-like kinase in cancer therapy. Clin Cancer Res (2010), 16(2):384.389.

Dikic I., Elazar Z. Mechanism and medical implications of mammalian autophagy. Nature Reviews. Molecular Cell Biology (2018), 19(6):349-364.

Dong D., Zheng L., Lin J., Zhang B., Zhu Y., Li N., Xie S., Wang Y., Gao N., Huang Z. Structural basis of the assembly of the human T cell receptor-CD3 complex. Nature (2019), 573:546-552.

Dowling S.D., Macian F. Autophagy and T cell metabolism. Cancer Letters (2018), 419:20-26.

Etienne-Manneville S. From signaling pathways to microtubule dynamics: the key players. Curr Opin Cell Biol (2010), 22:104-111.

Fallon P., Jolin H., Smith P., Emson C., Townsend M., Fallon R., Smith P., McKenzie A. IL-4 induces characteristic Th2 responses even in the combined absence of IL-5, IL-9, and IL-13. Immunity (2002), 17(1):7-17.

Farber D.L., Netea M.G., Radbruch A., Rajewsky K., Zinkernagel, R.M. Immunological memory: lessons from the past and a look to the future. Nature Reviews in Immunology (2016), 16:124-128.

Finetti F., Paccani S.R., Riparbelli M.G., Giacomello E., Perinetti G., Pazour G.J., Rosenbaum J.L., Baldari C.T. Intraflagellar transport is required for polarized recycling of the TCR/CD3 complex to the immune synapse. Nature Cell Biology (2009), 11(11):1332-9.

Finetti F., Patrussi L., Masi G., Onnis A., Galgano D., Lucherini O.M., Pazour G.J., Baldari C.T. Specific recycling receptors are targeted to the immune synapse by the intraflagellar transport system. Jounal of Cell Science (2014), 127(Pt 9):1924-37.

Finetti F., Cassioli C., Cianfanelli V., Onnis A., Paccagnini E., Kabanova A., Baldari C.T. The intraflagellar transport protein IFT20 controls lysosome biogenesis by regulating the post-Golgi transport of acid hydrolases. Cell Death and Differentiation (2020), 27(1):310-328.

Finetti F., Cassioli C., Cianfanelli V., Zevolini F., Onnis A., Gesualdo M., Brunetti J., Cecconi F., Baldari C.T. The intraflagellar transport protein IFT20 recruits ATG16L1 to early endosomes to promote autophagosome formation in T cells. Frontiers in Cell and Developmental Biology (2021), 9:634003.

Follit J. A., Tuft R. A., Fogarty K. E., Pazour G. J. The intraflagellar transport protein IFT20 is associated with the Golgi complex and is required for cilia assembly. Molecular Biology of the Cell (2006), 17:3781–3792.

Follit J.A., Xu F., Keady B.T., Pazour G.J. Characterization of mouse IFT complex B. Cell Motil Cytoskeleton (2009), 66:457-468.

Fraser J., Simpson J., Fontana R., Kishi−Itakura C., Ktistakis N. T., Gammoh, N. Targeting of early endosomes by autophagy facilitates EGFR recycling and signalling. EMBO Reports (2019), 20:e47734.

Fujishima Y., Nishiumi S., Masuda A., Inoue J., Nguyen N., Irino Y., Komatsu M., Tanaka K., Kutsumi H., Azuma T., Yoshida M. Autophagy in the intestinal epithelium reduces endotoxin-induced inflammatory responses by inhibiting NF-κB activation. Archives of Biochemistry and Biophysics (2011), 506(2):223-235.

Fujita N., Itoh T., Omori H., Fukuda M., Noda T., Yoshimori T. The Atg16L complex specifies the site of LC3 lipidation for membrane biogenesis in autophagy. Molecular Biology of the Cell (2002), 19:2092-2100.

Gammoh N. The multifaceted functions of ATG16L1 in autophagy and related processes. Journal of Cell Science (2020), 133:jcs249227.

Gao G.F., Rao Z., Bell J.I. Molecular coordination of αβ T-cell receptors and coreceptors CD8 and CD4 in their recognition of peptide-MHC ligands. Trends in Immunology (2002), 23:408-13.

Gaud G., Lesourne R., Love P.E. Regulatory mechanisms in T cell receptor signalling. Nature Review Immunology (2018), 18:485-497.

Gawden-Bone C.M., Frazer G., Richard A., Ma C., Strege K., Griffiths G.M. PIP5 kinases regulate membrane phosphoinositide and actin composition for targeted granule secretion by cytotoxic lymphocytes. Immunity (2018), 49:427–437 e4.

Geisler C. TCR trafficking in resting and stimulated T cells. Crit Rev Immunol (2004), 24:67-86.

Gray J.I., Westerhof L.M., MacLeod, M.K.L. The roles of resident, central and effector memory CD4 T-cells in protective immunity following infection or vaccination. Immunology (2018), 154:574-581.

Gray S.M., Kaech S.M., Staron M.M. The Interface Between Transcriptional and Epigenetic Control of Effector and Memory CD8(+) T-Cell Differentiation. Immunology Reviews (2014), 261:157-68.

Griffiths G.M., Isaaz S. Granzymes A and B are targeted to the lytic granules of lymphocytes by the mannose-6-phosphate receptor. J Cell Biol (1993), 120(4):885-896.

Griffiths G.M., Tsun A., Stinchcombe J.C. The immunological synapse: a focal point for endocytosis and exocytosis. J. Cell Biol. (2010), 189:399-406.

Gruenberg J. The endocytic pathway: a mosaic of domains. Nature Reviews Molecular Cell Biology (2001), 2:721–730.

Gutteridge R., Ndiaye M., Liu X., Ahmad N. Plk1 inhibitors in cancer therapy: from laboratory to clinics. Mol. Cancer Ther. (2016), 15(7):1427-1435.

Haeussler M., Schönig K., Eckert H., Eschstruth A., Mianné J., Renaud J.B., Schneider-Maunoury S., Shkumatava A., Teboul L., Kent J. *et al*. Evaluation of off-target and on-target scoring algorithms and integration into the guide RNA selection tool CRISPOR. Genome Biol. (2016), 17:148.

Halwani R., Al-Kufaidy R., Vazquez-Tello A., Pureza M.A., BaHammam A.S., Al-Jahdali H., Alnassar S.A., Hamid Q., Al-Muhsen S. IL-17 Enhances Chemotaxis of Primary Human B Cells during Asthma. PLoS One (2014), 9(12):e114604.

Hamasaki M., Shibutani S.T., Cuervo A.M., Klionsky D.J. Current Opinions in Cell Biology (2013), 25:455-460.

Hashimoto-Tane A., Yokosuka T., Sakata-Sogawa K., Sakuma M., Ishihara C., Tokunaga M., Saito T. Dynein-driven transport of T cell receptor microclusters regulates immune synapse formation and T cell activation. Immunity (2011), 34:919-931.

Heinzel S., Binh Giang T., Kan A., Marchingo J.M., Lye B.K., Corcoran L.M., Hodgkin P.D. A Myc-dependent division timer complements a cell-death timer to regulate T cell and B cell responses. Nature Immunology (2017), 18:96-103.

Henry E.K., Inclan-Rico J.M., Siracusa M.C. Type 2 cytokine responses: regulating immunity to helminth parasites and allergic inflammation. Current pharmacology reports (2017), 3(6):346-359.

Heras-Sandoval D., Pérez-Rojas J., Hernandez-Damian J., Pedraza-Chaverri J. The role of PI3K/AKT/mTOR pathway in the modulation of autophagy and the clearance of protein aggregates in neurodegeneration. Cellular Signaling (2014), 26(12):2694-2701.

Hogan P.G., Lewis R.S., Rao A. Molecular basis of calcium signaling in lymphocytes: STIM and ORAI. Annual Review in Immunology (2010), 28:491-533.

Holtrich U., Wolf G., Brauninger A., Karn T., Bohme B., Rubsamen-Waigmann H., Strebhardt K. Induction and down-regulation of PLK, a human serine/threonine kinase expressed in proliferating cells and tumors. Proc. Natl Acad. Sci. USA (1994), 91:1736-1740.

Honing S., Hunziker W. Cytoplasmic Determinants Involved in Direct Lysosomal Sorting, Endocytosis, and Basolateral Targeting of Rat Lgp120 (Lamp-I) in MDCK Cells. J Cell Biol (1995), 128:321-32.

Hurley J.H. ESCRT Complexes and the Biogenesis of Multivesicular Bodies. Curr Opin Cell Biol (2008), 20:4-11.

Iliaki S., Beyaert R., Afonina I. Polo-like kinase 1 (PLK1) signaling in cancer and beyond. Biochemical Pharmacology (2021), 193:114747.

Itoh T., Fujita N., Kanno E., Yamamoto A., Yoshimori T., Fukuda M. Golgi-resident small GTPase Rab33B interacts with Atg16L and modulates autophagosome formation. Molecular Biology of the Cell (2008), 19:2916-22925.

Jacquin E., Apetoh L. Cell-intrinsic roles for autophagy in modulating CD4 T cell function. Frontiers in Immunology (2018), 9:1023.

Janeway C.A., Travers P., Walport M., Shlomchik M.J. Immunobiology. New York: Garland Science (2001).

Jenkins M.R., Stinchcombe J., Yeung B., Asano Y., Ritter A., Weiss A., Griffiths G.M. Distinct structural and catalytic roles for Zap70 in formation of the immunological synapse in CTL. eLife (2014), 3:e01310.

Jensen P.E. Mechanisms of antigen presentation. Clinical Chemistry and Laboratory Medicine (1999), 37(3):179-186.

Johnston R.J., Poholek A.C., DiToro D., Yusuf I., Eto D., Barnett B., Dent A.L., Craft J., Crotty S. Bcl6 and Blimp-1 are reciprocal and antagonistic regulators of T follicular helper cell differentiation. Science (2009), 325(5943):1006-1010.

Jongsma M., Guarda G., Spaapen R. The regulatory network behind MHC class I expression. Molecular Immunology (2019), 113:16-21.

Joukov V., De Nicolo A. Aurora-PLK1 cascades as key signaling modules in the regulation of mitosis. Sci.Signal. (2018), 11:eaar4195.

Jutel M., Akdis M., Budak F., Aebischer-Casaulta C., Wrzyszcz M., Blaser K., Akdis C.A. IL-10 and TGF-beta cooperate in the regulatory T cell response to mucosal allergens in normal immunity and specific immunotherapy. European Journal of Immunology (2003), 33(5):1205-1214.

Kabat A.M., Harrison O.J., Riffelmacher T., Moghaddam A.E., Pearson C.F., Laing A., Abeler-Dorner L., Forman S., Grencis R., Sattentau Q., Simon A., Pott J., Maloy K. The autophagy gene Atg16l1 differentially regulates Treg and TH2 cells to control intestinal inflammation. Elife (2016), 5:e12444.

Kasai M., Tanida I., Ueno T., Kominami E., Seki S., Ikeda T., Mizuochi T. Autophagic compartments gain access to the MHC class II compartments in thymic epithelium. Journal of Immunology (2009), 183:7278-7285.

Kaufmann S., Winau F. From bacteriology to immunology: the dualism of specificity. Nature immunology (2005), 11(6):1063-1066.

Kaushik S., Cuervo A.M. Chaperone-mediated autophagy: a unique way to enter the lysosome world. Trends in Cell Biology (2012), 22:407-417.

Kim J., Lim Y.M., Lee M.S. The role of autophagic systemic metabolism and humen-type diabetes. Molecules and Cells (2018), 41(1):11-17.

Kim Y., Guan K.L. mTOR: a pharmacological target for autophagy regulation. The Journal of Clinical Investigation (2015), 125(1):25-32.

Kishi-Itakura C., Ktistakis N., Buss F. Ultrastructural insight into pathogen clearance by autophagy. Traffic (2020), 21(4):310-323.

Kitada M., Koya D. Autophagy in metabolic disease and ageing. Nature Reviews Endocrinology (2021), 17(11):647-661.

Klionsky D.J., Abdelmohsen,K., Abe A., Abedin M. J., Abeliovich H., Arozena A.A., et al. Guidelines for the use and interpretation of assays for monitoring autophagy (3rd edition). Autophagy (2016), 12:1-222.

Kocaturk N.M., Akkoc Y., Kig C., Bayraktar O., Gozuacik D., Kutlu O. Autophagy as a molecular target for cancer treatment. European Journal of Pharmaceutical Science (2019), 134:116-137.

Kolset S.O., Tveit H. Serglycin–structure and Biology. Cell Mol Life Sci (2008), 65:1073-85.

Kopf A. and Kiermaier E. Dynamic microtubule arrays in leukocytes and their role in cell migration and immune synapse formation. Front Cell Dev Biol (2021), 9:635511.

Kothe M., Kohls D., Low S., Coli R., Rennie G., Feru F., Kuhn C., Ding Y. Selectivity-determining residues in Plk1. Chem Biol Drug Des (2007), 70(6):540-546.

Kotsias F., Cebrian I., Alloatti A. Antigen processing and presentation. International Review of Cell and Molecular Biology (2019), 348:69-121.

Kovacs J.R., Li C., Yang Q., Li G., Garcia I.G., Ju S., Roodman D., Windle J., Zhang X., Lu B. Autophagy promotes T-cell survival through degradation of proteins of the cell death machinery. Cell Death Differentiation (2012), 19:144-152.

Kravtsov D.S., Erbe A.K., Sondel P.M. and Rakhmilevich A.L. Roles of CD4+ T cells as mediators of antitumor immunity. Front. Immunol. (2022), 13:972021.

Krishnamoorthy V., Kannanganat S., Maienschein-Cline M., Cook S.L., Chen J., Bahroos N., Sievert E., Corse E., Chong A., Sciammas R. The IRF4 gene regulatory module functions

as a read-write integrator to dynamically coordinate T helper cell fate. Immunity (2017), 47:481-497 e487.

Krzewski K., Gil-Krzewska A., Nguyen V., Peruzzi G., Coligan J.E. LAMP1/CD107a is Required for Efficient Perforin Delivery to Lytic Granules and NK- Cell Cytotoxicity. Blood (2013), 121:4672-83.

Kuhn J.R. and Poenie M. Dynamic polarization of the microtubule cytoskeleton during CTL-mediated killing. Immunity (2002), 16:111-121.

Lamb C., Longatti A., Tooze S. Rabs and GAPs in starvation-induced autophagy. Small GTPases (2016), 7(4):265-269.

Lane H.A., Nigg E.A. Antibody microinjection reveals an essential role for human polo-like kinase 1 (Plk1) in the functional maturation of mitotic centrosomes. J. Cell Biol. (1996), 135:1701-1713.

Langemeyer L., Fröhlich F., Ungermann C. Rab GTPase function in endosome and lysosome biogenesis. Trends in Cell Biology (2018), 28(11):957-970.

Langford G.M. Actin- and microtubule-dependent organelle motors: interrelationships between the two motility systems. Curr. Opin. Cell Biol. (1995), 7:82-88.

Lee K.H., Holdorf A.D., Dustin M.L., Chan A.C., Allen P., Shaw A. T cell receptor signaling precedes immunological synapse formation. Science (2002), 295: 1539-1542.

Li C., Jiang P., Wei S., Xu X., Wang J. Regulatory T cells in tumor microenvironment: new mechanisms, potential therapeutic strategies and future perspective. Molecular Cancer (2020), 19:116.

Li R., Gundersen G.G. Beyond polymer polarity: how the cytoskeleton builds a polarized cell. Nat Rev Mol Cell Biol (2008), 9:860-873.

Li W.W., Li J., Bao J.K. Microautophagy: lesser-known self-eating. Cellular and Molecular Life Sciences (2012), 69:1125-1136.

Li Y., Chen Y. AMPK and autophagy. Advances in Experimental Medicine and Biology (2019), 1206:85-108.

Liccardi G., RamosGarcia L., Tenev T., Annibaldi A., Legrand A.J., Robertson D., *et al.* RIPK1 and caspase-8 ensure chromosome stability independently of their role in cell death and inflammation. Mol Cell. (2019), 73(3):413-428.

Lin S., Mallet W., Huang A. and Maxfield F. Endocytosed cation-independent mannose 6-phosphate receptor traffics via the endocytic recycling compartment en route to the trans-Golgi network and subpopulation of late endosomes. Mol Biol Cell (2004), 15:721-733.

Liu X., Kapoor T.M., Chen J.K., Huse M. Diacylglycerol promotes centrosome polarization in T cells via reciprocal localization of dynein and myosin II. Proc. Natl Acad. Sci. USA (2013), 110:11976-11981.

Liu X., Sun Q., Wang X. PLK1, a potential target for cancer therapy. Trans. Onc. (2017), 10(1):22-32.

Lopez J.A., Brennan A.J., Whisstock J.C., Voskoboinik I., Trapani J.A. Protecting a Serial Killer: Pathways for Perforin Trafficking and Self-Defence Ensure Sequential Target Cell Death. Trends Immunol (2012), 33:406-12.

Luckheeram R.V., Zhou R., Verma A.D., Xia B. CD4+T Cells: differentiation and functions. Clinical and Developmental Immunology (2012), 925135.

Ma X., Godar R.J., Liu H., Diwan A. Enhancing lysosome biogenesis attenuates BNIP3-induced cardiomyocyte death. Autophagy (2012), 8:297-309.

Manders E.M., Stap J., Brakenhoff G.J., van Driel R. and Aten J.A. Dynamics of three-dimensional replication patterns during the S-phase, analysed by double labelling of DNA and confocal microscopy. J. Cell Sci. (1992), 103:857-862.

Marinari B., Costanzo A., Marzano V., Piccolella E., Tuosto L. CD28 delivers a unique signal leading to the selective recruitment of RelA and p52 NF- kappaB subunits on IL-8 and Bcl-xL gene promoters. Proceeding of the National Academy of Sciences USA (2004), 101:6098-6103.

Martin-Cofreces N., Baixauli F., Lopez M., Gil D., Monjas A., Alarcon B. and Sanchez-Madrid F. End-binding protein 1 controls signal propagation from the T cell receptor. EMBO J (2012), 31(21):4140-4152.

Martin-Cofreces N.B., Baixauli F., Sanchez- Madrid F. Immune synapse: conductor of orchestrated organelle movement. Trends Cell Biol (2014), 24: 61-72.

Mastrogiovanni M., Juzans M., Alcover A. and Di Bartolo V. Coordinating Cytoskeleton and Molecular Traffic in T Cell Migration, Activation, and Effector Functions. Front. Cell Dev. Biol. (2020), 8:591348.

Matthews S.A., Cantrell D.A. New insights into the regulation and function of serine/threonine kinases in T lymphocytes. Immunological Reviews (2009), 228:241-252.

Mauthe M., Orhon I., Rocchi C., Zhou X., Luhr M., Hijkema K.J., Coppes R., Engedal N., Meri M., Reggiori F. Cloroquine inhibits autophagic flux by decreasing autophagosome-lysosome fusion. Autophagy (2018), 14(8):1435-1455.

McKenzie B., Khazen R., Valitutti S. Greek Fire, poison Arrows, and scorpion bombs: how tumor cells defend against the siege weapons of cytotoxic T Lymphocytes. Front. Immunol. (2022), 13:894306.

Merkley S.D., Chock C.J., Yang X.O., Harris J., Castillo E.F. Modulating T Cell Responses via Autophagy: The Intrinsic Influence Controlling the Function of Both Antigen-Presenting Cells and T Cells. Frontiers in Immunology (2018), 9:2914.

Mijaljica D., Prescott M., Devenish R.J. Microautophagy in mammalian cells: revisiting a 40-year-old conundrum. Autophagy (2011), 7:673-682.

Mitchell D.M., Ravkov E.V., Williams M.A. Distinct roles for IL-2 and IL-15 in the differentiation and survival of $CD8^+$ effector and memory T cells. Journal of Immunology (2010), 184:6719-30.

Mizushima N., Levine B. Autophagy in human diseases. The New England Journal of Medicine (2020), 383:1564-1576.

Mullbacher A., Waring P., Hla R., Tran T., Chin S., Stehle T., Museteanu C., Simon M. Granzymes are the essential downstream effector molecules for the control of primary virus infections by cytolytic leukocytes. PNAS (1999), 96:13950-13955.

Murphy K. and Weaver C. Cytotoxic effector proteins that trigger apoptosis are contained in the granules of CD8 cytotoxic T cells. In: Janeway's Immunobiology (9th Edition). 9 edn (2016).

Nakagawa I., Amano A., Mizushima N., Yamamoto A., Yamaguchi H., Kamimoto T., Nara A. Autophagy defends cells against invading group A Streptococcus. Science (2004), 306:1037-1040.

Nedjic J., Aichinger M., Emmerich J., Mizushima N., Klein L. Autophagy in thymic epithelium shapes the T-cell repertoire and is essential for tolerance. Nature (2008), 455:396-400.

Noda N., Inagaki F. Mechanisms of autophagy. Annual Review of Biophysics (2015), 44:101-122.

O'Keefe J.P., Blaine K., Alegr M. L., Gajewski T.F. Formation of a central supramolecular activation cluster is not required for activation of naive $CD8^+$ T cells. Proc. Natl Acad. Sci. USA (2004), 101:9351-9356.

Oh-hora M., Rao A. Calcium signaling in lymphocytes. Current Opinions in Immunology (2008), 20:250-258.

Onnis A., Finetti F., Baldari C.T. Vesicular trafficking to the immune synapse assembly: how to assemble receptor-tailored pathways from a basic building set. Front. Immunol. (2016), 7:50.

Onnis A., Andreano E., Cassioli C., Finetti F., Della Bella C., Staufer O., Pantano E., Abbiento V., Marotta G., D'Elios M.M., Rappuoli R., Baldari C.T. SARS-CoV-2 Spike protein suppresses CTL-mediated killing by inhibiting immune synapse assembly. J Exp Med (2022), 220(2):e20220906.

Omori Y., Zhao C., Saras A., Mukhopadhyay S., Kim W., Furukawa T., Sengupta P., Veraksa A., Malicki J. Elipsa is an early determinant of ciliogenesis that links the IFT particle to membrane-associated small GTPase Rab8. Nature Cell Biology (2003), 10:437-444.

Onodera J., Ohsumi Y. Autophagy is required for maintenance of amino acid levels and protein synthesis under nitrogen starvation. The Journal of Biological Chemistry (2005), 280(36):31582-31586.

Onorati A., Dyczynski M., Ojha R., Amaravadi R. Targeting autophagy in cancer. Cancer (2018), 124(16):3307-3318.

Oral O., Yedier O., Kilic S., Gozuacik D. Involvement of autophagy in T cell biology. Histology and Histopathology (2017), 32(1):11-20.

Ouyang W., Kolls J., Zheng Y. The biological functions of T helper 17 cell effector cytokines in inflammation. Immunity (2008), 28(4):454-467.

Pageon S.V., Tabarin T., Yamamoto Y., Ma Y., Bridgeman J.S., Cohnen A., Benzing C., Gao Y., Crowther M.D., Tungatt K., et al. Functional role of T-cell receptor nanoclusters in signal initiation and antigen discrimination. Proc. Natl. Acad. Sci. USA (2016), 113:E5454-E5463.

Palacios E.H., Weiss A. Function of the Src-family kinases, Lck and Fyn, in T-cell development and activation. Oncogene (2004), 23:7990-8000.

Palmieri M., Impey S., Kang H., di Ronza A., Pelz C., Sardiello M., Ballabio A. Characterization of the CLEAR network reveals an integrated control of cellular clearance pathways. Hum. Mol. Genet. (2011), 20:3852-3866.

Pampliega O., Orhon I., Patel B., Sridhar S., Dìaz-Carretero A., Beau I., Codogno P., Satir P., Cuervo A.M. Functional interaction between autophagy and ciliogenesis. Nature (2013), 502(7470):194-200.

Parkin J., Cohen B. An overview of the immune system. The Lancet Immunology (2001), 357:1777-1789.

Parzych K., Klionsky D. An overview of autophagy: morphology, mechanism and regulation. Antioxidants and Redox Signaling (2014), 20(3):460-473.

Pazour G.J., Baker S.A., Deane J.A., Cole D.G., Dickert B.L., Rosenbaum J.L., *et al*. The intraflagellar transport protein, IFT88, is essential for vertebrate photoreceptor assembly and maintenance. J. Cell Biol. (2002), 157:103-113.

Pihan G. Centrosome dysfunction contributes to chromosome instability, chromoanagenesis, and genome reprograming in cancer. Front. Oncol. (2013), 3:277.

Pipkin M., Sacks A., Cruz-Guillot F., Lichtenheld M., Bevan M., Rao A. Interleukin-2 and inflammation induce distinct transcriptional programs that promote the differentiation of effector cytolytic T cells. Immunity (2010), 32(1):79-90.

Peters P.J., Borst J., Oorschot V., Fukuda M., Krahenbuhl O., Tschopp J., Slot J.W., Geuze H.J. Cytotoxic T Lymphocyte Granules are Secretory Lysosomes, Containing Both Perforin and Granzymes. The Journal of Experimental Medicine (1991), 173:1099-109.

Peters P.J., Geuze H.J., Van der Donk H.A., Slot J.W., Griffith J.M., Stam N.J.., Clevers H.C., Borst J. Molecules relevant for T cell-target cell interaction are present in cytolytic granules of human T lymphocytes. European Journal of Immunology (1989), 19:1469-1475.

Pishesha N., Harmand T.J., Ploegh, H.L. A guide to antigen processing and presentation. Nature Review Immunology (2022), 2:10.1038.

Podack E.R., Kupfer A. T-cell effector functions: mechanisms for delivery of cytotoxicity and help. Annu Rev Cell Biol (1991), 7:479-504.

Potter T.A., Grebe K., Freiberg B., Kupfer A. Formation of supramolecular activation clusters on fresh ex vivo $CD8^+$ T cells after engagement of the T cell antigen receptor and CD8 by antigen-presenting cells. Proc. Natl Acad. Sci. USA (2001), 98:12624-12629.

Prevo B., Scholey J.M., Peterman E.J.G. Intraflagellar transport: mechanisms of motor action, cooperation, and cargo delivery. FEBS Journal (2017), 284:2905-2931.

Progida C., Cogli L., Piro F., De Luca A., Bakke O. and Bucci C. Rab7b controls trafficking from endosomes to the TGN. J. Cell Sci. (2010), 123:1480-1491.

Pua H.H., Dzhagalov I., Chuck M., Mizushima N., He Y.W. A critical role for the autophagy gene Atg5 in T cell survival and proliferation. Journal of Experimental Medicine (2007), 204:25-31.

Puleston D.J., Zhang H., Powell T.J., Lipina E., Sims S., Panse I., Watson A., Cerundolo V., Townsend A., Klenerman P., Simon A.K. Autophagy is a critical regulator of memory $CD8^+$ T cell formation. Elife (2014), 3:1-21.

Puri C., Renna M., Bento C. F., Moreau K., Rubinsztein D.C. Diverse autophagosome membrane sources coalesce in recycling endosomes. Cell (2013), 154:1285-1299.

Quann E.J., Merino E., Furuta T., Huse M. Localized diacylglycerol drives the polarization of the microtubule-organizing center in T cells. Nat. Immunol. (2009), 10:627-635.

Rak G., Mace E.M., Banerjee P., Svitkina T., Orange J.S. Natural killer cell lytic granule secretion occurs through a pervasive actin network at the immune synapse. PLoS Biol. (2011), 9:e1001151.

Raposo G., Marks M.S., Cutler D.F. Lysosome-related organelles: driving post-Golgi compartments into specialisation. Current Opinions in Cell Biology (2007), 19:394-401.

Ravikumar B., Imarisio S., Sarkar S., O'Kane C.J., Rubinsztein D.C. Rab5 modulates aggregation and toxicity of mutant huntingtin through macroautophagy in cell and fly models of Huntington disease. Journal of Cell Science (2008), 121:1649-1660.

Ravanan P., Srikumar I.F., Talwar P. Autophagy: The spotlight for cellular stress responses. Life Sciences (2017), 188:53-67.

Reddy P.H., Yin X., Manczak M., Kumar S., Pradeepkiran A., Vijayan M., Reddy A. Mutant App and amyloid beta-induced defective autophagy, mitophagy, mitochondrial structural and functional changes and synaptic damage in hippocampal neurons from Alzheimer's disease. Human Molecular Genetics (2018), 27(14):2502-2516.

Redmann M., Benavides G., Berryhill T., Wani W., Ouyang X., Johnson M., Ravi S., Barnes S., Darley-Usmar V., Zhang J. Inhibition of autophagy with bafilomycin and chloroquine decreases mitochondrial quality and bioenergetic function in primary neurons. Redox Biology (2017), 11:73-81.

Reggiori F., Komatsu M., Finley K., Simonsen A. Autophagy: more than a nonselective pathway. International Journal of Cell Biology (2012), 2012:219625.

Reith W., LeibundGut-Landmann S., Waldburger J.M. Regulation of MHC class II gene expression by the class II transactivator. Nature Reviews Immunology (2005), 5:793-806.

Reinhardt H.C., Yaffe M. Phospho-Ser/Thr-binding domains: Navigating the cell cycle and DNA damage response. Nat. Rev. Mol. Cell Biol. (2013), 14:563-580.

Rijnboutt S., Aerts H.M., Geuze H.J., Tager J.M., Strous G.J. Mannose 6-phosphate-independent membrane association of cathepsin D, glucocerebrosidase, and sphingolipid-activating protein in HepG2 cells, J. Biol. Chem. (1991), 266:4862-4868.

Ritter A.T., Asano Y., Stinchcombe J., Dieckmann N., Chen B., Gawden-Bone C., van Engelenburg S., Legant W., Gao L., et al. Actin depletion initiates events leading to granule secretion at the immunological synapse. Immunity (2015), 42:864-876.

de la Roche M., Ritter A., Angus K., Dinsmore C., Earnshaw C., Reiter J. and Griffiths G.M. Hedgehog signaling controls T cell killing at the immunological synapse. Science (2013), 342:1247–1250.

de la Roche M., Asano Y., Griffiths G.M. Origins of the cytolytic synapse. Nature Reviews Immunology (2016), 16(7):421-432.

Rosenbaum J.L., Witman G.B. Intraflagellar transport. Nature Reviews Molecular Cell Biology (2002), 3:813-825.

Rossy J., Williamson D.J., Gaus K. How does the kinase Lck phosphorylate the T cell receptor? Spatial organization as a regulatory mechanism. Frontiers in Immunology (2012), 3:167.

Ruf S., Heberle A.M., Langelaar-Makkinje M., Gelino S., Wilkinson D., Gerbeth C., et al., PLK1 (polo like kinase 1) inhibits MTOR complex 1 and promotes autophagy, Autophagy. (2017), 13(3):486-505.

de Saint Basile G., Ménasché G., Fischer A. Molecular mechanisms of biogenesis and exocytosis of cytotoxic granules. Nature Reviews Immunology (2010), 11:568-579.

Sakaguchi S., Mikami N., Wing J.B., Tanaka A., Ichiyama K., Ohkura N. Regulatory T cells and human disease. Annu Rev Immunol (2020), 38:541-566.

Sallusto F., Lenig D., Forster R., Lipp M., Lanzavecchia A. Two subsets of memory T lymphocytes with instinct homing potentials and effector functions. Nature (1999), 401:708-12.

Sallusto F. Heterogeneity of human $CD4^+$ T cells against microbes. Annual Review of Immunology (2016), 34:317-334.

Sanchez-Ruiz Y., Valitutti S., Dupre L. Stepwise maturation of lytic granules during differentiation and activation of human $CD8^+$ T lymphocytes. Plos ONE (2011), 6(11):e27057.

Satir P., Pedersen L.B., Christensen S.T. The primary cilium at a glance. The Journal of Cell Science (2010), 123:499-503.

Sardiello M., Palmieri M., di Ronza A., Medina D.L., Valenza M., Gennarino V.A., et al. A gene network regulating lysosomal biogenesis and function. Science (2009), 325:473-7.

Sardon T., Peset I., Petrova B., Vernos I. Dissecting the role of Aurora A during spindle assembly. EMBO J. (2008), 27:2567-2579.

Schmitz M.L., Krappmann D. Controlling NF-κB activation in T cells by costimulatory receptors. Cell death and differentiation (2006), 13:834-842.

Schmucker S., Sumara I. Molecular dynamics of PLK1 during mitosis. Mol Cell Oncol (2014), 1(2):e954507.

Settembre C., Fraldi A., Medina D.L., Ballabio A. Signals from the lysosome: a control centre for cellular clearance and energy metabolism. Nat Rev Mol Cell Biol. (2013), 14:283-296.

Shahrara S., Pickens S., Dorfleutner A., Pope R. IL-17 induces monocyte migration in rheumatoid arthritis. The Journal of Immunology (2009), 182(6):3884-3891.

Shao C., Chien S.J., Farah E., Li Z., Ahmad N., Liu X. Plk1 phosphorylation of numb leads to impaired DNA damage response, Oncogene. 37 (6) (2018) 810–820.

Skjeldal F., Haugen L., Marteus D., Frei D., Rodseth A., Hu X., Bakke O. De novo formation of early endosomes during Rab5-to-Rab7a transition. Journal of Cell Science (2021), 134(8):jcs254185.

Smith N., Rise M., Christian S. A comparison of the innate and adaptive immune system in cartilaginous fish, ray-finned fish and lobe-finned fish. Frontiers in immunology (2019), 10:2292.

Soares H., Henriques R., Sachse M., Ventimiglia L., Alonso M., Zimmer C., Thoulouze M.I., Alcover A. Regulated vesicle fusion generates signaling nanoterritories that control T cell activation at the immunological synapse. J. Exp. Med. (2013), 210:2415-2433.

Sparrow E., Bodman-Smith M.D. Granulysin: The Attractive Side of a Natural Born Killer. Immunol Lett (2020), 217:126-32.

Spicer B.A., Conroy P.J., Law R.H.P., Voskoboinik I., Whisstock J.C. Perforin-A Key (Shaped) Weapon in the Immunological Arsenal. Semin Cell Dev Biol (2017), 72:117-23.

Staiano L., Zappa F. Hijacking intracellular membranes to feed autophagosomal growth. FEBS Letters (2019), 593:3120-3134.

Steegmaier M., Hoffman M., Baum A., Lenart P., Petronczki M., Krssak M., Gurtler U., Garin-Chesa P., Lieb S. et al. BI2536, a potent and selective inhibitor of Polo-like Kinase 1, inhibits tumor growth in vivo. Current Biology (2007), 17:316-322.

Stinchcombe J.C., Page L. J., Griffiths G.M. Secretory lysosome biogenesis in cytotoxic T lymphocytes from normal and Chediak–Higashi syndrome patients. Traffic (2000), 1:435-444.

Stinchcombe J.C., Bossi G., Booth S., Griffiths G.M. The Immunological Synapse of CTL Contains a Secretory Domain and Membrane Bridges. Immunity (2001), 15:751-61.

Stinchcombe J.C., Bossi G., Griffiths G.M. Linking albinism and immunity: the secrets of secretory lysosomes. Science (2004), 305: 55-59.

Stinchcombe J.C., Majorovits E., Bossi G., Fuller S., Griffiths G.M. Centrosome polarization delivers secretory granules to the immunological synapse. Nature Letters (2006), 443:462-465.

Stinchcombe J., Griffiths G.M. Secretory mechanisms in cell-mediated cytotoxicity. Annu. Rev. Cell Dev. Biol. (2007), 23:495–517.

Stöckli J., Höning S., Rohrer J. The acidic cluster of the CK2 site of the cation-dependent mannose 6-phosphate receptor (CD-MPR) but not its phosphorylation is required for GGA1 and AP-1 binding. J Biol Chem (2004), 279(22):23542-9.

Strebhardt K. Multifaceted polo-like kinases: drug targets and antitargets for cancer therapy. Nat Rev Drug Disc (2010), 9:643-660.

Südhof T.C. Calcium control of neurotransmitter release. Cold Spring Harb. Perspect. Biol. (2012), 4:a011353.

Sugimoto N., Oida T., Hirota K., Nakamura K., Nomura T., Uchiyama T., Sakaguchi S. Foxp3-dependent and -independent molecules specific for $CD25^{+}CD4^{+}$ natural regulatory T cells revealed by DNA microarray analysis. Int Immunol (2006), 18(8):1197-1209.

Swain S.L., McKinstry K., Strutt T. Expanding roles for CD4+ T cells in immunity to viruses. Nature Reviews Immunology (2012), 12:136-148.

Takahashi K., Nagai T., Chiba S., Nakayama K., Mizuno K. Glucose deprivation induces primary cilium formation through mTORC1 inactivation. The Journal of Cell Science (2018), 131(1):jcs208769.

Takeuchi A., Saito T. CD4 CTL, A Cytotoxic Subset of CD4(+) T Cells, Their Differentiation and Function. Frontiers in Immunology (2017), 8:194.

Takeuchi O., Akira S. Pattern recognition receptors and inflammation. Cell (2010), 140:805-820.

Tamzalit F., Tran D., Jin W., Boyko V., Bazzi H., Kepecs A., Kam L., Anderson K and Huse M. Centrioled control the capacity, but not the specificity, of cytotoxic T cell killing. PNAS (2020), 117(8):4310-4319.

Taschner M., Bhogaraju S., Lorentzen E. Architecture and function of IFT complex proteins in ciliogenesis. Differentiation (2012), 83:S12-S22.

Taschner M., Lorentzen E. The intraflagellar transport machinery. Cold Spring Harbour Perspectives in Biology (2016), 8:a028092.

Tian Q., Streuli M., Saito H., Schlossman S.F., Anderson P. A polyadenylate binding protein localized to the granules of cytolytic lymphocytes induces DNA fragmentation in target cells. Cell (1991), 67: 629-639.

Togashi Y., Shitara K., Nishikawa H. Regulatory T cells in cancer immunosuppression - implications for anticancer therapy. Nat Rev Clin Oncol (2019), 16(6):356-71.

Tsun A., Qureshi I., Stinchcombe J., Jenkins M., de la Roche M., Kleczkowska J., Zamyoska R., Griffiths G.M. Centrosome docking at the immunological synapse is controlled by Lck signaling. J. Cell Biol. (2011), 192:663–674.

Tu H.Y., Yuan B.S., Hou X.O., Zhang X.J., Pei C.S., Ma Y.T., Yang Y.P., Fan Y., Qin Z.H., Liu C.F., Hu L.F. α-synuclein suppresses microglieal autophagy and promotes neurodegeneration in a mouse model of Parkinson's disease. Aging Cell (2021), 20(12):e13522.

Trapani J., Smyth M. Functional significance of the perforin/granzyme cell death pathway. Nat Rev Immunol (2002), 2:735-747.

Valdor R., Macian F. Mechanisms of self-inactivation in anergic T cells. Immunologia (2010), 29:20-33.

Van Vugt M.A.T.M., Van De Weerdt B.C.M., Vader G., Janssen H., Calafat J., R. Klompmaker, *et al.*, Polo-like kinase-1 is required for bipolar spindle formation but is dispensable for anaphase promoting complex/Cdc20 activation and initiation of cytokinesis, J Biol Chem. (2004), 279(35):36841-36854.

Vivar O.I., Masi G., Carpier J., Magalhaes J.G., Galgano D., Pazour G. J., Amigorena S., Hivroz C., Baldari C. IFT20 controls LAT recruitment to the immune synapse and T-cell activation in vivo. PNAS (2016), 113:386-391.

Wang F., Jia J., Rodrigues B. Autophagy, metabolic disease, and pathogenesis of heart dysfunction. Canadian Journal of Cardiology (2017), 33(7):850-859.

Wang J.H., Reinherz E.L. The structural basis of αβ T-lineage immune recognition: TCR docking topologies, mechanotransduction, and co-receptor function. Immunological Reviews (2012), 250:102-119.

Wang G., Chen Q., Zhang X., Zhang B., Zhou X., Liu J., Jiang Q., Zhang C. PCM1 recruits Plk1 to the pericentriolar matrix to promote primary cilia disassembly before mitotic entry. J Cell Sci (2013), 126(6):1355-1365.

Watanabe R., Fujii H., Shirai T., Saito S., Ishii T., Harigae H. Autophagy plays a protective role as an anti-oxidant system in human T cells and represents a novel strategy for induction of T-cell apoptosis. European Journal of Immunology (2014), 44:2508-2520.

Wei J., Long L., Yang K., Guy C., Shrestha S., Chen Z., Wu C., Vogel P., Neale G., Green D., Chi H. Autophagy enforces functional integrity of regulatory T cells by coupling environmental cues and metabolic homeostasis. Nature Immunology (2016), 17:277-285.

Wen H., Zhan L., Chen S., Long L., Xu E. Rab7 may be a novel therapeutic target for neurologic diseases as a key regulator in autophagy. Journal of Neuroscience Research (2017), 95(10):1993-2004.

White E., Mehnert J., Chan S. Autophagy, metabolism, and cancer. Clinical Cancer Research (2015), 21(22):5037-5046.

Wucherpfennig K.W., Gagnon E., Call M.J., Huseby E.S., Call M.E. Structural biology of the T-cell receptor: insights into receptor assembly, ligand recognition, and initiation of signaling. Cold Spring Harbor Perspectives in Biology (2010), 2:a005140.

Xiong Q., Li W., Li P., Yang M., Wu C., Eichinger L. The Role of ATG16 in autophagy and the ubiquitin proteasome system. Cells (2018), 8:2.

Xu J., Shen C., Wang T, Quan J. Structural basis for the inhibition of Polo-like kinase 1. Nat. Struct. Mol. Biol. (2013), 20:1047-1053.

Xu X., Araki K., Li S., Han J.H., Ye L., Tan W., Konieczny B., Bruinsma M., Martinez J., Pearce E., Green D., Jones D., Virgin H., Ahmed R. Autophagy is essential for effector CD8+ T cell survival and memory formation. Nature Immunology (2014), 15(12):1152-63.

Yang G., Song W., Postoak J.L., Chen J., Martinez J., Zhang J., Wu L., Van Kaer J. Autophagy-related protein PIK3C3/VPS34 controls T cell metabolism and function. Autophagy (2021), 17(5):1193-1204.

Yang Q., Wang R., Zhu L. Chaperone-mediated autophagy. Advances in Experimental Medicine and Biology (2019), 1206:435-452.

Yang Z., Klionsky D.J. Mammalian autophagy: core molecular machinery and sinaling regulation. Current Opinions in Cell Biology (2010), 22:124-131.

Yeste A., Mascanfroni I., Nadeau M., Burns E., Tukpah A.M., Santiago A., Wu C., Patel B., Kumar D., Quintana F. IL-21 induces IL-22 production in $CD4^+$ T cells. Nature Communications (2014), 5:3753.

Yu L., Chen Y., Tooze S. Autophagy pathway: cellular and molecular mechanisms. Autophagy (2018), 14(2):207-215.

Zaffagnini G., Martens S. Mechanisms of selective autophagy. Journal of Molecular Biology (2016), 428:1714-1724.

Zheng J., Koda T., Fujwara T., Kishi M., Ikehara Y., Kakinuma M. Journal of Cell Science (1998), 111:1061-1069.

Zitouni S., Nabais C., Jana S., Guerrero A., Bettencourt-Dias M. Polo-like kinases: structural variations lead to multiple functions. Nat- Rev. Mol. Cell Biol. (2014), 15:433-452.

Zucchetti A.E., Bataille L., Carpier J.M., Dogniaux S., San Roman-Jouve M., Maurin M., Stuck M., Rios R., Baldari C., Pazour G.J., Hivroz C. Tethering of vesicles to the Golgi by GMAP210 controls LAT delivery to the immune synapse. Nature Communications (2019), 10:2864.

LIST OF PUBLICATIONS

- Finetti F., Cassioli C., Cianfanelli V., **Zevolini F.**, Onnis A., Gesualdo M., Brunetti J., Cecconi F., Baldari C.T. The intraflagellar transport protein IFT20 recruits ATG16L1 to early endosomes to promote autophagosome formation in T cells. Frontiers in Cell and Developmental Biology (2021), 9:634003 (*attached paper*).
- Herrera-Leon C., Ramos-Martin F., El Btaouri H., Antonietti V., Sonnet P., Martiny L., **Zevolini F.**, Falciani C., Sarazin C., D'Amelio N. The influence of short motifs on the anticancer activity of HB43 peptide. Pharmaceutics (2022), 14(5):1089.
- Falciani C., **Zevolini F.**, Brunetti J., Riolo G., Gracia R., Marradi M., Loinaz I., Ziemann C., Cossio U., Llop J., Bracci L., Pini A. Antimicrobial peptide-loaded nanoparticles as inhalation therapy for Pseudomonas aeruginosa infections. International Journal of Nanomedicine (2020), 15:1117-1128.
- Castiglia F., **Zevolini F.**, Riolo G., Brunetti J., De Lazzeri A., Moretto A., Manetto G, Pini A., Fragai M., Bracci L., Falciani C. NMR study of the secondary structure of an active branched antimicrobial peptide. Molecules (2019), 24(23):4290.

frontiers in Cell and Developmental Biology

ORIGINAL RESEARCH
published: 22 March 2021
doi: 10.3389/fcell.2021.634003

The Intraflagellar Transport Protein IFT20 Recruits ATG16L1 to Early Endosomes to Promote Autophagosome Formation in T Cells

Francesca Finetti[1], Chiara Cassioli[1], Valentina Cianfanelli[2,3], Fabrizia Zevolini[1], Anna Onnis[1], Monica Gesualdo[1], Jlenia Brunetti[4], Francesco Cecconi[2,3,5] and Cosima T. Baldari[1]**

[1] Department of Life Sciences, University of Siena, Siena, Italy, [2] Cell Stress and Survival Unit, Center for Autophagy, Recycling and Disease (CARD), Danish Cancer Society Research Center, Copenhagen, Denmark, [3] Department of Pediatric Hemato-Oncology and Cell and Gene Therapy, IRCCS Bambino Gesù Children's Hospital, Rome, Italy, [4] Department of Medical Biotechnologies, University of Siena, Siena, Italy, [5] Department of Biology, University of Rome Tor Vergata, Rome, Italy

OPEN ACCESS

Edited by:
Angela Wandinger-Ness, University of New Mexico, United States

Reviewed by:
Martin Lowe, The University of Manchester, United Kingdom
Mingqun Lin, The Ohio State University, United States

***Correspondence:**
Francesca Finetti
finetti4@unisi.it
Cosima T. Baldari
baldari@unisi.it;
cosima.baldari@unisi.it

Specialty section:
This article was submitted to Membrane Traffic, a section of the journal Frontiers in Cell and Developmental Biology

Received: *26 November 2020*
Accepted: *23 February 2021*
Published: *22 March 2021*

Citation:
Finetti F, Cassioli C, Cianfanelli V, Zevolini F, Onnis A, Gesualdo M, Brunetti J, Cecconi F and Baldari CT (2021) The Intraflagellar Transport Protein IFT20 Recruits ATG16L1 to Early Endosomes to Promote Autophagosome Formation in T Cells. Front. Cell Dev. Biol. 9:634003. doi: 10.3389/fcell.2021.634003

Lymphocyte homeostasis, activation and differentiation crucially rely on basal autophagy. The fine-tuning of this process depends on autophagy-related (ATG) proteins and their interaction with the trafficking machinery that orchestrates the membrane rearrangements leading to autophagosome biogenesis. The underlying mechanisms are as yet not fully understood. The intraflagellar transport (IFT) system, known for its role in cargo transport along the axonemal microtubules of the primary cilium, has emerged as a regulator of autophagy in ciliated cells. Growing evidence indicates that ciliogenesis proteins participate in cilia-independent processes, including autophagy, in the non-ciliated T cell. Here we investigate the mechanism by which IFT20, an integral component of the IFT system, regulates basal T cell autophagy. We show that IFT20 interacts with the core autophagy protein ATG16L1 and that its CC domain is essential for its pro-autophagic activity. We demonstrate that IFT20 is required for the association of ATG16L1 with the Golgi complex and early endosomes, both of which have been identified as membrane sources for phagophore elongation. This involves the ability of IFT20 to interact with proteins that are resident at these subcellular localizations, namely the golgin GMAP210 at the Golgi apparatus and Rab5 at early endosomes. GMAP210 depletion, while leading to a dispersion of ATG16L1 from the Golgi, did not affect basal autophagy. Conversely, IFT20 was found to recruit ATG16L1 to early endosomes tagged for autophagosome formation by the BECLIN 1/VPS34/Rab5 complex, which resulted in the local accumulation of LC3. Hence IFT20 participates in autophagosome biogenesis under basal conditions by regulating the localization of ATG16L1 at early endosomes to promote autophagosome biogenesis. These data identify IFT20 as a new regulator of an early step of basal autophagy in T cells.

Keywords: intraflagellar transport, vesicular trafficking, ATG16L1, early endosomes, autophagy, T cell

INTRODUCTION

Autophagy is a degradative process that subserves the dual function of eliminating damaged macromolecules and organelles while providing endogenous energy sources and building blocks to maintain cellular homeostasis (Dikic and Elazar, 2018). Similar to other cell types, T cells exploit autophagy as a quality control and pro-survival mechanism which is essential for the long-lasting maintenance of the naive peripheral T cell repertoire. The roles of autophagy are, however, not limited to T cell homeostasis. Autophagy participates in thymocyte development by sustaining the survival of double negative thymocytes and their transition to the double positive stage (Nedjic et al., 2008) and regulates both positive and negative selection via the MHCII loading pathway in thymic epithelial cells (Kasai et al., 2009). In the periphery, T cell activation and proliferation are fine-tuned by selective autophagy (Zaffagnini and Martens, 2016). In this context, the autophagy cargo is initially switched from mitochondria to macromolecules including inhibitors of T cell receptor (TCR) signaling (Hubbard et al., 2010; Valdor et al., 2014) and cell cycle (Jia et al., 2015). Subsequently, as T cells undergo differentiation, the autophagic degradation of the NF-κB regulator Bcl10 occurs (Paul et al., 2012). Autophagy also impacts on helper and cytotoxic T cell effectors, with Th1, Th2, and Treg cells relying on autophagy for survival (Kovacs et al., 2012; Kabat et al., 2016; Wei et al., 2016) and cytotoxic T lymphocytes (CTL) for their function and for memory maintenance (Puleston et al., 2014; Xu et al., 2014).

The autophagy machinery has been extensively characterized. Autophagy is initiated by the ULK complex, consisting of ULK1/2, ATG13, FIP200, and ATG101, which promotes phagophore nucleation through the class III PI3-K complex, consisting of VPS34, VPS15, BECLIN 1, and ATG14L. In order to engulf the cargo, the phagophore elongates and subsequently closes. These two steps involve the ATG12-ATG5 conjugation system, which is recruited to the phagophore by ATG16L. The conjugation system acts as an E3-like ligase to promote the cleavage and lipidation of ATG8/LC3, resulting in the phosphatidyl ethanolamine-conjugated form that binds to the phagophore membrane. Following phagophore closure, the resulting autophagosomes undergo dynein-dependent transport along the microtubules to a perinuclear location, where they fuse with lysosomes to become autolysosomes, delivering their cargo for degradation (Dikic and Elazar, 2018). This basic process is fine-tuned by a plethora of regulators and effectors. Among these is the intraflagellar transport (IFT) system, a multimolecular protein complex which controls the assembly of the primary cilium, a signaling organelle present in the majority of vertebrate cells (Pampliega et al., 2013; Prevo et al., 2017). Two integral components of the IFT system, IFT20 and IFT88, have been shown to mediate the transport of some components of the autophagic machinery to the cilium during cell starvation, with IFT20 binding ATG16L1 at the Golgi apparatus and shuttling it to the base of the cilium, wherefrom it enters the cilium with the assistance of IFT88 (Pampliega et al., 2013).

We have previously shown that, unexpectedly, IFT20 plays a key role in the activation of the non-ciliated T cells in a complex with other IFT components by regulating the assembly of the immune synapse, a specialized signaling interface that forms when a T cell encounters a cognate antigen presenting cell (Finetti et al., 2009, 2011). This function involves the ability of IFT20 to associate with the Golgi complex and endocytic compartments, the primary one among the latter being the early endosome, to control the intracellular traffic of the T cell antigen receptor and the transmembrane adaptor linker for activation of T cells (LAT) (Finetti et al., 2009, 2014; Vivar et al., 2016). Interestingly, we have recently implicated IFT20 in another vesicular trafficking-related process, the mannose-6-phosphate receptor-dependent transport of acid hydrolases to lysosomes, on which lysosome biogenesis and function depend (Finetti et al., 2020). Consistent with the central role of lysosomes in autophagy, both basal and starvation-induced autophagy are impaired in IFT20-deficient T cells (Finetti et al., 2020). However, the implication of the IFT system at early steps of autophagy in ciliated cells (Pampliega et al., 2013) suggests that IFT20 could participate in T cell autophagy also directly. Here, we show that IFT20 promotes ATG16L1 localization to the Golgi complex and early endosomes through its interaction with GMAP210 and Rab5, respectively. We demonstrate that under basal conditions IFT20 participates in autophagosome formation at early endosomes, but not at the Golgi apparatus, by allowing for the recruitment of ATG16L1 to early endosome-associated BECLIN 1 complex, thereby promoting local LC3-II accumulation. Our results identify IFT20 as an adaptor that targets ATG16L1 and downstream autophagy regulators to a specific endomembrane compartment, resulting in autophagosome biogenesis in T cells.

MATERIALS AND METHODS

Cells, Plasmids, and Transfections

Control, IFT20KD, and GMAPKD Jurkat T cell lines were generated as previously described (Finetti et al., 2009; Galgano et al., 2017). Jurkat T cells were stably transfected with the pEGFP-N1 plasmid construct encoding full-length IFT20, or a deletion mutant of IFT20 lacking aminoacid residues 73–132, which include the coiled-coil domain (ΔCC IFT20), or the respective empty vector. Stably transfected cells were selected in G418-containing medium at the final concentration of 1 mg/ml (Gibco/Thermo Fisher Scientific, MA, United States). Transient transfections were carried out by electroporation using pCMV-EGFP-C3-Rab5a (kindly provided by M. Zerial), pEGFP 2xFYVE (kindly provided by A. De Matteis), pEGFP-N1 IFT20-GFP, or pEGFP-N1 ΔCC IFT20-GFP [1 μg/1 × 10^6 cells in 800 μl of OPTI-MEM (Gibco/Thermo Fisher Scientific, MA, United States)] and analyzed 24 h post-transfection.

Cloning and Purification of Recombinant Proteins

GFP- and GST-tagged mutants of IFT20 were generated by cloning the sequences that encode the IFT20 N-terminus lacking the coiled-coil domain (ΔCC-IFT20, aa 1–73), the IFT20 C-terminus including the coiled-coil domain (CC-IFT20, aa 74–132), and the full-length protein (IFT20, aa 1–132) in-frame with the tags into the pEGFP-N1 (#6085-1 Addgene) and pGEX-6P-2

vectors (#27-4598-01 Addgene). The sequences were amplified by PCR using the primers listed in **Supplementary Table 1**. The 5'-ends of the primers were modified to add compatible restriction sites (*Xho*I and *Kpn*I for pEGFP-N1, *Eco*RI and *Xho*I for pGEX-6P-2) and extra base pairs that ensure efficient DNA cleavage by restriction enzymes.

The recombinant GST fusion proteins were affinity purified on GSH-Sepharose (GE Healthcare, Italy) from bacterial cultures incubated with 0.25 mM isopropyl-β-D-thiogalactopyranoside (Sigma-Aldrich) overnight at RT and lysed in B-PER Complete Bacterial Protein Extraction Reagent (Thermo Fisher Scientific, MA, United States) according to the manufacturers' instructions.

Antibodies and Reagents

All primary commercial antibodies used in this manuscript are listed in **Supplementary Table 2**, where information about the dilutions used for immunoblotting and immunofluorescence is specified. Polyclonal anti-IFT20 antibodies (Pazour et al., 2002) were kindly provided by G. Pazour. Secondary peroxidase-labeled antibodies were from Amersham Biosciences. Alexa Fluor 488- and 555-labeled secondary Abs were from Thermo Fisher Scientific (anti-mouse 488, #A11001; anti-rabbit 488, #A11008; anti-mouse 555, #A21422; and anti-rabbit 555, #A21428). Chloroquine was purchased from Sigma-Aldrich (C6628).

Immunoprecipitation, *in vitro* Binding Assays and Immunoblotting

Immunoprecipitation experiments were performed as previously described (Finetti et al., 2020). Briefly, 5×10^7 cells/sample were lysed in 0.5% Triton X-100 in 20 mM Tris–HCl (pH 8), 150 mM NaCl in the presence of protease inhibitors (Sigma-Aldrich) and the phosphatase inhibitor sodium vanadate (Sigma-Aldrich). Postnuclear supernatants (2 mg/sample) were immunoprecipitated for 2 h at 4°C with gentle agitation using 2 μg of rabbit anti-IFT20 antibody (#13615-1-AP, Proteintech, United Kingdom), anti-ATG16L1 antibody (#8089S, Cell Signaling) or mouse anti-BECLIN 1 mAb (sc-48341, Santa Cruz), and protein A-Sepharose (PAS, 3 mg/sample, GE Healthcare, Italy), after a preclearing step on PAS (1 h, 3 mg/sample). Subsequently, all samples were washed 4X with 1 ml 0.5% Triton X-100 lysis buffer, resuspended in 15 μl Laemmli buffer (#B0007, Life Technologies/Thermo Fisher Scientific, MA, United States), boiled for 5 min and then subjected to SDS-PAGE.

In vitro-binding assays were carried out using recombinant GST, IFT20-GST, ΔCC IFT20-GST, or CC IFT20-GST on GSH-Sepharose precleared postnuclear supernatants from 5×10^7 cells/sample lysed in 0.5% Triton X-100 in the presence of protease and phosphatase inhibitors as described (Pacini et al., 1998). The binding reaction was performed for 2 h at 4°C with gentle agitation. Samples were washed 4X with 1 ml 0.5% Triton X-100 lysis buffer in the presence of protease and phosphatase inhibitors, resuspended in 15 μl Laemmli buffer, boiled for 5 min and subjected to SDS-PAGE.

Immunoblotting was carried out using peroxidase-labeled secondary antibodies and a chemiluminescence detection kit (#34578, Thermo Fisher Scientific, MA, United States). Membranes were reprobed with control antibodies after stripping carried out using ReBlot Plus Mild Antibody Stripping Solution, 10× (#2502, Merck Millipore, Italy). Blots were scanned using a laser densitometer (Duoscan T2500; Agfa, Belgium) and quantified by using ImageJ 1.46r (National Institutes of Health, United States).

Immunofluorescence Microscopy and Colocalization Analyses

For immunofluorescence analysis, Jurkat cells were allowed to adhere for 15 min to poly-L-lysine-coated wells and then fixed by immersion in methanol for 10 min at −20°C. Alternatively, for LC3B labeling, Jurkat cells were incubated 10 min in 50 mM NH_4Cl after fixation in 4% paraformaldehyde for 10 min at RT, and then permeabilized in methanol for 10 min at −20°C. Fixed and permeabilized samples were washed for 5 min in PBS and incubated with primary antibodies overnight at 4°C, after blocking in 5% normal goat serum and 1% BSA for 1 h. Samples were washed for 5 min in PBS and incubated for 45 min at RT with Alexa-Fluor- 488-, Alexa-Fluor- 555-, and Alexa-Fluor-647-labeled secondary antibodies.

Confocal microscopy was carried out on a Zeiss LSM700 or a TCS SP8 Confocal laser scanning microscopy (Leica, Germany) using a 63× objective with pinholes opened to obtain 0.8 μm-thick sections. For the analyses shown in **Figures 2A**, **3A,D**, **4A** confocal microscopy imaging was carried out with a 0.2 Airy Unit pinhole which allows to obtain thinner optical section (less than 0.4 μm) from a single image. Detectors were set to detect an optimal signal below the saturation limits. Images were processed with Zen 2009 image software (Carl Zeiss, Jena, Germany).

The quantitative colocalization analysis was performed on median optical sections using ImageJ and JACoP plug-in to determine Mander's coefficient as previously described (Finetti et al., 2014). The ATG16L1 dispersion was quantified by measuring fluorescence intensity in concentric regions using ImageJ. Circular regions were centered on the point of ATG16L1 maximal intensity and designed proportionally to the cell size (inner circle, middle ring, and outer ring diameters, corresponding to 1/9, 1/4.5, and 1/2.25 of cell diameter, respectively) (Progida et al., 2010). Alternatively, ATG16L1 dispersion was measured using ImageJ by calculating the distance of $ATG16L1^+$ dots (identified using the same fluorescence threshold in control and IFT20KD cells in each experiments) from the centrosome (identified by pericentrin staining).

Autophagic Flux and $LC3^+$ Dot Number Measurement

To analyze the autophagic flux, 1×10^6 cells/sample were incubated in RPMI 1640 added with 7.5% BCS for 30 min at 37°C in the presence or absence of 40 μM chloroquine. Subsequently, cells were harvested and lysed in 1% Triton X-100 in 20 mM Tris–HCl pH 8.0, 150 mM NaCl in the presence of protease and phosphatase inhibitors, and processed for immunoblotting with anti-LC3B antibodies. Autophagy flux was calculated as

the difference in LC3-II levels, normalized to actin, between chloroquine-treated and untreated cells.

The number of LC3B$^+$ vesicles was determined by immunofluorescence microscopy. 1×10^5 cells/sample were incubated in RPMI 1640 added with 7.5% BCS for 30 min at 37°C with or without 40 μM chloroquine and allowed to adhere to poly-L-lysine-coated wells. Subsequently, the samples were fixed, permeabilized and stained as described above.

Membrane Fractionation

Cytosolic and membrane fractions were purified as previously described (Finetti et al., 2014). Jurkat cells (3×10^7/sample) were resuspended in 1 ml homogenization medium (0.25 M sucrose, 1 mM EDTA, 10 mM Tris–HCl pH 7.4) in the presence of protease and phosphatase inhibitors. The samples were homogenized by 10 pestle strokes through Dounce homogenization (tight Dounce homogenizer, Wheaton, United States) and 10 passages through a 26-gauge syringe needle. The homogenate was centrifuged at 3,000 × *g* for 5 min at 4°C to remove nuclei and the supernatant was centrifuged at 65,000 × *g* for 1 h at 4°C. The supernatant (cytosolic fraction) was collected, while the pellet (membrane fraction) was lysed in homogenization buffer containing protease and phosphatase inhibitors with 0.5% Triton, and centrifuged at 16,100 × *g* for 20 min at 4°C to eliminate insoluble material. The same quantities of membrane protein-enriched supernatant and cytosolic fraction were analyzed by SDS-PAGE.

Statistical Analysis

GraphPad (Prism Software) was used to calculate mean values, standard deviation values and statistical significance. Values with Gaussian distribution were analyzed using Student's *t* test (paired or unpaired), one sample *t* test (theoretical mean = 1) or one-way ANOVA. Values without normal distribution were analyzed using Mann–Withney test or Kruskal–Wallis test. A level of $P < 0.05$ was considered statistically significant.

RESULTS

IFT20 Interacts Constitutively With ATG16L1 in T Cells

IFT20 interacts with ATG16L1 and colocalizes with this protein at intracellular vesicles in ciliated cells (Pampliega et al., 2013). The evidence that T cells share common regulators of vesicular trafficking with ciliated cells (Cassioli and Baldari, 2019) and that IFT20 deficiency is associated to impaired autophagic flux in T cells (Finetti et al., 2020) raises the question of whether IFT20 may interact with ATG16L1 also in non-ciliated T cells to promote autophagy. To address this issue, we performed co-immunoprecipitation experiments in Jurkat T cells, which showed that IFT20 interacts with ATG16L1 (**Figure 1A**). Consistent with this finding, IFT20 displayed partial colocalization with ATG16L1 in Jurkat T cells, as assessed by immunofluorescence (**Figure 1B**). The ability of IFT20 to interact with ATG16L1 was confirmed by *in vitro* GSH-Sepharose pull-down assays using an IFT20-GST fusion protein (**Figures 1C,D**). Hence, similar to ciliated cells, IFT20 interacts with ATG16L1 in the non-ciliated T cell.

IFT20 is a small protein containing a single coiled-coil (CC) domain at its C-terminus (**Figure 1C**) that has been implicated in its heterodimerization with other CC domain-containing components of the IFT complex (Baker et al., 2003; Omori et al., 2008). To map the interaction of ATG16L1 on IFT20 we generated GST fusion proteins with the IFT20 CC domain (amino acid residues 74–132; CC IFT20) or the full-length protein lacking the CC domain (amino acid residues 1–73; ΔCC IFT20). The GST-pull down assays showed that ATG16L1 binds to IFT20 regardless of the presence of the CC-domain (**Figure 1D**). These results indicate that IFT20 interacts with ATG16L1 mostly through a molecular determinant localized within its unstructured region, potentially using its CC domain to couple ATG16L1 to sites of autophagosome formation.

To investigate the role of the CC domain in basal IFT20-dependent autophagy we generated Jurkat T cells transfectants expressing IFT20-GFP or a deletion mutant lacking the CC domain, fused to GFP (ΔCC IFT20-GFP) (**Figure 1E** and **Supplementary Figure 1A**). A similar construct encoding the isolated GFP-tagged CC domain was not expressed at detectable levels, likely due to low protein stability (data not shown). The impact of ΔCC IFT20 expression on the autophagic flux was assessed by immunoblot. Cells were either untreated or treated with chloroquine, which blocks the degradation of LC3-II by impairing autophagosome fusion with lysosomes (Mauthe et al., 2018). Immunoblot analysis with anti-LC3B antibodies showed that under basal conditions the autophagic flux was decreased in cells expressing ΔCC IFT20-GFP compared to controls expressing full-length IFT20-GFP (**Figure 1F**). This result was confirmed by immunofluorescence analysis of LC3$^+$ dots, which showed a decreased autophagic flux in ΔCC IFT20-GFP-expressing cells compared to controls expressing the full-length GFP fusion protein (**Figure 1G**). Hence, the pro-autophagic function of IFT20 requires its CC domain.

IFT20 Tethers ATG16L1 to Cellular Membranes

ATG16L1 is a cytoplasmic protein that is recruited to multiple cellular membranes which can serve as membrane sources for autophagosomes (Xiong et al., 2018). Although the mechanism of ATG16L1 recruitment to membranes is not fully understood, ATG16L1 has been reported to interact with the autophagy regulator FIP200 and with the phosphatidylinositol 3-phosphate [PI(3)P]-binding protein WIPI2. Both these interactions are functional to the association of ATG16L1 with isolation membranes, particularly at the endoplasmic reticulum, during autophagosome formation. ATG16L1 also interacts with the small GTPase Rab33 at the Golgi complex, SNX18/Rab11 at recycling endosomes, and the membrane coat protein clathrin at the plasma membrane, wherefrom it is transferred to the endocytic compartment (Itoh et al., 2008; Ravikumar et al., 2010; Gammoh et al., 2013).

The association of IFT20 with the Golgi apparatus and endocytic compartments (Finetti et al., 2009) and its ability to

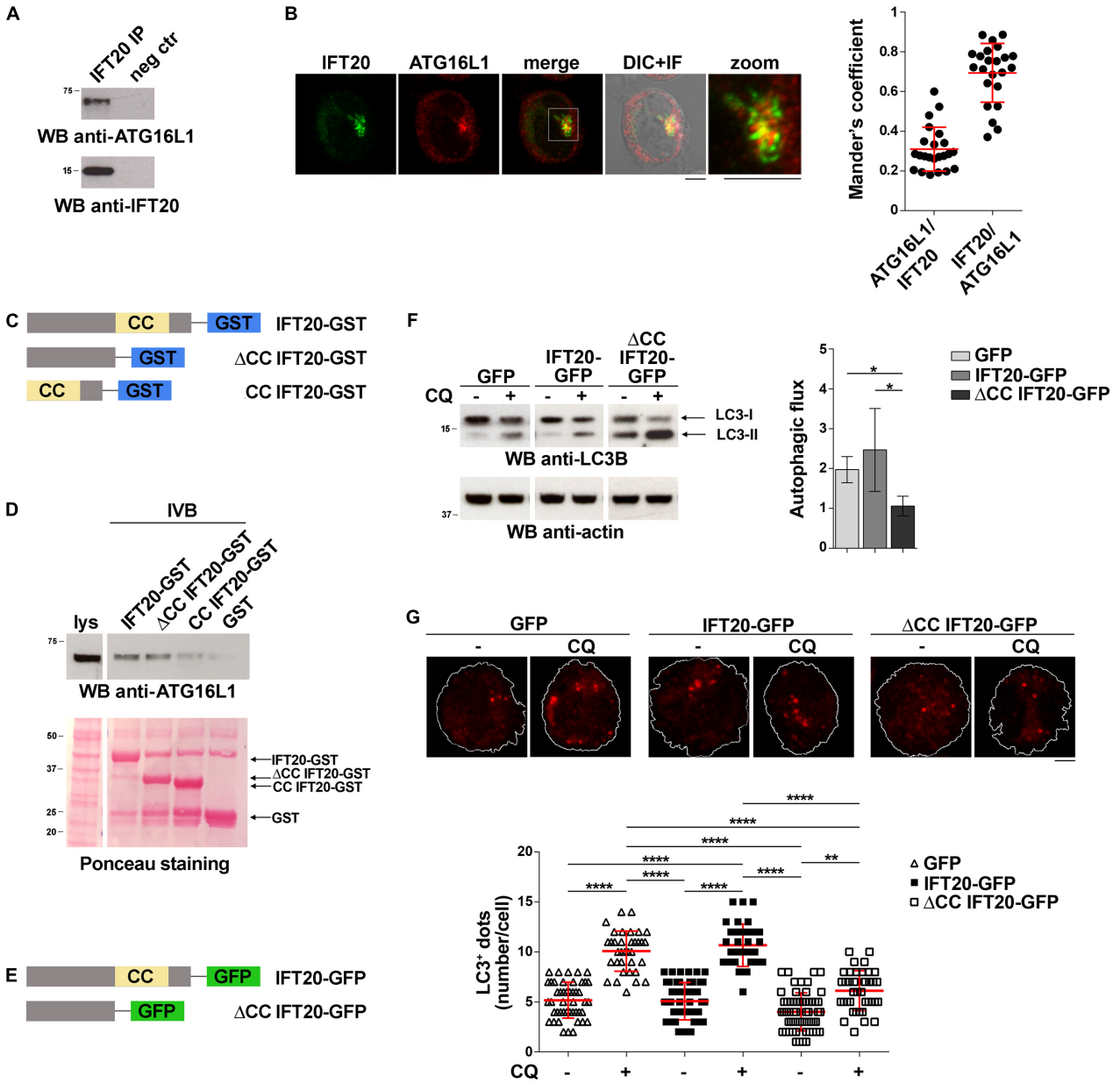

FIGURE 1 | IFT20 binds to ATG16L1 and promotes T cell autophagy through its CC domain. **(A)** Western blot (WB) analysis with anti-ATG16L1 antibodies of IFT20-specific immunoprecipitates from lysates of Jurkat T cells. A preclearing control (proteins bound to Protein-A–Sepharose before the addition of primary antibody) is included in each blot (neg ctr). The migration of molecular mass markers is indicated. The immunoblots shown are representative of at least 3 independent experiments. **(B)** Immunofluorescence analysis of IFT20 and ATG16L1 in Jurkat cells. Representative medial optical sections and overlay of immunofluorescence (IF) and differential interference contrast (DIC) images are shown (IF + DIC). The graph shows the quantification (using Mander's coefficient) of the weighted colocalization of IFT20 and ATG16L1 in Jurkat cells. The data are expressed as mean ± SD (23 cells/sample; $n = 3$). Scale bars: 5 μm. **(C)** Schematic representation of the GST fusion proteins with full-length IFT20 (IFT20-GST), or the full-length protein lacking the CC domain (ΔCC IFT20-GST) or the CC domain (CC IFT20-GST). The CC domain is highlighted as a yellow box. **(D)** Immunoblot analysis with anti-ATG16L1 antibodies of *in vitro*-binding assays carried out on post-nuclear supernatants of Jurkat cells using IFT20-GST, ΔCC IFT20-GST, and CC IFT20-GST fusion proteins, or GST as negative control. The Ponceau red staining of the same filter is shown to compare the levels of fusion proteins and GST used in the assay. The immunoblot shown is representative of three independent experiments. **(E)** Schematic representation of the GFP fusion protein with IFT20 (IFT20-GFP) or with the full-length protein lacking the CC domain (ΔCC IFT20-GFP). The CC domain is highlighted as a yellow box. **(F)** Immunoblot analysis of LC3B in lysates of Jurkat cells expressing GFP, IFT20-GFP, or ΔCC IFT20-GFP in the presence or absence of chloroquine (CQ, 40 μM). The migration of molecular mass markers is indicated. The graph shows the autophagic flux in Jurkat transfectants, calculated as the difference in the levels of LC3II/actin between CQ-treated and CQ-untreated samples (mean fold ± SD; one-way ANOVA; $n \geq 3$). **(G)** Immunofluorescence analysis of LC3B in Jurkat cells expressing GFP, IFT20-GFP, or ΔCC IFT20-GFP either untreated or treated for 30 min with chloroquine (CQ, 40 μM). The *z*-projection of maximum intensity and the quantification of the number of $LC3^+$ dots/cell are shown. At least 35 cells from three independent experiments were analyzed (mean ± SD; Kruskal–Wallis test). $^*P < 0.05$; $^{**}P < 0.01$; $^{****}P < 0.0001$.

interact with ATG16L1 (**Figure 1**) suggest a role for IFT20 in tethering ATG16L1 to endomembranes. To test this hypothesis we addressed the outcome of RNAi-mediated IFT20 depletion (IFT20KD; **Supplementary Figure 1B**) on the subcellular localization of ATG16L1. Immunofluorescence analysis showed that ATG16L1 was concentrated at a vesicular-like compartment in control cells, as previously reported in NIH3T3 cells (Itoh et al., 2008). The localization of ATG16L1 was altered to a significant extent in Jurkat cells stably knocked down for IFT20 expression, where it showed a dispersed pattern, as assessed by measuring the distance of ATG16L1^{+} vesicles from the centrosome as well as by quantifying the fluorescence intensity in concentric cellular regions from the point of maximal intensity (**Figures 2A,B**; Progida et al., 2010). These results support the notion that IFT20 contributes to the vesicular localization of ATG16L1 in T cells.

To confirm this function of IFT20, the association of ATG16L1 with cellular membranes was addressed biochemically by immunoblot analysis of cytosolic and membrane fractions obtained from control and IFT20KD Jurkat cells. ATG16L1 was detected both in cytosolic and in membrane fractions. IFT20 deficiency resulted in a decrease in the amount of ATG16L1 associated with the membrane fractions (**Figure 2C**), suggesting that the loss of ATG16L1 compartmentalization observed by immunofluorescence in IFT20KD cells results from its release from cellular membranes to the cytosol.

To understand whether the CC domain of IFT20, which is required for the pro-autophagic function of IFT20 (**Figures 1F,G**) but not for ATG16L1 binding (**Figure 1D**), affects the subcellular localization of ATG16L1, we carried out an immunofluorescence analysis of ATG16L1 in Jurkat T cells expressing IFT20-GFP or the ΔCC IFT20-GFP mutant (**Figure 1E** and **Supplementary Figure 1A**). At variance with IFT20-GFP, which did not elicit any detectable effect, the absence of the CC domain resulted in a complete loss of the vesicular pattern of ATG16L1 (**Figure 2D**), similar to that observed in IFT20KD cells (**Figures 2A,B**). The alteration in the subcellular localization of ATG16L1 was paralleled by a diffuse staining throughout the cell of ΔCC IFT20-GFP, with only the centrosomal localization remaining unaffected (**Figure 2E**). This suggests that ΔCC IFT20-GFP acts in a dominant negative fashion to prevent the interaction of endogenous, membrane-associated IFT20 with ATG16L1. Importantly, the defect in ATG16L1 localization observed in IFT20KD cells was rescued by restoring IFT20 expression, while ΔCC-IFT20 was unable to correct this defect (**Figure 2F** and **Supplementary Figure 1C**). Hence IFT20 mediates the vesicular localization of ATG16L1 in T cells and this function maps to its CC domain.

IFT20 Is Required for the Association of ATG16L1 With the Golgi Apparatus

To identify the membrane compartment ATG16L1 associates with in T cells, we carried out a colocalization analysis of ATG16L1 with the Golgi complex, one of the most IFT20-enriched subcellular compartments (Follit et al., 2006; Finetti et al., 2009). A decrease in the colocalization of ATG16L1 with the Golgi marker giantin was observed in IFT20KD cells compared to controls (**Figure 3A**), implicating IFT20 in the Golgi localization of ATG16L1.

IFT20 is known to associate with the Golgi apparatus through its interaction with the golgin GMAP210 (Follit et al., 2008). This interaction is mediated by the CC domain of GMAP210 (Follit et al., 2008; Zucchetti et al., 2019). To understand whether the IFT20-dependent association of ATG16L1 with the Golgi is mediated by GMAP210 we analyzed the subcellular localization of ATG16L1 in Jurkat cells knocked down for GMAP210 expression by RNA interference (**Supplementary Figure 1D**). Similar to IFT20KD cells, GMAP210KD cells showed a dispersed pattern of ATG16L1 staining, with a decrease in its association with the Golgi apparatus (**Figures 3B,C**). This was paralleled by a loss of IFT20 co-localization with the Golgi (**Figure 3D**), consistent with the ability of IFT20 to interact with GMAP210 in T cells (Galgano et al., 2017; Zucchetti et al., 2019).

To map the GMAP210 binding site on IFT20 we carried out pull-down assays using the IFT20-GST, ΔCC IFT20-GST, and CC IFT20-GST fusion proteins (**Figure 1C**). As expected, GMAP210 was found to interact with full-length IFT20 (**Figure 3E**). The CC domain of IFT20 was largely responsible for this interaction, as shown by the preferential binding to GMAP210 to the isolated CC domain compared to the fusion protein lacking the CC domain (**Figure 3E**). Consistent with this finding, the CC domain of IFT20 was essential for its association with the Golgi apparatus, as assessed in Jurkat cell transfectants expressing ΔCC IFT20-GFP (**Figure 3F**).

The Golgi apparatus has been identified as a source of autophagosomal membranes, contributing to phagophore elongation through ATG16L1 recruitment (Itoh et al., 2008; Staiano and Zappa, 2019). To understand whether the GMAP210-dependent, IFT20-mediated recruitment of ATG16L1 to the Golgi is implicated in the pro-autophagic function of IFT20 we measured the autophagic flux in GMAP210KD cells. Remarkably, GMAP210 deficiency did not impair basal autophagy, as assessed both by immunoblot and by immunofluorescence analysis of LC3 (**Figures 3G,H**). Hence, while IFT20 couples ATG16L1 to the Golgi in T cells through its CC domain-dependent interaction with GMAP210, the resulting Golgi association of ATG16L1 does not lead to autophagosome formation. Accordingly, the recruitment of BECLIN 1 to the Golgi complex is minimal in Jurkat cells, as assessed by immunofluorescence analysis of the colocalization of BECLIN 1 with the *cis*-Golgi marker GM130 (**Supplementary Figure 2**).

IFT20 Is Required for the Association of ATG16L1 With Early Endosomes

In T cells IFT20 is associated not only with the Golgi apparatus, but also with other endomembrane compartments, a major one being early endosomes, where it interacts with Rab5 (Finetti et al., 2014). Of relevance, Rab5 is a component of the macromolecular complex containing BECLIN 1 and the class III phosphatidylinositol-3 kinase VPS34 that regulates autophagosome formation (Ravikumar et al., 2008). An association of ATG16L1 with both early and recycling endosomes

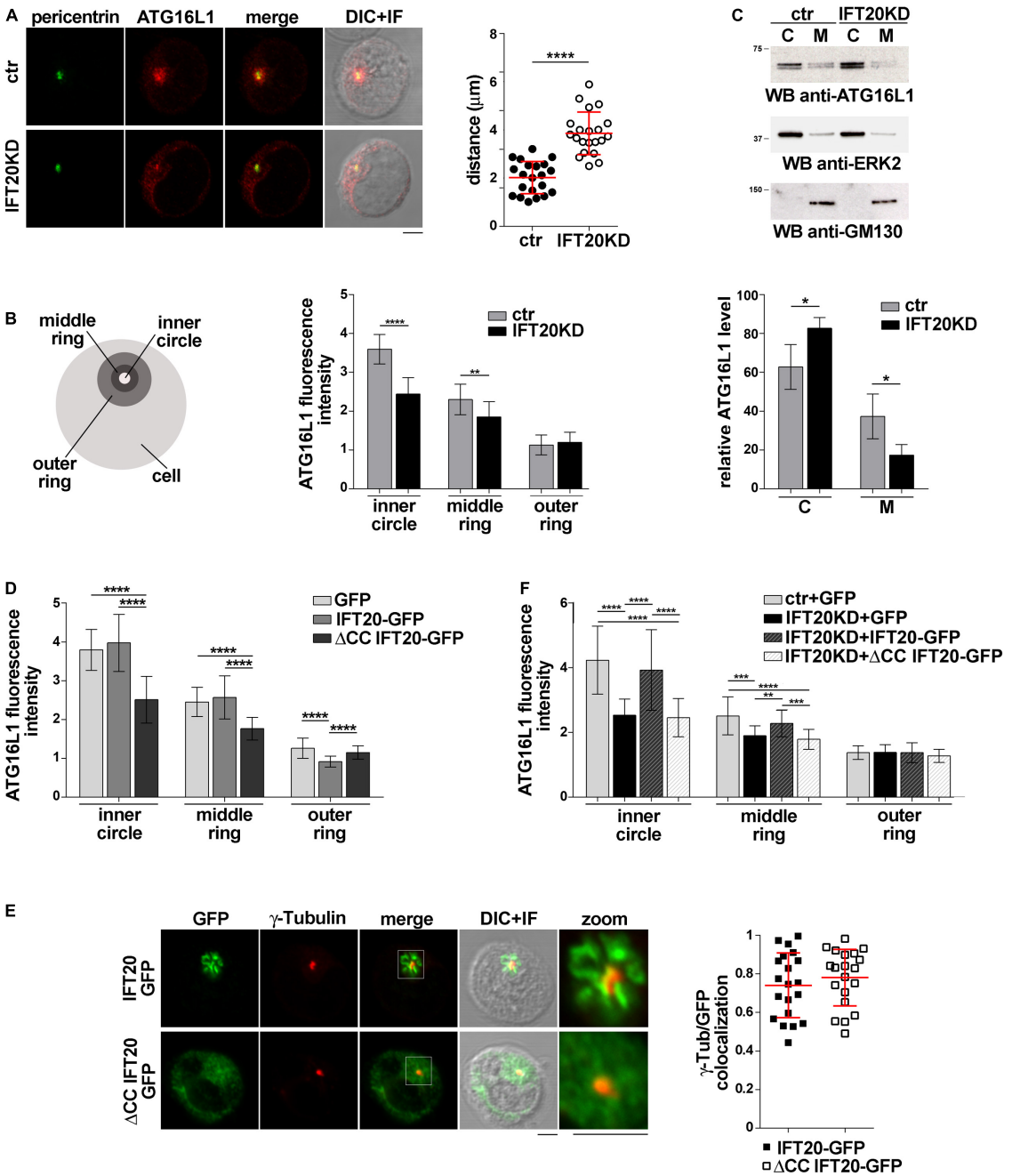

FIGURE 2 | IFT20 regulates the intracellular localization of ATG16L1. **(A,B)** Immunofluorescence analysis of ATG16L1 and the centrosomal protein pericentrin in control (ctr) and IFT20KD Jurkat cells. Representative medial optical sections and overlay of immunofluorescence and DIC images are shown (IF + DIC). Scale bars: 5 μm. **(A)** The graph shows the quantification of the distance of ATG16L1^{+} vesicles from the centrosome (mean ± SD, 21 cells; $n = 3$; Student's t-test). **(B)** Histogram showing the quantification of fluorescence intensity in the concentric regions indicated in the scheme and defined from the point of ATG16L1 maximal intensity (mean ± SD, ≥ 20 cells/sample; $n = 3$; Mann–Whitney test). **(C)** Immunoblot analysis of ATG16L1 in cytosolic (C) and membrane (M) fractions purified from control and IFT20KD Jurkat cells. The cytosolic protein ERK2 and the *cis*-Golgi marker GM130 were used to assess the purity of cytosolic and membrane fractions, respectively. The migration of molecular mass markers is indicated. The histogram shows the quantification of the percentage of ATG16L1 in the cellular fractions obtained from 4 independent experiments (mean ± SD; Student's t-test). **(D)** Immunofluorescence analysis of ATG16L1 in GFP, IFT20-GFP, and ΔCC IFT20-GFP Jurkat transfectants. The histograms show the quantification of fluorescence intensity in the concentric regions described above (mean ± SD, ≥ 25 cells/sample; $n = 3$; Mann–Whitney test). **(E)** Quantification (using Mander's coefficient) of the weighted colocalization of γ-tubulin with GFP in medial confocal sections of IFT20-GFP or ΔCC IFT20-GFP expressing Jurkat cells (mean ± SD; ≥ 20 cells/line; $n = 3$). Representative images (medial optical sections and overlay DIC + IF) are shown. Scale bar: 5 μm. **(F)** Immunofluorescence analysis of ATG16L1 in control and IFT20KD cells transiently transfected with either empty vector (GFP), or the IFT20-GFP construct or the ΔCC IFT20-GFP construct. The graph shows the quantification of fluorescence intensity in the concentric regions described above (mean ± SD, ≥ 25 cells/sample; $n = 3$; Mann–Whitney test). $^{*}P < 0.05$; $^{**}P < 0.01$; $^{***}P < 0.001$; $^{****}P < 0.0001$.

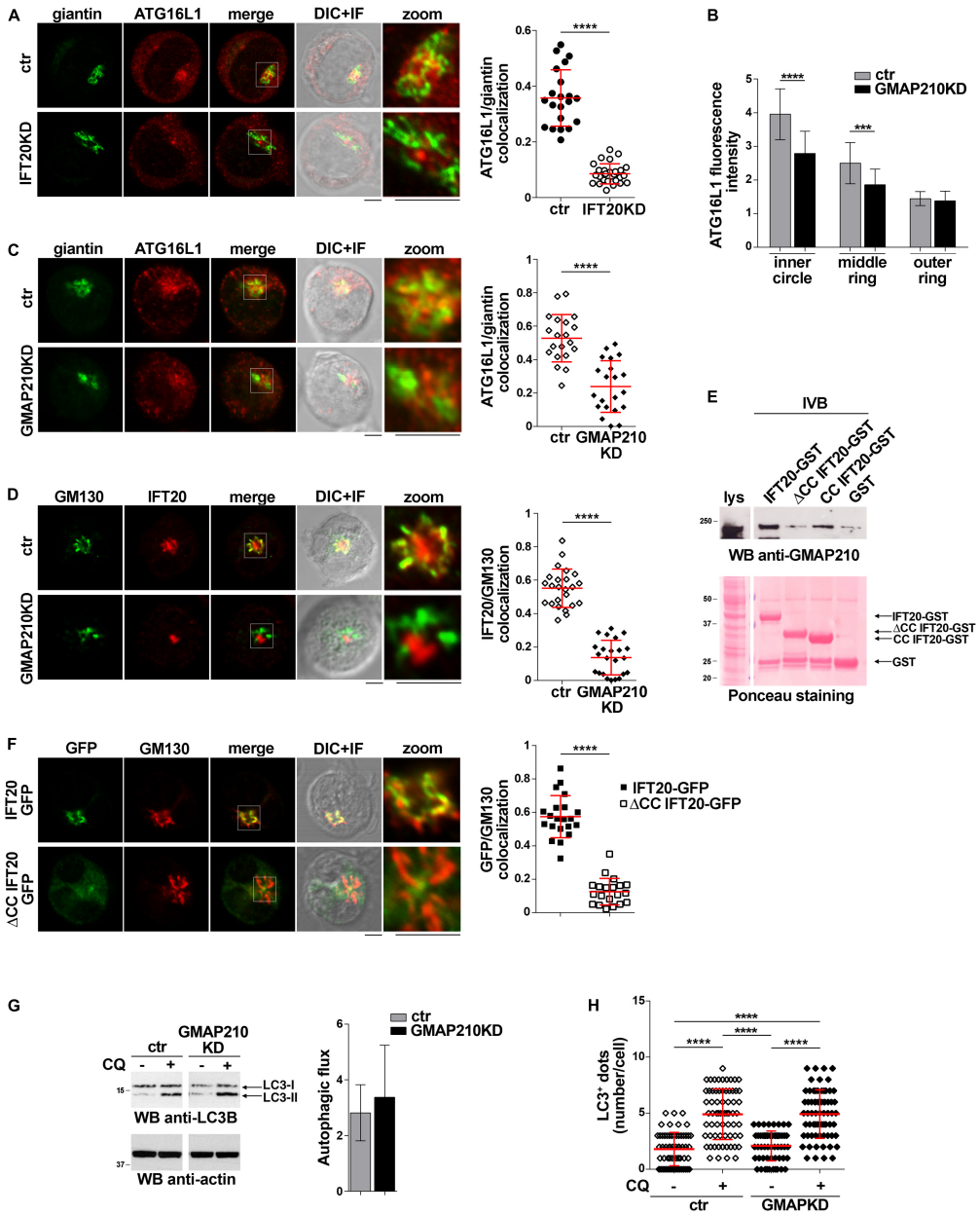

FIGURE 3 | IFT20 couples ATG16L1 to the Golgi through its CC domain-mediated interaction with GMAP210. **(A)** Quantification using Mander's coefficient of the weighted colocalization of ATG16L1 and the Golgi marker giantin in ctr and IFT20KD Jurkat cells (≥ 21 cells/sample, $n = 3$; mean ± SD; Student's *t*-test). Representative images (medial optical sections and the overlay DIC + IF) are shown. Scale bar: 5 μm. **(B)** Quantification of fluorescence intensity of ATG16L1 in the concentric regions previously described (**Figure 2B**) in control and GMAP210KD cells (mean ± SD, ≥ 25 cells/sample; $n = 3$; Mann–Whitney test). **(C,D)** Immunofluorescence analysis of ATG16L1 and giantin **(C)** or IFT20 and the Golgi marker GM130 **(D)** in control and GMAP210KD cells. Representative medial optical sections and overlay of immunofluorescence (IF) and differential interference contrast (DIC) images are shown (IF + DIC). The graph shows the quantification (using Mander's coefficient) of the weighted colocalization of ATG16L1 and giantin **(C)** or IFT20 and GM130 **(D)**. The data are expressed as mean ± SD (≥ 20 cells/sample; $n = 3$; Mann–Whitney test). Scale bars: 5 μm. **(E)** Immunoblot analysis with anti-GMAP210 antibodies of *in vitro*-binding assays carried out on post-nuclear supernatants of Jurkat cells using IFT20-GST, ΔCC IFT20-GST and CC IFT20-GST fusion proteins, or GST as negative control. The Ponceau red staining of the same filter is shown to compare the levels of fusion proteins and GST used in the assay. The immunoblot shown is representative of three independent experiments. **(F)** Quantification (using Mander's coefficient) of the weighted colocalization of the *cis*-Golgi marker GM130 with GFP in medial confocal sections of IFT20-GFP or ΔCC IFT20-GFP expressing Jurkat cells (mean ± SD; ≥ 20 cells/line; $n = 3$; Mann–Whitney test). Representative images (medial optical sections and overlay DIC + IF) are shown. Scale bar: 5 μm. **(G)** Immunoblot analysis of LC3B in lysates of control or GMAP210KD cells in the presence or absence of chloroquine (CQ, 40 μM). The migration of molecular mass markers is indicated. The histograms show the autophagic flux calculated as the difference in the levels of LC3II/actin between CQ-treated and CQ-untreated samples (mean fold ± SD; Student's *t*-test; $n \geq 3$). **(H)** Quantification of the number of $LC3^+$ dots/cell in control or GMAP210KD cells either untreated or treated for 30 min with chloroquine (CQ, 40 μM). At least 35 cells from three independent experiments were analyzed (mean ± SD; Kruskal–Wallis test). $^{**}P < 0.01$; $^{***}P < 0.001$; $^{****}P < 0.0001$.

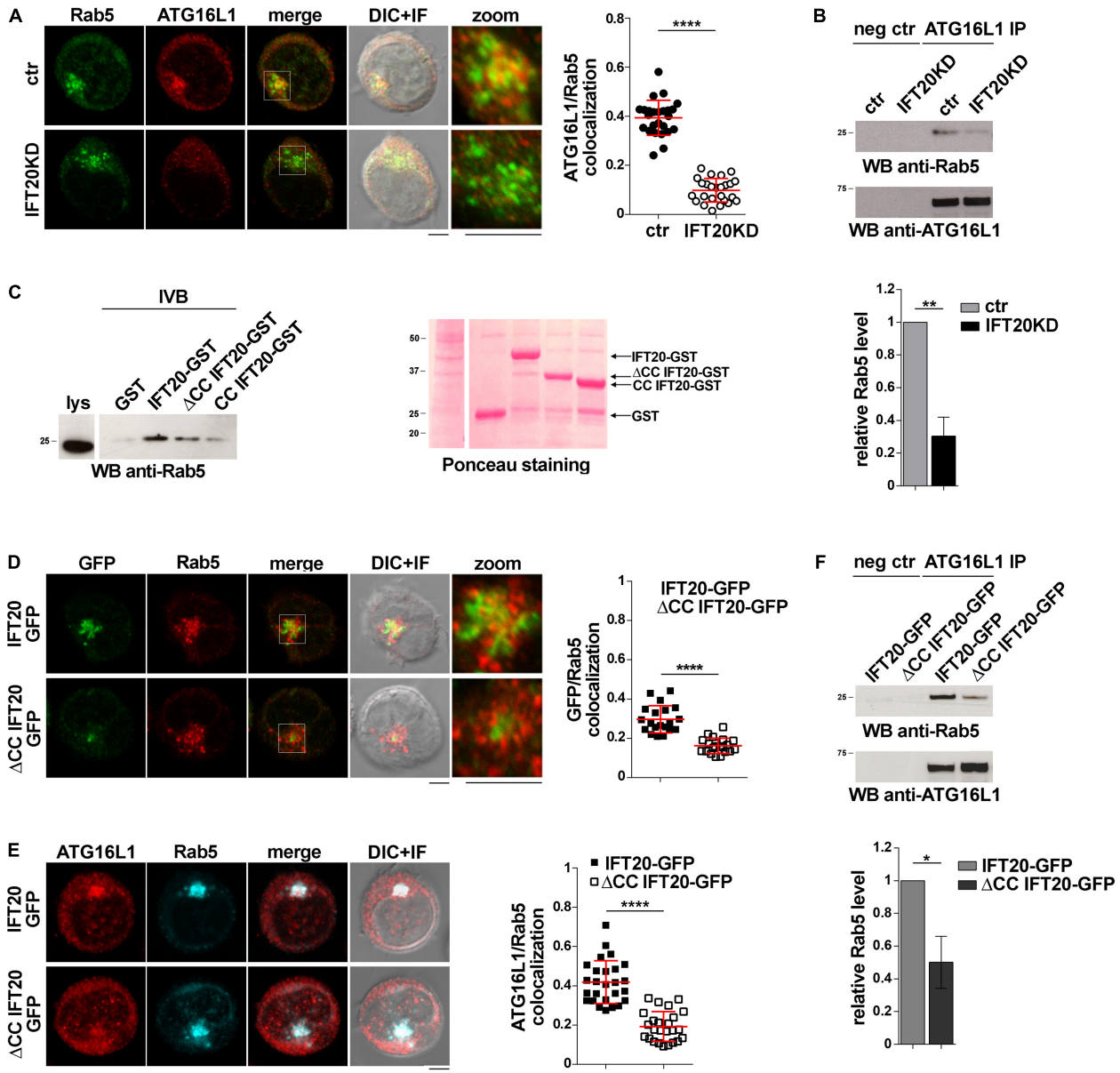

FIGURE 4 | IFT20 couples ATG16L1 to early endosomes through interaction with Rab5. **(A)** Immunofluorescence analysis of ATG16L1 and Rab5 GFP in control and IFT20KD Jurkat cells. Representative medial optical sections and overlay of immunofluorescence and DIC images are shown (IF + DIC). Scale bar: 5 μm. The graph shows the quantification of the weighted colocalization (Mander's coefficient) of ATG16L1 and the early endosome marker Rab5 in ctr and IFT20KD Jurkat cells (= 25 cells/sample, $n = 3$; mean ± SD; Student's *t*-test). **(B)** Immunoblot analysis with anti-Rab5 antibodies of ATG16L1-specific immunoprecipitates from lysates of control and IFT20KD Jurkat cells. Preclearing controls are included in each blot (neg ctr). Tested proteins show comparable expression in total cell lysate from ctr and IFT20KD Jurkat cells (**Supplementary Figures 3A,B**). The migration of molecular mass markers is indicated. The quantification of the relative protein expression normalized to ATG16L1 (mean fold ± SD; ctr value = 1) is reported for each blot ($n = 3$; mean ± SD; Student's *t*-test). **(C)** Immunoblot analysis with anti-Rab5 antibodies of *in vitro*-binding assays carried out on post-nuclear supernatants of Jurkat cells using IFT20-GST, ΔCC IFT20-GST, and CC IFT20-GST fusion proteins, or GST as negative control. The Ponceau red staining of the same filter is shown to compare the levels of fusion proteins and GST used in the assay. The immunoblot shown is representative of three independent experiments. **(D)** Immunofluorescence analysis of GFP and Rab5 in Jurkat cells expressing IFT20-GFP and ΔCC IFT20-GFP. The graph shows the quantification using Mander's coefficient of the weighted colocalization of GFP and Rab5 in Jurkat transfectants reported as mean value/cell calculated on individual Rab5$^+$ dot (= 20 cells/sample, $n = 3$; mean ± SD; Student's *t*-test). **(E)** Immunofluorescence analysis of ATG16L1 and Rab5 in IFT20-GFP and ΔCC IFT20-GFP Jurkat transfectants. The graph shows the quantification of the weighted colocalization (Mander's coefficient) of ATG16L1 and Rab5 (≥ 25 cells/sample, $n = 3$; mean ± SD; Student's *t*-test) in Jurkat transfectants. Representative medial optical sections and overlay of immunofluorescence and DIC images are shown (IF + DIC). Scale bar: 5 μm. **(F)** Immunoblot analysis with anti-Rab5 antibodies of ATG16L1-specific immunoprecipitates from lysates of Jurkat cells expressing IFT20-GFP or ΔCC IFT20-GFP. Preclearing controls are included in each blot (neg ctr). The migration of molecular mass markers is indicated. The quantification of Rab5 levels normalized to ATG16L1 (mean fold ± SD; ctr value = 1) is shown ($n = 3$; mean ± SD; Student's *t*-test). $^{**}P < 0.01$; $^{***}P < 0.001$; $^{****}P < 0.0001$.

has been reported in other cell types (Ravikumar et al., 2010; Puri et al., 2013; Fraser et al., 2019), suggesting the possibility that IFT20 may exploit its interaction with Rab5 to recruit ATG16L1 to early endosomes to promote autophagy.

To investigate whether ATG16L1 associates with early endosomes in T cells and whether IFT20 is required for its localization, we carried out a colocalization analysis of ATG16L1 and Rab5 in control and IFT20KD T cells. Interestingly, we found that a pool of ATG16L1 was associated with Rab5$^+$ endosomes in control cells, as reported for glial cells (Fraser et al., 2019). IFT20 depletion resulted in a significant decrease in the colocalization of ATG16L1 with Rab5 (**Figure 4A**). Additionally, ATG16L1 was found to interact with Rab5 in co-immunoprecipitation experiments (**Figure 4B**). This interaction was impaired in IFT20 KD cells (**Figure 4B**).

To map the interaction of IFT20 with Rab5 we carried out pull-down assays using the IFT20-GST, CC IFT20-GST, and ΔCC IFT20-GST fusion proteins (**Figure 1C**). Rab5 interacted both with the GST-tagged isolated CC domain and with the fusion protein lacking the CC domain, indicating that molecular determinants mapping to different parts of IFT20 contribute to its ability to bind Rab5 (**Figure 4C**). Interestingly, the CC domain of IFT20 was found to be required for its association with early endosomes, as assessed in Jurkat cell transfectants expressing ΔCC IFT20-GFP and stained for Rab5 (**Figure 4D**). Additionally, ATG16L1 co-localization and interaction with Rab5 was compromised in these cells (**Figures 4E,F**). These results indicate that, by interacting with Rab5 and ATG16L1 using both its unstructured portion and its CC domain, IFT20 promotes the association of ATG16L1 with early endosomes.

IFT20 Is Required for the Interaction of ATG16L1 With Autophagy Regulators

The autophagy regulator BECLIN 1 assists the localization of ATG16L1 to the sites of autophagosome formation both indirectly and directly. BECLIN 1 forms a complex with VPS34, which induces a local increase in PI(3)P at the isolation membrane (Funderburk et al., 2010), leading to ATG16L1 recruitment through binding to the PI(3)P-binding adaptor WIPI2 (Dooley et al., 2014). Additionally, ATG16L1 interacts with BECLIN 1 in a complex that includes the gap junction protein connexin 43 (Bejarano et al., 2014). Compartment-specific interactors, such as Rab5 for early endosomes in HeLa cells (Ravikumar et al., 2008; Otomo et al., 2011), promote local autophagosome formation by recruiting BECLIN 1.

The finding that IFT20 is required for the association of ATG16L1 with membrane compartments in T cells raises the question of whether IFT20 is implicated in the formation of the autophagy-regulating complexes in which ATG16L1 participates. Since the IFT20-dependent recruitment of ATG16L1 to the Golgi apparatus does not appear to contribute to its pro-autophagic function in T cells (**Figures 3G,H**), we focused on early endosomes. In particular, we addressed the role of IFT20 in the interaction of ATG16L1 with BECLIN 1 at this membrane compartment. Similar to other cell types (Bejarano et al., 2014), ATG16L1 was found to co-immunoprecipitate and co-localize with BECLIN 1 in T cells. This association was impaired in IFT20KD T cells (**Figures 5A,B**). Conversely, IFT20 deficiency did not affect the ability of ATG16L1 to interact with its downstream autophagy-regulating partner ATG5 (**Figure 5C**), which is covalently bound to ATG12 (Mizushima et al., 1998). Additionally, neither the interaction of BECLIN 1 with Rab5 (**Figure 5D**) nor their co-localization (**Figure 5E**) were affected by IFT20 deficiency. Accordingly, PI(3)P production at early endosomes was comparable to controls in IFT20KD cells, as assessed by quantifying the co-localization of Rab5 with GFP in cells transiently transfected with a GFP-tagged reporter construct encoding the tandem FYVE domains of hepatocyte growth factor-regulated tyrosine kinase substrate, which specifically interacts with PI(3)P (**Figure 5F**). Together, these results suggest that IFT20 is required for the recruitment of the ATG16L1-ATG5-ATG12 complex to early endosomes that have been tagged for autophagosome formation by Rab5-associated BECLIN 1.

ATG16L1 is involved in determining the site of LC3 lipidation, functioning as a scaffold to recruit the ATG12-ATG5 conjugating enzyme and LC3 to allow for the transfer reaction of LC3 from ATG3 to phosphatidylethanolamine at the phagophore membrane (Hanada et al., 2007; Fujita et al., 2008). The potential impact of IFT20 depletion on the ability of ATG16L1 to interact with LC3 was assessed in co-immunoprecipitation experiments. ATG16L1 was found to co-immunoprecipitate with LC3-I (**Figure 6A**). This suggests that the pool of ATG16L1 recruited to early endosomes by IFT20 might in turn recruit LC3-I to promote its local cleavage and lipidation to LC3-II. In support of this notion, the interaction of ATG16L1 with LC3-I was significantly impaired in IFT20-deficient T cells (**Figure 6A**). To further address this issue cells were co-stained for LC3 and ATG16L1. IFT20 deficiency resulted in a decrease in the co-localization of ATG16L1 with LC3$^+$ dots (**Figure 6B**). As previously reported, the number of LC3$^+$ dots was higher in IFT20KD cells due to their impaired ability to clear autolysosomes (Finetti et al., 2020). Importantly, a decrease in the co-localization of LC3 with Rab5 was also observed under these conditions (**Figure 6C**). Taken together, these results indicate that IFT20 participates in autophagosome formation by targeting ATG16L1 and its partners ATG5-ATG12 to Rab5$^+$ and BECLIN-1$^+$ vesicles, allowing for the recruitment of LC3 to promote the local generation of isolation membranes at early endosomes.

DISCUSSION

We have previously reported that IFT20 indirectly promotes T cell autophagy by regulating the mannose-6-P receptor-dependent transport of acid hydrolases to lysosomes (Finetti et al., 2020). Based on the implication of IFT20 in autophagosome formation in ciliated cells (Pampliega et al., 2013), here we investigated the potential direct implication of IFT20 in this process in the non-ciliated T cell. We show that, under basal conditions, IFT20 interacts with the autophagy regulator ATG16L1 and recruits it to both the Golgi apparatus and early endosomes. For this function IFT20 exploits its CC domain to bind the golgin GMAP210 at the Golgi, and

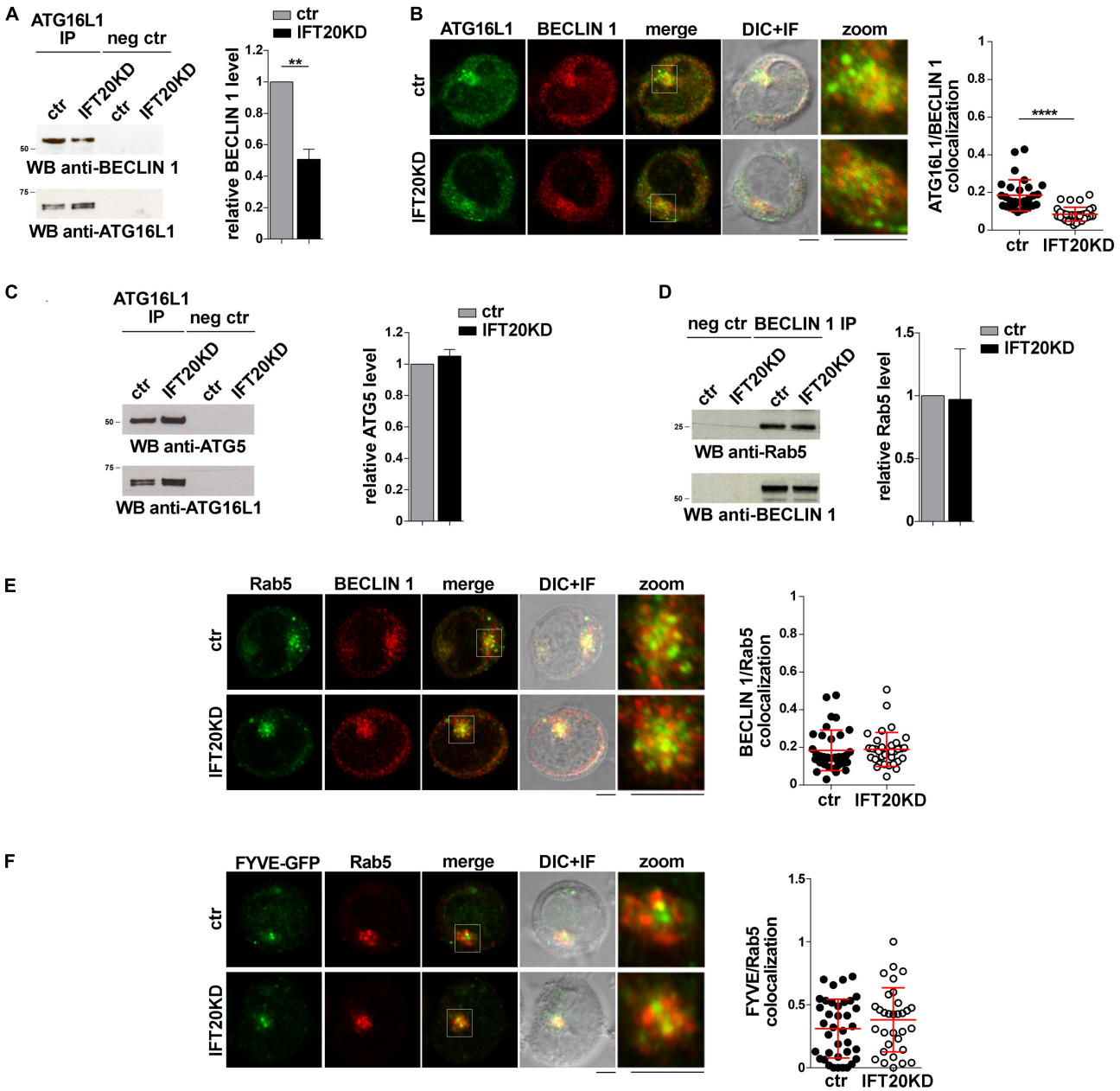

FIGURE 5 | IFT20 recruits ATG16L1 to early endosomes tagged for autophagosome formation. **(A)** Immunoblot analysis with BECLIN 1 antibodies of ATG16L1-specific immunoprecipitates from lysates of control and IFT20KD Jurkat cells. Preclearing controls are included in each blot (neg ctr). Tested proteins show comparable expression in total cell lysate from ctr and IFT20KD Jurkat cells (**Supplementary Figures 3A,C**). The migration of molecular mass markers is indicated. The quantification of the relative protein expression normalized to ATG16L1 (mean fold ± SD; ctr value = 1) is reported for each blot (n = 3; mean ± SD; Student's t-test). **(B)** Quantification (using Mander's coefficient) of the weighted colocalization of ATG16L1 with BECLIN 1 in medial confocal sections of control and IFT20KD Jurkat cells (mean ± SD; ≥ 30 cells/line; n = 3; Mann–Whitney test). Representative images (medial optical sections and overlay DIC + IF) are shown. Scale bar: 5 μm. **(C)** Immunoblot analysis with ATG5 antibodies of ATG16L1-specific immunoprecipitates from lysates of control and IFT20KD Jurkat cells. Preclearing controls are included in each blot (neg ctr). Tested proteins show comparable expression in total cell lysate from ctr and IFT20KD Jurkat cells (**Supplementary Figures 3A,D**). The migration of molecular mass markers is indicated. The quantification of the relative protein expression normalized to ATG16L1 (mean fold ± SD; ctr value = 1) is reported for each blot (n = 3; mean ± SD). **(D)** Immunoblot analysis with Rab5 antibodies of BECLIN 1-specific immunoprecipitates from lysates of control and IFT20KD Jurkat cells. Preclearing controls are included in each blot (neg ctr). Tested proteins show comparable expression in total cell lysate from ctr and IFT20KD Jurkat cells (**Supplementary Figures 3B,C**). The migration of molecular mass markers is indicated. The quantification of the relative protein expression normalized to ATG16L1 (mean fold ± SD; ctr value = 1) is reported for each blot (n = 3; mean ± SD). **(E,F)** Immunofluorescence analysis of BECLIN 1 and Rab5 **(E)** or FYVE-GFP and Rab5 **(F)** in control and IFT20KD Jurkat cells. Representative medial optical sections and overlay of immunofluorescence and DIC images are shown (IF + DIC). Scale bar: 5 μm. The graphs show the quantification of the weighted colocalization (Mander's coefficient) of BECLIN 1 **(E)** or FYVE-GFP **(F)** and Rab5 in ctr and IFT20KD Jurkat cells (mean ± SD; ≥ 32 cells/line; n = 3; Mann–Whitney test). $^{****}P < 0.0001$.

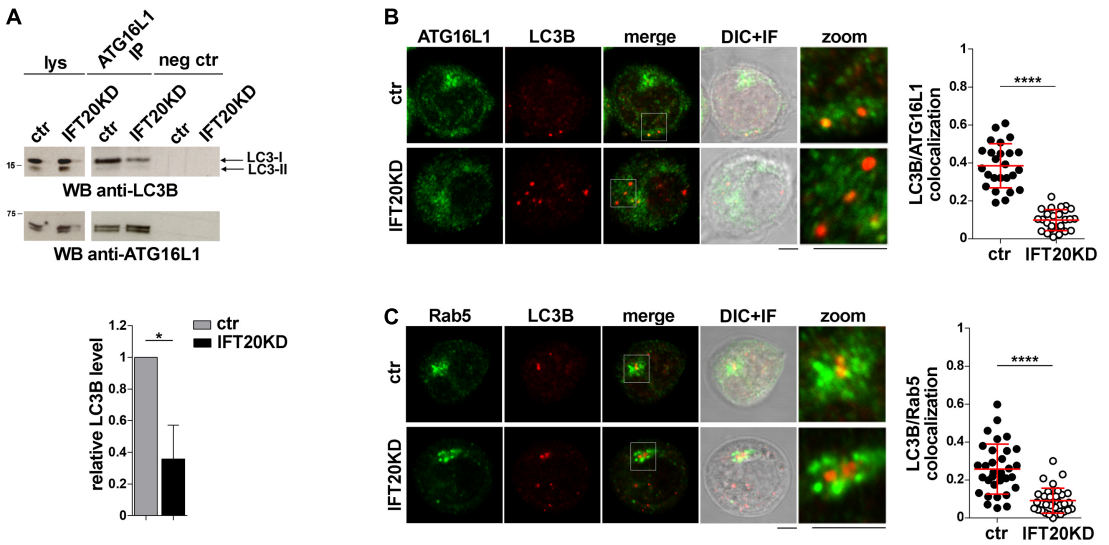

FIGURE 6 | IFT20 is required for LC3 recruitment to ATG16L1 at early endosomes. **(A)** Western blot analysis with anti-LC3B antibodies of ATG16L1-specific immunoprecipitates from lysates of control and IFT20KD Jurkat cells. Preclearing controls and total cell lysates are included in each blot (neg ctr). The migration of molecular mass markers is indicated. The quantification of the relative protein levels normalized to ATG16L1 (mean fold ± SD; ctr value = 1) is shown (n = 3; mean ± SD; Student's t-test). **(B,C)** Immunofluorescence analysis of ATG16L1 **(B)** or Rab5 **(C)** and LC3B in control and IFT20KD Jurkat cells. The graph shows the quantification using Mander's coefficient of the weighted colocalization of LC3B and ATG16L1 **(B)** or Rab5 **(C)** in ctr and IFT20KD Jurkat cells reported as mean value/cell calculated on single dot LC3$^+$ (≥ 25 cells/sample, n = 3; mean ± SD; Mann–Whitney test). Representative images (medial optical sections and the overlay DIC + IF) are shown. Scale bar: 5 μm. *P < 0.05; ****P < 0.0001.

molecular determinants mapping to both the CC domain and the unstructured domain to bind the small GTPase Rab5 at early endosomes. We provide evidence that the IFT20-dependent ATG16L1 localization to early endosomes, but not to the Golgi apparatus, results in the local formation of autophagosomes downstream of BECLIN 1 recruitment and PI(3)P production. The results highlight a dual role of IFT20 in basal T cell autophagy.

IFT20 has been previously demonstrated to regulate both basal and starvation-induced autophagy in ciliated cells (Pampliega et al., 2013). Our data, implicating IFT20 in basal T cell autophagy, underscore the notion that the ciliogenesis machinery is exploited by the non-ciliated T cell beyond immune synapse assembly. In support of this notion, we have recently demonstrated that IFT20 participates in lysosome biogenesis, a function that we found to be shared by ciliated cells (Finetti et al., 2020). The autophagy-related mechanism appears, however, to differ, at least in part. In ciliated cells the IFT system is required for the transport of autophagy regulators – including VPS34, ATG14, ATG16L1, and ATG7 – to the base of the cilium (Pampliega et al., 2013). Additionally, IFT20 co-localizes with ATG16L1 at small Golgi-proximal vesicles that undergo trafficking to the cilium upon cell starvation, independently of other components of the IFT system (Pampliega et al., 2013). Here we show that IFT20 co-localizes with ATG16L1 at the Golgi apparatus. Additionally, the IFT20-dependent Golgi localization of ATG16L1 does not appear relevant to the pro-autophagic function of IFT20, at least under basal conditions. Indeed, untethering IFT20 from the Golgi through depletion of its interactor GMAP210 did not compromize autophagy, despite the dissipation of ATG16L1 away from the Golgi. The Golgi apparatus has been identified as one of the membrane sources for phagophore elongation in other cell types, with ATG16L1 promoting the local recruitment and lipidation of LC3 (Fujita et al., 2008; Davis et al., 2017). Our data suggest that other ATG16L1 pools, recruited to the Golgi apparatus by alternative interactors, such as Rab33 (Itoh et al., 2008), might contribute to the local formation of autophagosomes. However, we have detected minimal co-localization of BECLIN 1 with the Golgi in T cells. As an alternative possibility, Golgi-associated ATG16L1 may play autophagy-independent functions in these cells, as recently reported in *Dictyostelium discoideum* (Karow et al., 2020).

We found that, as opposed to the Golgi, early endosomes are sites of autophagosome formation in T cells, as shown by the local accumulation of BECLIN 1, PI(3)P, ATG16L1, and LC3. Interestingly, while IFT20 appears dispensable for the association of a functional class III PI3-K complex with early endosomes, it is essential for the recruitment of ATG16L1 to this location. PI(3)P is known to promote the WIPI2-dependent association of ATG16L1 with sites of autophagosome formation (Dooley et al., 2014). However, additional interactors participate in its targeting to specific membrane compartments, including Rab33 at the Golgi apparatus, SNX18/Rab11 at recycling endosomes and clathrin at the plasma membrane (Itoh et al., 2008; Ravikumar et al., 2010; Knævelsrud et al., 2013; Puri et al., 2013). Here we identify Rab5 as an early endosome-specific binding partner of ATG16L1 in T cells, which may account for the association of ATG16L1 with early endosomes reported for other cell types (Fraser et al., 2019). Of note, Rab5 participates in a complex

with BECLIN 1 and VPS34 (Ravikumar et al., 2008). Our results implicate Rab5 not only in marking early endosomes as sites of autophagosome formation by promoting the VPS34-dependent production of PI(3)P, but also in assisting the subsequent recruitment and/or stabilization of ATG16L1 at these sites using IFT20 as an adaptor.

Our data provide evidence that the association of IFT20 with both the Golgi apparatus and early endosomes is mediated by compartment-specific interactors, namely GMAP210, as previously reported (Follit et al., 2008) and Rab5, respectively. Both these interactions map to the CC domain of IFT20, as shown both in pull-down assays and by co-localization analysis of cells expressing an IFT20 deletion mutant lacking the CC domain. The site of interaction of IFT20 on GMAP210 has been mapped to the CC domain of the latter (Follit et al., 2008; Zucchetti et al., 2019). Hence GMAP210 and IFT20 heterodimerize through their respective CC domain, consistent with the function of CC domains in establishing protein-protein interactions (Mason and Arndt, 2004). IFT20 exploits its CC domain to also interact with Rab5, however, the pull-down assays with the GST-tagged IFT20 construct lacking the CC domain show that the unstructured domain also binds Rab5, indicating the cooperation of multiple molecular determinants of IFT20 in this interaction. Of note, at variance with its compartment-specific binding partners, the interaction of IFT20 with ATG16L1 is CC domain-independent and maps to the unstructured N-terminal portion of the protein. While the only protein-protein interaction domain of IFT20 is its CC domain, which is used for binding IFT54 and IFT57 within the IFT complex (Baker et al., 2003; Omori et al., 2008), IFT20 is able to recognize and bind a number of proteins at the Golgi apparatus for sorting and targeting to the ciliary membrane, as exemplified by rhodopsin, opsin, and polycystin-2 (Follit et al., 2006; Keady et al., 2011). Hence, similar to these interactors, ATG16L1 might bind directly or indirectly to a molecular determinant within the IFT20 N-terminus that remains to be identified.

Longevity is a key feature of both naive and memory T cells as it ensures the maintenance of the immune repertoire as well as long-lasting protection from pathogens toward which the organism has mounted an effective immune response. Basal autophagy is one of the main mechanisms that underlie this extended T cell survival (Pua et al., 2007; Kovacs et al., 2012; Xu et al., 2014). Our finding of a dual role of IFT20 in autophagy, i.e., promoting autophagosome formation by recruiting ATG16L1 at early endosomes, and allowing for the degradation of the autolysosome contents by controlling lysosome biogenesis (Finetti et al., 2020), highlights IFT20 as a key player in T cell homeostasis.

DATA AVAILABILITY STATEMENT

The raw data supporting the conclusions of this article will be made available by the authors, without undue reservation.

AUTHOR CONTRIBUTIONS

All authors listed have made a substantial, direct and intellectual contribution to the work, and approved it for publication. FF and CB wrote the manuscript. FF prepared the figures.

FUNDING

This work was carried out with the support of the Fondazione Telethon, Italy (Grant GGP16003) and the Associazione Italiana per la Ricerca sul Cancro (Grant IG 20148) to CB, and Ministero dell'Istruzione, dell'Università e della Ricerca (Grant PRIN bando 2017-2017FS5SHL) to CB and FC. VC was supported by the Lundbeck Foundation (R209-2015-3505) and the KBVU from the Danish Cancer Society (R146-A9471), and is currently supported by the Fondazione Umberto Veronesi. The support of the Associazione Italiana per la Ricerca sul Cancro (AIRC IG-23543) and the BKVU from Danish Cancer Society R231-A14034 to FC was also acknowledged. FC laboratory in Copenhagen is part of the Center of Excellence for Autophagy, Recycling and Disease (CARD), funded by the Danmarks Grundforskningsfond (DNRF125).

ACKNOWLEDGMENTS

The authors wish to thank Greg Pazour, Marino Zerial, and Antonella De Matteis for generously providing key reagents and Noa Martin-Cofreces for interesting suggestions.

SUPPLEMENTARY MATERIAL

The Supplementary Material for this article can be found online at: https://www.frontiersin.org/articles/10.3389/fcell.2021.634003/full#supplementary-material

REFERENCES

Baker, S. A., Freeman, K., Luby-Phelps, K., Pazour, G. J., and Besharse, J. C. (2003). IFT20 links kinesin ii with a mammalian intraflagellar transport complex that is conserved in motile flagella and sensory cilia. *J. Biol. Chem.* 278, 34211–34218. doi: 10.1074/jbc.M300156200

Bejarano, E., Yuste, A., Patel, B., Randy, R. F., Spray, D. C., and Cuervo, A. M. (2014). Connexins modulate autophagosome biogenesis. *Nat. Cell Biol.* 16, 401–414. doi: 10.1038/ncb2934

Cassioli, C., and Baldari, C. T. (2019). A ciliary view of the immunological synapse. *Cells* 8:789. doi: 10.3390/cells8080789

Davis, S., Wang, J., and Ferro-Novick, S. (2017). Developmental cell review crosstalk between the secretory and autophagy pathways regulates autophagosome formation. *Dev. Cell* 41, 23–32. doi: 10.1016/j.devcel.2017.03.015

Dikic, I., and Elazar, Z. (2018). Mechanism and medical implications of mammalian autophagy. *Nat. Rev. Mol. Cell Biol.* 19, 349–364. doi: 10.1038/s41580-018-0003-4

Dooley, H. C., Razi, M., Polson, H. E. J., Girardin, S. E., Wilson, M. I., and Tooze, S. A. (2014). WIPI2 links LC3 conjugation with PI3P, autophagosome formation, and pathogen clearance by recruiting Atg12-5-16L1. *Mol. Cell* 55, 238–252. doi: 10.1016/j.molcel.2014.05.021

Finetti, F., Cassioli, C., Cianfanelli, V., Onnis, A., Paccagnini, E., Kabanova, A., et al. (2020). The intraflagellar transport protein IFT20 controls lysosome biogenesis by regulating the post-Golgi transport of acid hydrolases. *Cell Death Differ.* 27, 310–328. doi: 10.1038/s41418-019-0357-y

Finetti, F., Paccani, S. R., Riparbelli, M. G., Giacomello, E., Perinetti, G., Pazour, G. J., et al. (2009). Intraflagellar transport is required for polarized recycling of the TCR/CD3 complex to the immune synapse. *Nat. Cell Biol.* 11, 1332–1339. doi: 10.1038/ncb1977

Finetti, F., Paccani, S. R., Rosenbaum, J., and Baldari, C. T. (2011). Intraflagellar transport: a new player at the immune synapse. *Trends Immunol.* 32, 139–145. doi: 10.1016/j.it.2011.02.001

Finetti, F., Patrussi, L., Masi, G., Onnis, A., Galgano, D., Lucherini, O. M., et al. (2014). Specific recycling receptors are targeted to the immune synapse by the intraflagellar transport system. *J. Cell Sci.* 127, 1924–1937. doi: 10.1242/jcs.139337

Follit, J. A., San Agustin, J. T., Xu, F., Jonassen, J. A., Samtani, R., Lo, C. W., et al. (2008). The Golgin GMAP210/TRIP11 anchors IFT20 to the Golgi complex. *PLoS Genet.* 4:e1000315. doi: 10.1371/journal.pgen.1000315

Follit, J. A., Tuft, R. A., Fogarty, K. E., and Pazour, G. J. (2006). The intraflagellar transport protein IFT20 is associated with the golgi complex and is required for cilia assembly. *Mol. Biol. Cell* 17, 3781–3792. doi: 10.1091/mbc.e06-02-0133

Fraser, J., Simpson, J., Fontana, R., Kishi−Itakura, C., Ktistakis, N. T., and Gammoh, N. (2019). Targeting of early endosomes by autophagy facilitates EGFR recycling and signalling. *EMBO Rep.* 20:e47734. doi: 10.15252/embr.201947734

Fujita, N., Itoh, T., Omori, H., Fukuda, M., Noda, T., and Yoshimori, T. (2008). The Atg16L complex specifies the site of LC3 lipidation for membrane biogenesis in autophagy. *Mol. Biol. Cell* 19, 2092–2100. doi: 10.1091/mbc.E07-12-1257

Funderburk, S. F., Wang, Q. J., and Yue, Z. (2010). Beclin 1-VPS34 complex-at the crossroads of autophagy and beyond. *Trends Cell Biol.* 20, 355–362. doi: 10.1016/j.tcb.2010.03.002

Galgano, D., Onnis, A., Pappalardo, E., Galvagni, F., Acuto, O., and Baldari, C. T. (2017). The T cell IFT20 interactome reveals new players in immune synapse assembly. *J. Cell Sci.* 130, 1110–1121. doi: 10.1242/jcs.200006

Gammoh, N., Florey, O., Overholtzer, M., and Jiang, X. (2013). Interaction between FIP200 and ATG16L1 distinguishes ULK1 complex-dependent and-independent autophagy. *Nat. Struct. Mol. Biol.* 20, 144–149. doi: 10.1038/nsmb.2475

Hanada, T., Noda, N. N., Satomi, Y., Ichimura, Y., Fujioka, Y., Takao, T., et al. (2007). The Atg12-Atg5 conjugate has a novel E3-like activity for protein lipidation in autophagy. *J. Biol. Chem.* 282, 37298–37302. doi: 10.1074/jbc.C700195200

Hubbard, V. M., Valdor, R., Patel, B., Singh, R., Cuervo, A. M., and Macian, F. (2010). Macroautophagy regulates energy metabolism during effector t cell activation. *J. Immunol.* 185, 7349–7357. doi: 10.4049/jimmunol.1000576

Itoh, T., Fujita, N., Kanno, E., Yamamoto, A., Yoshimori, T., and Fukuda, M. (2008). Golgi-resident small GTPase Rab33B interacts with Atg16L and modulates autophagosome formation. *Mol. Biol. Cell* 19, 2916–2925. doi: 10.1091/mbc.E07

Jia, W., He, M. X., McLeod, I. X., Guo, J., Ji, D., and He, Y. W. (2015). Autophagy regulates T lymphocyte proliferation through selective degradation of the cell-cycle inhibitor CDKN1B/p27Kip1. *Autophagy* 11, 2335–2345. doi: 10.1080/15548627.2015.1110666

Kabat, A. M., Harrison, O. J., Riffelmacher, T., Moghaddam, A. E., Pearson, C. F., Laing, A., et al. (2016). The autophagy gene Atg16l1 differentially regulates Treg and TH2 cells to control intestinal inflammation. *Elife* 5:e12444. doi: 10.7554/eLife.12444

Karow, M., Fischer, S., Meßling, S., Konertz, R., Riehl, J., Xiong, Q., et al. (2020). Functional characterisation of the autophagy ATG12˜5/16 complex in dictyostelium discoideum. *Cells* 9:1179. doi: 10.3390/cells9051179

Kasai, M., Tanida, I., Ueno, T., Kominami, E., Seki, S., Ikeda, T., et al. (2009). Autophagic compartments gain access to the mhc class ii compartments in thymic epithelium. *J. Immunol.* 183, 7278–7285. doi: 10.4049/jimmunol.0804087

Keady, B. T., Le, Y. Z., and Pazour, G. J. (2011). IFT20 is required for opsin trafficking and photoreceptor outer segment development. *Mol. Biol. Cell* 22, 921–930. doi: 10.1091/mbc.E10-09-0792

Knævelsrud, H., Søreng, K., Raiborg, C., Håberg, K., Rasmuson, F., Brech, A., et al. (2013). Membrane remodeling by the PX-BAR protein SNX18 promotes autophagosome formation. *J. Cell Biol.* 202, 331–349. doi: 10.1083/jcb.201205129

Kovacs, J. R., Li, C., Yang, Q., Li, G., Garcia, I. G., Ju, S., et al. (2012). Autophagy promotes T-cell survival through degradation of proteins of the cell death machinery. *Cell Death Differ.* 19, 144–152. doi: 10.1038/cdd.2011.78

Mason, J. M., and Arndt, K. M. (2004). Coiled coil domains: stability, specificity, and biological implications. *Chembiochem* 5, 170–176. doi: 10.1002/cbic.200300781

Mauthe, M., Orhon, I., Rocchi, C., Zhou, X., Luhr, M., Hijlkema, K. J., et al. (2018). Chloroquine inhibits autophagic flux by decreasing autophagosome-lysosome fusion. *Autophagy* 14, 1435–1455. doi: 10.1080/15548627.2018.1474314

Mizushima, N., Noda, T., Yoshimori, T., Tanaka, Y., Ishii, T., George, M. D., et al. (1998). A protein conjugation system essential for autophagy. *Nature* 395, 395–398. doi: 10.1038/26506

Nedjic, J., Aichinger, M., Emmerich, J., Mizushima, N., and Klein, L. (2008). Autophagy in thymic epithelium shapes the T-cell repertoire and is essential for tolerance. *Nature* 455, 396–400. doi: 10.1038/nature07208

Omori, Y., Zhao, C., Saras, A., Mukhopadhyay, S., Kim, W., Furukawa, T., et al. (2008). Elipsa is an early determinant of ciliogenesis that links the IFT particle to membrane-associated small GTPase Rab8. *Nat. Cell Biol.* 10, 437–444. doi: 10.1038/ncb1706

Otomo, A., Kunita, R., Suzuki-Utsunomiya, K., Ikeda, J. E., and Hadano, S. (2011). Defective relocalization of ALS2/alsin missense mutants to Rac1-induced macropinosomes accounts for loss of their cellular function and leads to disturbed amphisome formation. *FEBS Lett.* 585, 730–736. doi: 10.1016/j.febslet.2011.01.045

Pacini, S., Ulivieri, C., Di Somma, M. M., Isacchi, A., Lanfrancone, L., Pelicci, P. G., et al. (1998). Tyrosine 474 of ZAP-70 is required for association with the Shc adaptor and for T-cell antigen receptor-dependent gene activation. *J. Biol. Chem.* 273, 20487–20493. doi: 10.1074/jbc.273.32.20487

Pampliega, O., Orhon, I., Patel, B., Sridhar, S., Díaz-Carretero, A., Beau, I., et al. (2013). Functional interaction between autophagy and ciliogenesis. *Nature* 502, 194–200. doi: 10.1038/nature12639

Paul, S., Kashyap, A. K., Jia, W., He, Y. W., and Schaefer, B. C. (2012). Selective autophagy of the adaptor protein bcl10 modulates t cell receptor activation of NF-κB. *Immunity* 36, 947–958. doi: 10.1016/j.immuni.2012.04.008

Pazour, G. J., Baker, S. A., Deane, J. A., Cole, D. G., Dickert, B. L., Rosenbaum, J. L., et al. (2002). The intraflagellar transport protein, IFT88, is essential for vertebrate photoreceptor assembly and maintenance. *J. Cell Biol.* 157, 103–113. doi: 10.1083/jcb.200107108

Prevo, B., Scholey, J. M., and Peterman, E. J. G. (2017). Intraflagellar transport: mechanisms of motor action, cooperation, and cargo delivery. *FEBS J.* 284, 2905–2931. doi: 10.1111/febs.14068

Progida, C., Cogli, L., Piro, F., De Luca, A., Bakke, O., and Bucci, C. (2010). Rab7b controls trafficking from endosomes to the TGN. *J. Cell Sci.* 123, 1480–1491. doi: 10.1242/jcs.051474

Pua, H. H., Dzhagalov, I., Chuck, M., Mizushima, N., and He, Y.-W. (2007). A critical role for the autophagy gene Atg5 in T cell survival and proliferation. *J. Exp. Med.* 204, 25–31. doi: 10.1084/jem.20061303

Puleston, D. J., Zhang, H., Powell, T. J., Lipina, E., Sims, S., Panse, I., et al. (2014). Autophagy is a critical regulator of memory $CD8^+$ T cell formation. *Elife* 3, 1–21. doi: 10.7554/eLife.03706

Puri, C., Renna, M., Bento, C. F., Moreau, K., and Rubinsztein, D. C. (2013). Diverse autophagosome membrane sources coalesce in recycling endosomes. *Cell* 154, 1285–1299. doi: 10.1016/j.cell.2013.08.044

Ravikumar, B., Imarisio, S., Sarkar, S., O'Kane, C. J., and Rubinsztein, D. C. (2008). Rab5 modulates aggregation and toxicity of mutant huntingtin through macroautophagy in cell and fly models of Huntington disease. *J. Cell Sci.* 121, 1649–1660. doi: 10.1242/jcs.025726

Ravikumar, B., Moreau, K., Jahreiss, L., Puri, C., and Rubinsztein, D. C. (2010). Plasma membrane contributes to the formation of pre-autophagosomal structures Europe PMC Funders Group. *Nat.Cell Biol.* 12, 747–757. doi: 10.1038/ncb2078

Staiano, L., and Zappa, F. (2019). Hijacking intracellular membranes to feed autophagosomal growth. *FEBS Lett.* 593, 3120–3134. doi: 10.1002/1873-3468.13637

Valdor, R., Mocholi, E., Botbol, Y., Guerrero-Ros, I., Chandra, D., Koga, H., et al. (2014). Chaperone-mediated autophagy regulates T cell responses through targeted degradation of negative regulators of T cell activation. *Nat. Immunol.* 15, 1046–1054. doi: 10.1038/ni.3003

Vivar, O. I., Masi, G., Carpier, J., Magalhaes, J. G., Galgano, D., Pazour, G. J., et al. (2016). IFT20 controls LAT recruitment to the immune synapse and T-cell activation in vivo. *Proc. Natl. Acad. Sci. U.S.A.* 113, 386–391. doi: 10.1073/pnas.1513601113

Wei, J., Long, L., Yang, K., Guy, C., Shrestha, S., Chen, Z., et al. (2016). Autophagy enforces functional integrity of regulatory T cells by coupling environmental cues and metabolic homeostasis. *Nat. Immunol.* 17, 277–285. doi: 10.1038/ni.3365

Xiong, Q., Li, W., Li, P., Yang, M., Wu, C., and Eichinger, L. (2018). The Role of ATG16 in autophagy and the ubiquitin proteasome system. *Cells* 8:2. doi: 10.3390/cells8010002

Xu, X., Araki, K., Li, S., Han, J. H., Ye, L., Tan, W. G., et al. (2014). Autophagy is essential for effector CD8 + T cell survival and memory formation. *Nat. Immunol.* 15, 1152–1161. doi: 10.1038/ni.3025

Zaffagnini, G., and Martens, S. (2016). Mechanisms of selective autophagy. *J. Mol. Biol.* 428, 1714–1724. doi: 10.1016/j.jmb.2016.02.004

Zucchetti, A. E., Bataille, L., Carpier, J. M., Dogniaux, S., San Roman-Jouve, M., Maurin, M., et al. (2019). Tethering of vesicles to the Golgi by GMAP210 controls LAT delivery to the immune synapse. *Nat. Commun.* 10:2864. doi: 10.1038/s41467-019-10891-w

Conflict of Interest: The authors declare that the research was conducted in the absence of any commercial or financial relationships that could be construed as a potential conflict of interest.